An Innovative Injection and Mixing System for Diesel Fuel Reforming

Final Report for: July 1, 2006 - December 31, 2007

Submitting Organization:

Engine Components
Goodrich Corporation
811 4th Street
West Des Moines, IA 50265

Award Project Director and Principle Author:

Spencer D. Pack
Sr. Design Engineer
Engine Components
Goodrich Corporation
2200 Delavan Drive
West Des Moines, IA 50265-0100
Tel: (515) 633-3460
email: spencer.pack@goodrich.com

Award Identification Number: DE-FC26-04NT42229

Submittal Date: 2008FEB20
Report Completion Date: 2008JAN18
File Name: TR #1161.pdf

DISCLAIMER

Turbine Fuel Technologies
Goodrich Corporation
811 4th Street
West Des Moines, Iowa 50265-0100
515/274-1561

TECHNICAL REPORT

Technical Report Number	Issue / Revision
TR #1161	NC

Title
An Innovative Injection and Mixing System for Diesel Fuel Reforming

Project	GT#	Part Number	Date
DOE Fuel Cell	4035-102	N/A	2008JAN18

TRANSMITTAL OF TECHNICAL DATA (EAR)

THESE COMMODITIES, TECHNOLOGY OR SOFTWARE ARE CONTROLLED BY THE U.S. EXPORT ADMINISTRATION REGULATION (EAR). DIVERSION CONTRARY TO U.S. LAW IS PROHIBITED.

Technology ECCN(s):
EAR99

Executive Summary

This project focused on fuel stream preparation improvements prior to injection into a solid oxide fuel cell reformer. Each milestone and the results from each milestone are discussed in detail in this report. The first two milestones were the creation of a coking formation test rig and various testing performed on this rig. Initial tests indicated that three anti-carbon coatings showed improvement over an uncoated (bare metal) baseline. However, in follow-up 70 hour tests of the down selected coatings, Scanning Electron Microscope (SEM) analysis revealed that no carbon was generated on the test specimens. These follow-up tests were intended to enable a down selection to a single best anti-carbon coating. Without the formation of carbon it was impossible to draw conclusions as to which anti-carbon coating showed the best performance. The final 70 hour tests did show that AMCX AMC26 demonstrated the lowest discoloration of the metal out of the three down selected anti-carbon coatings. This discoloration did not relate to carbon but could be a useful result when carbon growth rate is not the only concern. Unplanned variations in the series of tests must be considered and may have altered the results. Reliable conclusions could only be drawn from consistent, repeatable testing beyond the allotted time and funding for this project.

Milestones 3 and 4 focused on the creation of a preheating pressure atomizer and mixing chamber. A design of experiment test helped identify a configuration of the preheating injector, Build 1, which showed a very uniform fuel spray flow field. This injector was improved upon by the creation of a Build 2 injector. Build 2 of the preheating injector demonstrated promising SMD results with only 22psi fuel pressure and 0.7 in H_2O of Air. It was apparent from testing and CFD that this Build 2 has flow field recirculation zones. These recirculation zones may suggest that this Build 2 atomizer and mixer would require steam injection to reduce the auto ignition potential. It is also important to note that to achieve uniform mixing within a short distance, some recirculation is necessary.

Milestone 5 generated CFD and FEA results that could be used to optimize the preheating injector. CFD results confirmed the recirculation zones seen in test data and confirmed that the flow field would not change when attached to a reformer. The FEA predicted fuel wetted wall temperatures which led to several suggested improvements that could possibly improve nozzle efficiency.

Milestone 6 (originally an optional task) took a different approach than the preheating pressure atomizer. It focused on creation and optimization of a piezoelectric injector which could perform at extremely low fuel pressures. The piezoelectric atomizer showed acceptable SMD results with fuel pressure less than 1.0 psig and air pressure less than 1.0 in H_2O. These SMD values were enhanced when a few components were changed, and it is expected would improve further still at elevated air temperatures. It was demonstrated that the piezoelectric injector could accomplish the desired task. The addition of phase tracking and a burst mode to the frequency controller increased the usability of the piezoelectric injector. This injector is ready to move on to the next phase of development.

Engine Components has met the required program milestones of this project. Some of the Milestones were adjusted to allow Milestone 6 to be completed in parallel with the other Milestones. Because of this, Task 3.10 and 3.13 were made optional instead of Milestone 6. Engine Components was extremely grateful for the support that was provided by NETL in support of this work.

Prepared By	Title
Spencer Pack	Sr. Design Engineer
John Short	Research Associate
Nick Overman	Design Engineer

AUTHORIZATION
APPROVAL PER
GOODRICH
PMI 2.094

Revision History

Revision	Date	Author	Revision	Date	Author
NC	2008JAN18	S. Pack			

#11-E

TABLE OF CONTENTS

1.0 Introduction 4
2.0 Milestone 1.0: Complete Data Acq. Software and Automated Coking Test Rig 4
Task 1.1 Document Test Set Up With Rig Schematics and Drawings 5
Task 1.3 Modify LabVIEW Data Acquisition Software for Anti Carbon Coating Testing. 10
Task 1.4 Perform Test Rig Calibration and Safety Check 12
3.0 Milestone 2.0: Anti-Carbon Coating Investigation and Endurance Tests 13
Task 2.1 Identify Potential Coating Candidates and Application Methods 13
Task 2.2 Prepare Coking Test Hardware and Coating Specimens 14
Task 2.3 Devise Test Matrix and Test Conditions 14
Task 2.4 Run Coking Tests Using Tube Specimens 16
Task 2.5 Analyze Test Results and Down-Select the Best Anti-Carbon Coating 16
Task 2.6 Apply the Selected Coating to a Fuel Injector Cartridge 28
Task 2.7 Conduct Endurance Tests for a Back-to-Back Comparison Between a Coated and a Non-Coated Injector 29
4.0 Milestone 3.0: Complete Optimized Preheating Simplex Injector 45
Task 3.1 Define Operation and Performance Requirements for the Injector/Mixer System 46
Task 3.2 Evaluate New Concepts for Operation and Performance Improvements 48
Task 3.3 Prepare Solid Models for the Optimized Preheating Simplex Injector 48
Task 3.4 Prepare Drawings for the Optimized Components 48
Task 3.5 Fabricate and Assemble Test Hardware for the First Build 48
Task 3.6 Run Injector Tests and Establish Performance Curves for the First Build 52
Task 3.7 Analyze test results and propose design refinement 59
Task 3.8 Fabricate and assemble test hardware for the second build 59
Task 3.9 Run injector tests and establish performance curves for the second build 59
Task 3.11 Optimize feedback sensor location 64
Task 3.12 Improve Injector Response Time and Stability During Flow Transition 65
Task 3.10 Optimize the Heating Efficiency and Miniaturize the Temperature Controller 65
Task 3.13 Perform Final Injector Tests With Improved Electronic Control 65
5.0 Milestone 4.0: Construct Integrated Preheating Injector/Mixer System 65
Task 4.1 Evaluate New Mixing Chamber Configurations for the Preheating Simplex Injector 66
Task 4.2 Prepare Solid Model and Drawings For the Improved Mixing Chamber 67
Task 4.3 Fabricate and Assemble Mixing Chamber 68
Task 4.4 Investigate Effect of Fuel Injection Location 70
Task 4.5 Optimize Injector Housing 70
Task 4.6 Optimize Swirl Mixer location, Configuration and Fabrication method 70
Task 4.7 Investigate Effect of Swirl mixer and Perforated Screens on fuel Mixture Characteristics 70
Task 4.8 Conduct Hot Flow Tests for the Optimized Injector/Mixer System 70
6.0 Milestone 5.0: Complete CFD analysis and Design of Experiment Study 74

Task 5.1 Perform CFD Analysis for the Preheating Simplex Injector/Mixer Having a Large Plenum as the Outlet Boundary 75
Task 5.2 Conduct Flow Field Measurements to Validate CFD Predictions 79
Task 5.3 Perform CFD Analysis for the Preheating Simplex Injector/Mixer Having a Simulated Reactor as the Outlet Boundary 79
Task 5.4 Conduct FE Analysis For the Injector Thermal and Material Stress Improvement 84
Task 5.5 Conduct SDE Study Using the Optimized Preheating Simplex Injector for Performance Prediction and Correlation 88
7.0 Milestone 6.0: Optimize Piezoelectric Injector and Mixer (Optional) 88
Task 6.1 Evaluate Improvement Ideas for the Piezoelectric Injector 89
Task 6.2 Prepare Solid Model and Drawings 89
Task 6.3 Fabricate and Assemble Test Hardware 89
Task 6.4 Conduct Experimental Tests 93
Task 6.5 Investigate Effect of Flow Rate, Temperature, and Fluid properties 94
Task 6.7 Conduct SDE Study to Fully Characterize the Injector performance 94
Task 6.6 Incorporate Pulse Modulation Device and Controller 97
8.0 Summary 98

1.0 Introduction

This Technical Report is a conclusive report out of all the work, testing, activities, results, etc of the Department of Energy (DOE) grant (Identification Number: DE-FC26-04NT42229) titled "An Innovative Injection and Mixing System for Diesel Fuel Reforming". Engine Components, Goodrich Corporation, utilized several disciplines and departments to accomplish this six quarter program. The departments were Design Engineering, Project Management, Purchasing, Manufacturing, and Engineering Technologies. The Design Engineers were utilized in creating the test rig schematics, drawings, CFD analysis, fuel injector design, and solid models. The Purchasing Department was utilized to obtain the required rig and atomizer components. Engineering Technologies Department created the desired rig test fixtures and completed rig testing. Project Management kept the team working together and on task to meet this project's goals and timeline.

This report is broken into eight sections. Each section covers one of the milestones which were proposed and agreed to in this project. The work performed to complete each milestone and the results obtained from that milestone are summarized. The work was not necessarily performed in series as suggested by this report. Rather most of the work was performed in parallel and out of milestone sequence. Engine Components greatly appreciates the funds provided by the DOE in support of this work.

It is Engine Components belief that fuel and air stream preparation is critical to solid oxide fuel cell (SOFC) reformers performance and life. It is reasoned that a reformer can produce hydrogen and carbon monoxide more effectively if the fuel and air are uniformly mixed prior to injection into the reformer. Also, the risk of hot spots and burn out in areas of the reformer would be minimized. This reduction of hot spots could also lead to increased reformer life. With this belief, Engine Components proposed and completed this project. This project focuses on fuel stream preparation prior to SOFC reformer injection.

2.0 Milestone 1.0: Complete Data Acq. Software and Automated Coking Test Rig

The objective of Milestone 1.0 was to create a test rig and data acquisition software that could perform tests and collect data on anti-carbon formation coatings. Solid Oxide Fuel Cells and fuel reformers require high air-fuel mixture temperatures. These temperatures are often well above the carbon or coke formation point of diesel fuels. Also, a promising injection technology for fuel reformer applications utilizes preheated fuel for improved atomization and evaporation. For these reasons, it was proposed that a test rig was needed to determine which of the many anti-carbon formation coatings would work best in diesel fuel cell applications. This section summarizes the work that was completed to create this test rig.

To complete this Milestone several sub tasks were required and accomplished. The first sub task was:

Task 1.1 Document Test Set Up With Rig Schematics and Drawings[1]

This coking test rig schematic can be seen in Figure 2.1. Some of the key features of this rig seen from this schematic are:

1) Up to 8 test samples can be run simultaneously.
2) Fuel back pressure regulated to ensure fuel is below boiling point.
3) Fuel heaters controlled to heat fuel up to desired temperatures.
4) Oven temperature is controlled.
5) Nitrogen purge available for fuel circuit and oven purge.
6) Heat exchanger utilized to cool fuel before entering catch tank.
7) Many pressure transducers and thermal couples that will be monitored which can shut the test down.
8) Optional Heated Air Circuit for the fuel line (not utilized at this time).

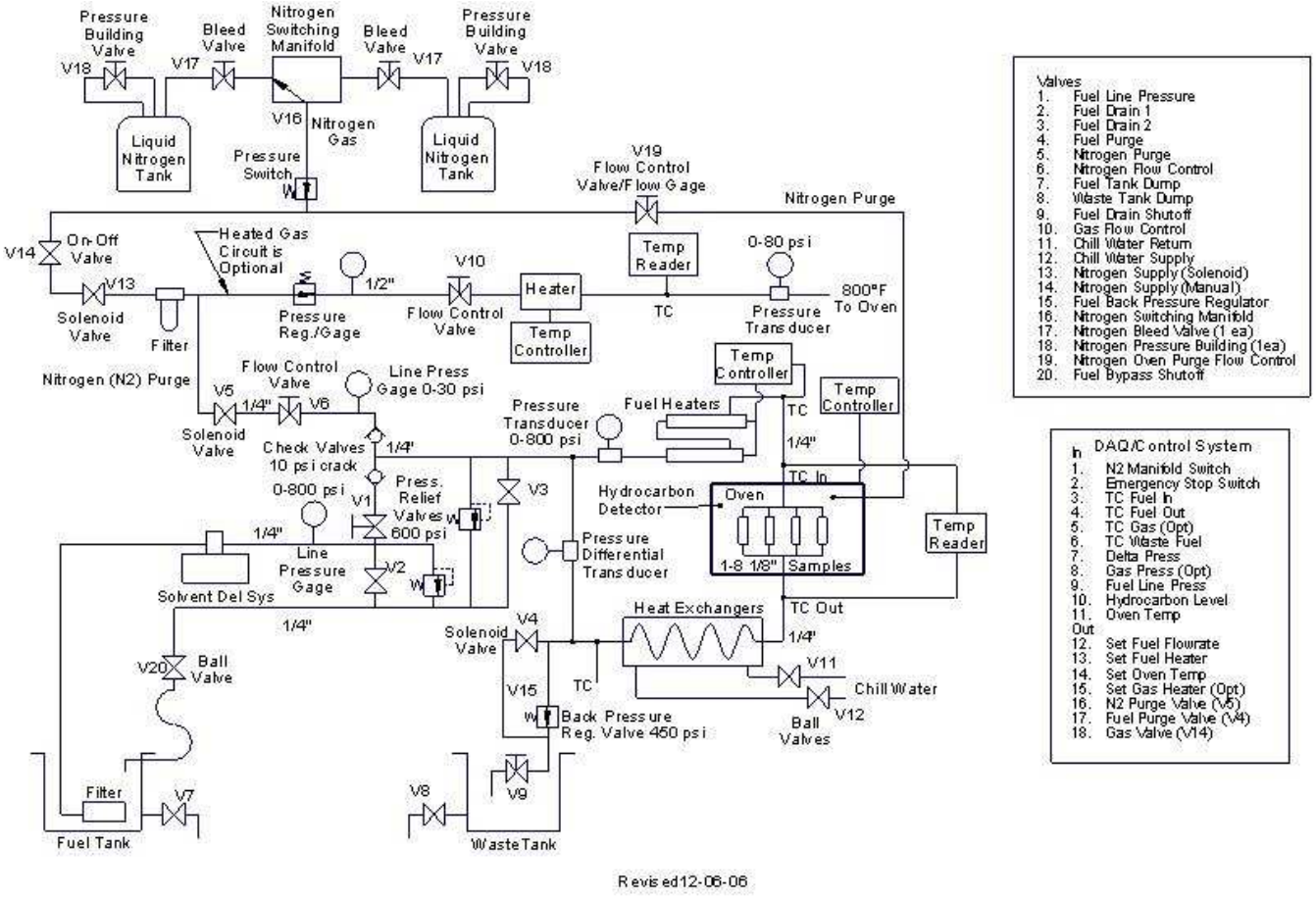

Figure 2.1: Coking Rig Schematic

This basic Coking Rig Schematic (Figure 2.1) was used to determine what parts were needed. With this in mind, the components were ordered and assembled to create the coking rig.

[1] Schematics and Drawings remain Goodrich Engine Components Proprietary Information.

Figures 2.2 through 2.9 show the construction of this coking rig. Figure 2.2 shows the entire rig setup in the room. Figure 2.3 shows the hood exhaust system. This exhaust hood closes when a fire is detected and the CO2 fire suppression system is activated. Figure 2.4 shows the CO_2 fire suppression system. This system is activated when 190°F is detected in the exhaust hood. The CO_2 nozzles are located above the rig (in and outside of exhaust hood). Figure 2.5 shows the optional heated air controller (not used in this project) and the fuel heater controller. The heater controller is used to heat the fuel to the desired test conditions before entering the test piece. Figure 2.6 shows the fuel flow controller as well as other various gages and instrumentation. Figure 2.7 shows the N_2 purge system manifold. This N_2 system constantly fills the oven with N_2 and can be used to purge the fuel lines during normal or emergency shut down. Figure 2.8 is another look at the fuel storage tanks. Figure 2.9 shows some of the safety marking required for the CO_2 fire suppression system.

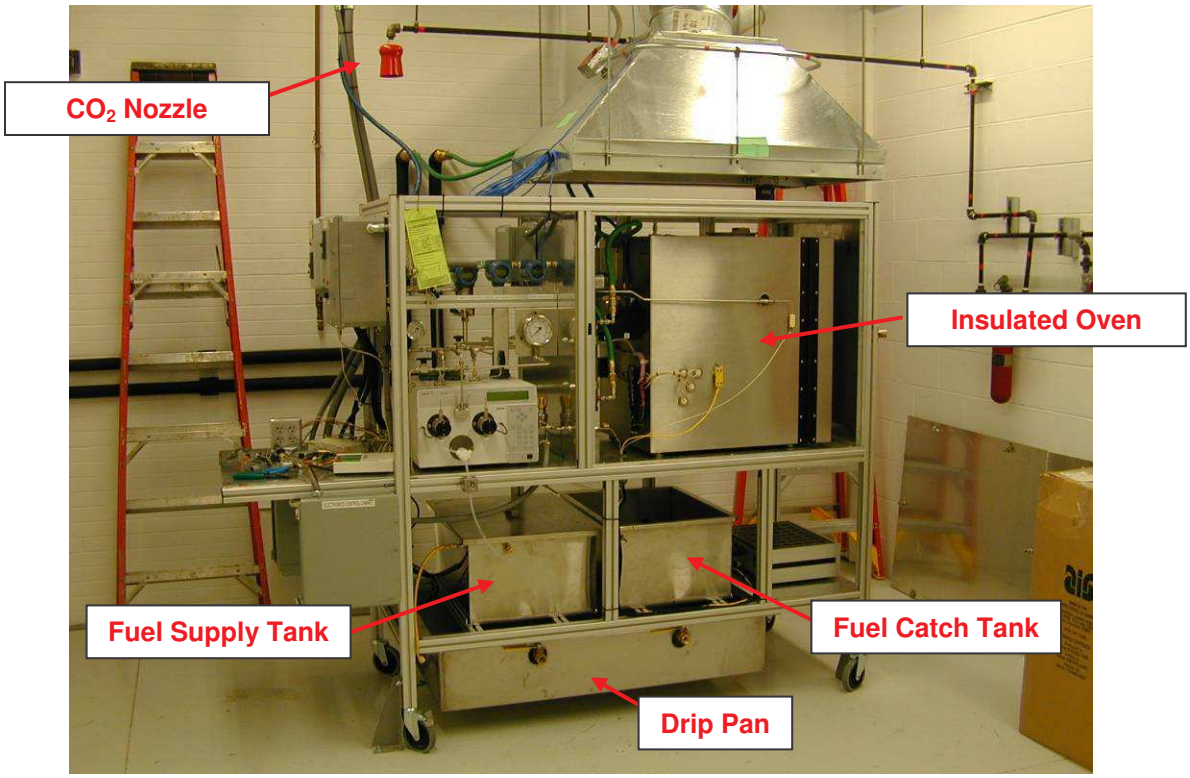

Figure 2.2: Coking Test Rig

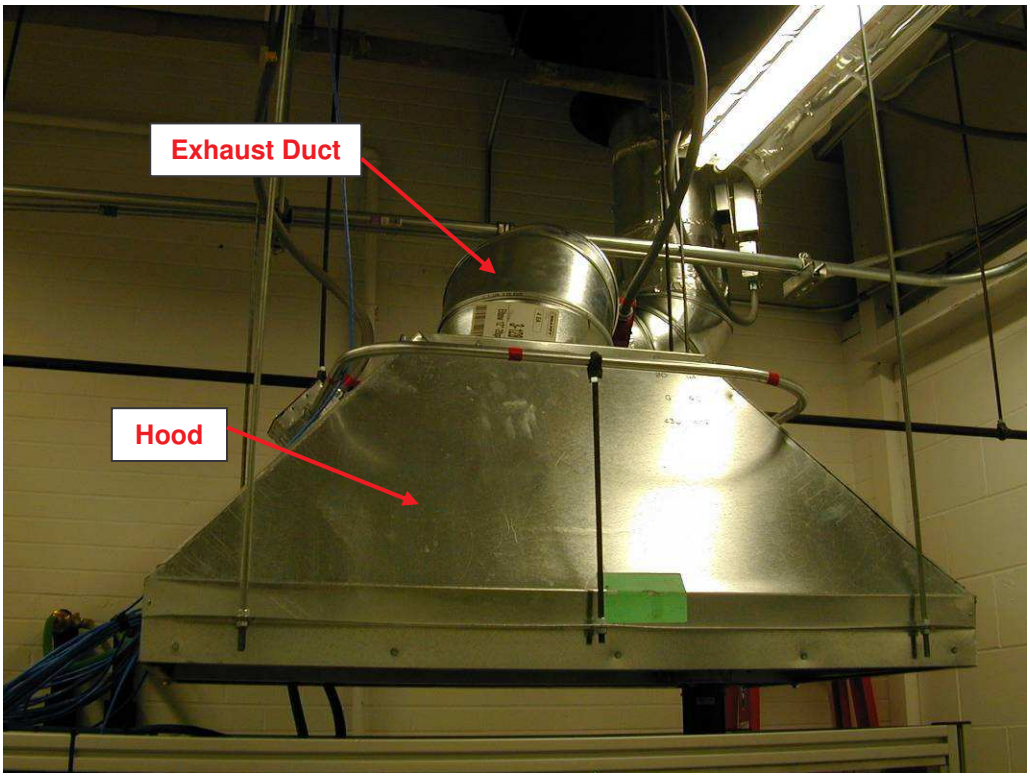

Figure 2.3: Coking Rig Exhaust Fan

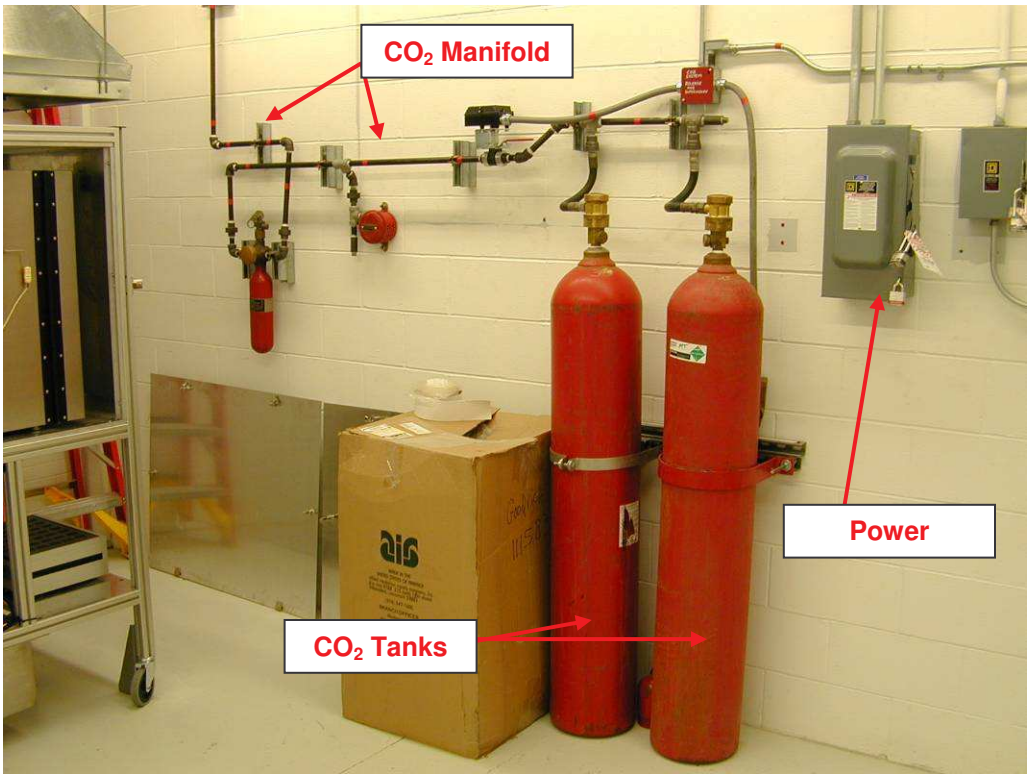

Figure 2.4: Coking Rig Room CO_2 Fire Suppression System

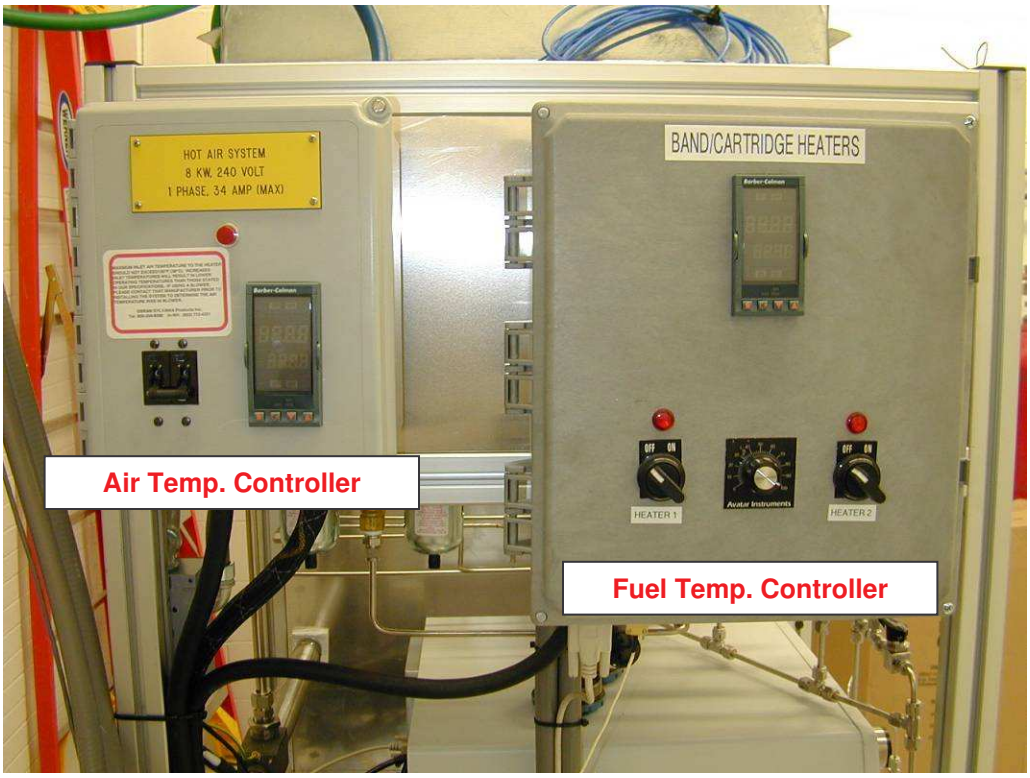

Figure 2.5: Fuel Heater Control Panel

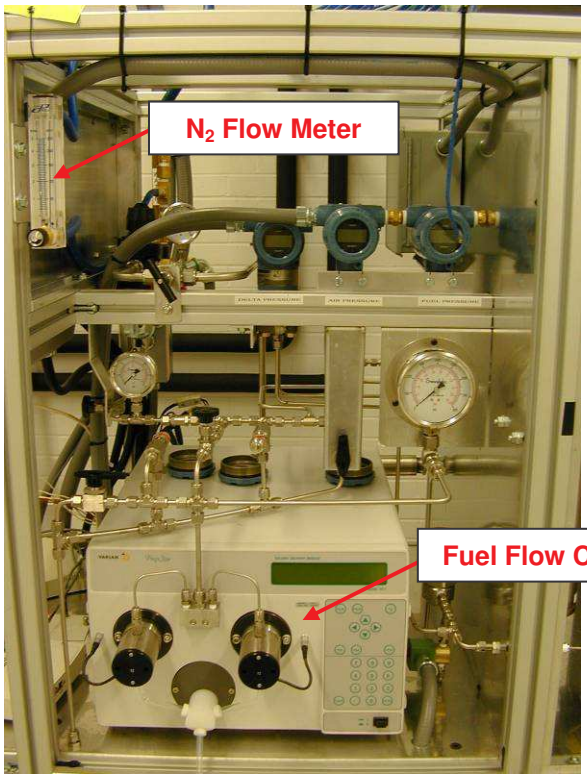

Figure 2.6: Coking Rig Fuel Controllers and Various Meters

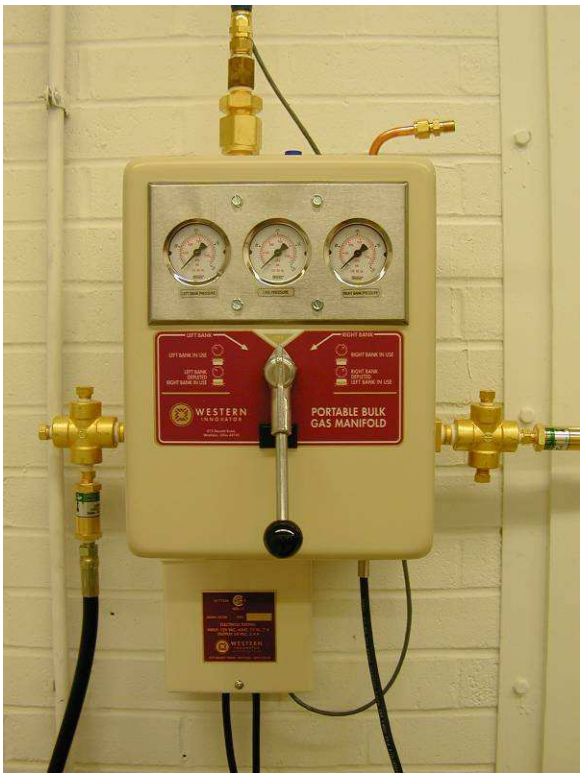

Figure 2.7: N_2 Oven Purge Manifold

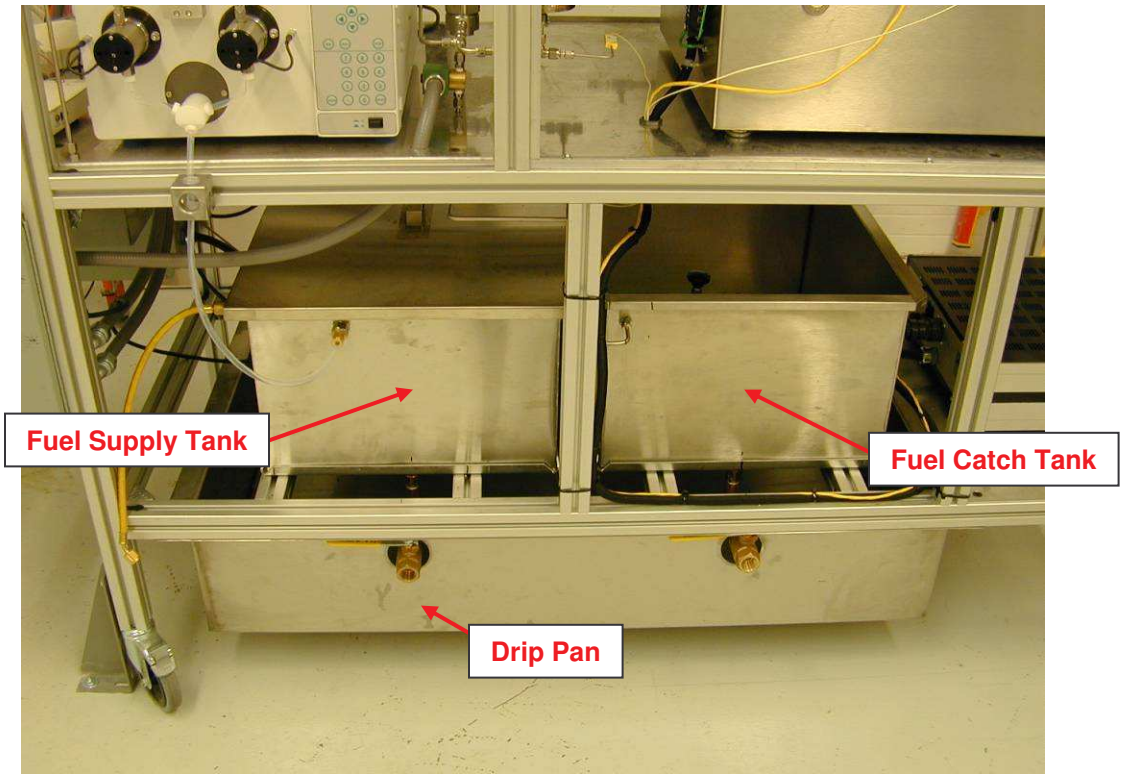

Figure 2.8: Liquid Fuel Supply and Return Tanks

Figure 2.9: Coking Rig Fire Door

The test rig shown in the previous figures is controlled by a laptop computer running the LabVIEW data acquisition software. This control program was the next sub task of Milestone 1.0. As a side note, task 1.2 was deleted from the requirements early on in the program and is not discussed in this report.

Task 1.3 Modify LabVIEW Data Acquisition Software for Anti Carbon Coating Testing.

This LabVIEW coking rig control program was written and used extensively throughout the carbon formation testing. Figure 2.10 through 2.12 show the graphical user interface of the program. Figure 2.10 shows how the fuel flow rate, fuel temp, oven temp, N_2 oven purge and N_2 fuel purge is tracked and monitored. This data is monitored for the entire test cycle. Figure 2.11 shows other monitored data such as fuel pressure, fuel temperature (before and after entrance to oven test specimens), and fuel temperature after waste heat exchanger. Figure 2.12 is the emergency shut down panel. This control panel activates the emergency shut down procedures in order to mitigate risk to equipment and personnel.

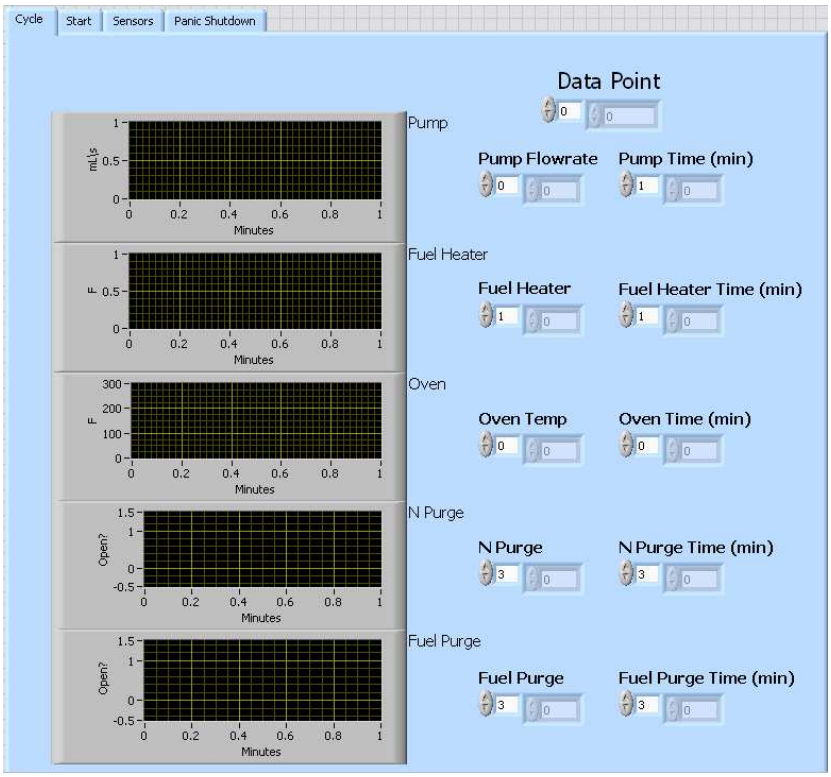

Figure 2.10: LabVIEW Control Program Front Panel

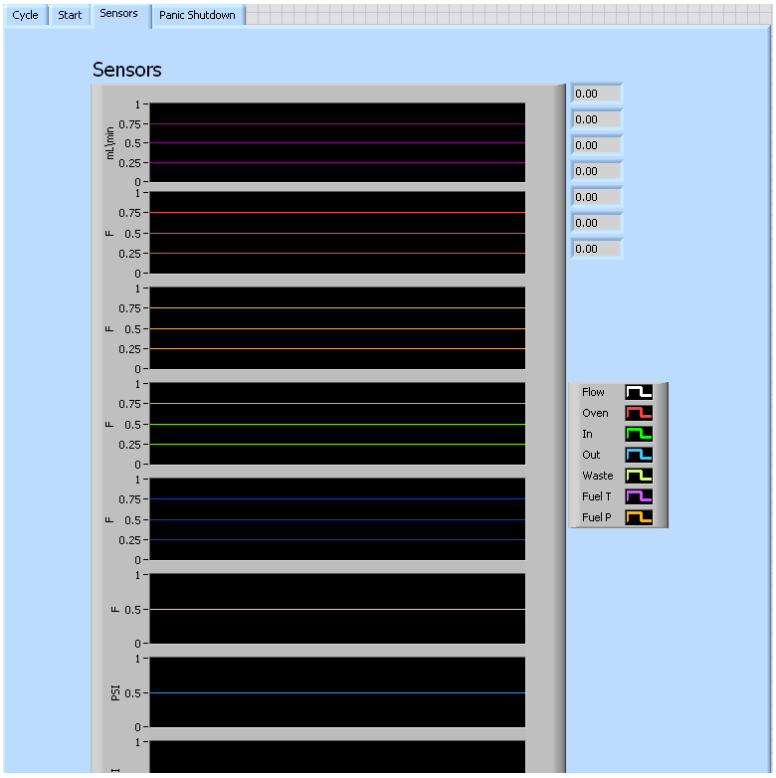

Figure 2.11: LabVIEW Control Program Sensors Panel

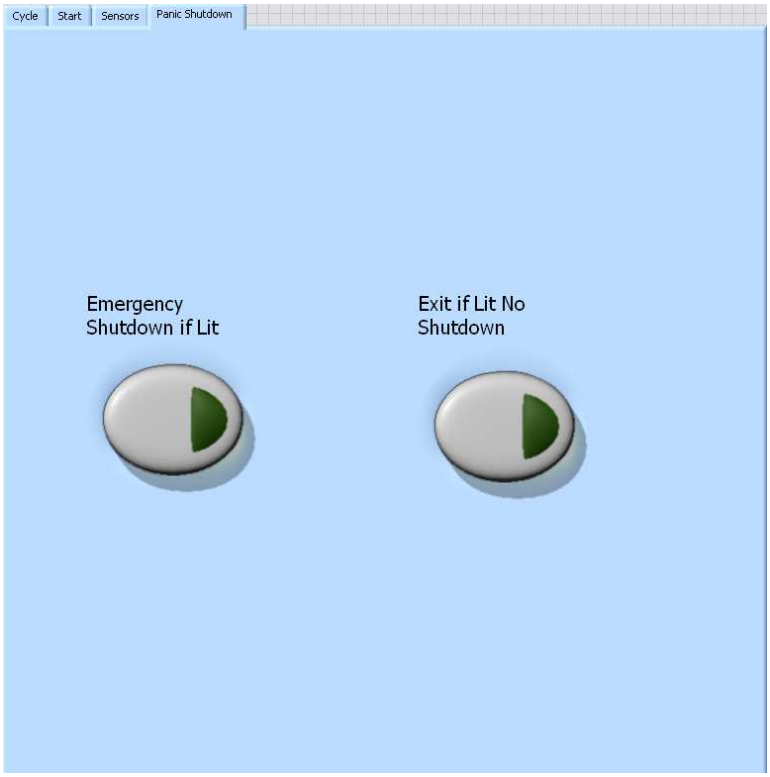

Figure 2.12: LabVIEW Control Program Emergency Shut Down Panel

The final subtask required for Milestone 1.0 was to calibrate the rig and perform a safety check.

Task 1.4 Perform Test Rig Calibration and Safety Check.

A safety review and check was conducted for the test rig to ensure compliance with all safety requirements. Safety is of utmost concern when dealing with pressurized fuel in a high temperature environment. Several safety rig tests were performed.

One test performed was the oven leak test. It is critical that oxygen be purged from the oven during heated testing. The concern is if one of the test specimens were to leak during a heated test, a fire could occur if oxygen is present in the test chamber. To minimize this risk the oven test chamber is constantly purged with nitrogen. To ensure the oven chamber is positively purged with Nitrogen, a leak test was developed and performed. During this test the chamber was positively charged with Freon (<1psi). A Freon detection device is utilized to determine the leak points. A major finding of the first test was that no Freon was detected at the point where the motor shaft, powering the fan, enters the oven. This point was expected to be a large leakage point. It was determined that the spinning fan (connected to the shaft) created a low pressure zone which drew air into the chamber even when the chamber was positively pressurized. A manifold was designed and installed around the shaft which displaced the air being drawn into the oven with nitrogen. This modification ensures that no air (oxygen) is brought into the chamber during the specimen testing. A second leak test was performed with positive results.

The oven leak test showed where oven leakage points occurred. These points were used to measure hydrocarbons in case of a fuel leak. A Hydrocarbon sensor was installed and tied into the LabVIEW software as well as the fire suppression system. This hydrocarbon sensor was mounted to the exhaust hood. The idea is, if a leak occurs, hydrocarbons will be instantly released into the chamber. These hydrocarbons will then leak out of the positively N_2 purged oven chamber. If the hydrocarbon sensor detects a certain level of hydrocarbons, the rig will immediately shut down and perform a nitrogen purge of the fuel lines. In this way, all fire risks will be minimized.

During operation the oven is purged with ~1 cfm of nitrogen. In addition, fuel lines are designed to incorporate a nitrogen purge system. The nitrogen gas is supplied by two tanks of liquid nitrogen connected via a manifold. This allows for replacement of the nitrogen tanks during an actual test (test shut down will not be needed). Figure 2.7 shows this N_2 manifold system.

This completes all the requirements for Milestone 1.0. This work was completed during the first quarter of the project. As a side note, the original Task 1.2 was deleted after negotiations between Engine Components and NETL. Task 1.2 was deleted because it potentially caused ownership concerns over the coking test rig. The coke formation test rig remains property of Engine Components.

3.0 Milestone 2.0: Anti-Carbon Coating Investigation and Endurance Tests

Milestone 2.0 is a follow on to the work performed in Milestone 1.0. Milestone 1.0 created the test rig for testing Anti-Carbon formation coatings. Milestone 2.0 is the actual testing of these coatings. As previously noted, Solid Oxide Fuel Cells and fuel reformers require high air fuel mixture temperatures. These temperatures are often well above the carbon or coke formation point of Diesel fuels. Also, a promising injection technology for fuel reformer applications utilizes preheated fuel for improved atomization and evaporation. For these reasons, it was proposed that testing was needed to determine which of the many anti-carbon formation coatings would work best in diesel fuel cell applications. This section summarizes the results of the anti-carbon coatings that were investigated.

Milestone 2 work began during the first quarter and was not fully completed until the final quarter of the project. The first sub task that was completed (during the second quarter) was:

Task 2.1 Identify Potential Coating Candidates and Application Methods

Six different coatings were selected for rig testing. The six selected anti-coating candidates can be seen in Table 3.1. Table 3.1 gives the coating vender, coating type, and application technique. Each coating specimen was given a dash number for ease of tracking and data collection. All of the following Figures and Tables reference this dash number. This table closes out subtask 2.1.

Coating Vendor	Coating Type	Application Technique	Dash #
AMCX	Inertium	Diffusion Bonded	-1A
AMCX	AMC26	Diffusion Bonded	-1B
Restek	Silcosteel AC	Chemical Vapor Deposition	-2
Chromalloy AZ	Aluminide	Chemical Vapor Deposition	-3
Advanced Polymer Solutions	Silicone Base Polymer	Molecular Bonding	-4
Danfoss Tantalum Technologies	Tantalum	Chemical Vapor Deposition	-5
Baseline	No Coating	N/A	N/A

Table 3.1: Coating Candidates Identified.

The next subtask completed was:

Task 2.2 Prepare Coking Test Hardware and Coating Specimens

Figure 3.1 shows the layout of the test specimen. All test specimens were machined from 347 stainless steel bar stock. All the interior surfaces were coated with the anti-carbon coating. Five of these specimens were obtained for each type of coating. The fuel flow thru this specimen is from left to right during the tests. The test specimen rod (shown in Figure 3.1) is designed to be removable; this allows measurements to be taken along the rod to determine the carbon formation rate. As the carbon builds on the test specimen rod the rod diameter increases.

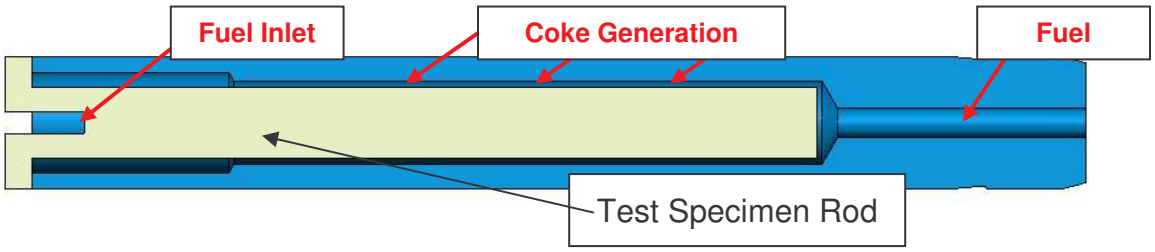

Figure 3.1: Coking Rig Test Specimen

The receipt of these test specimens closed subtask 2.2. The next subtask worked and completed was:

Task 2.3 Devise Test Matrix and Test Conditions

Engine Components devised a test matrix for the first stage coke build up testing. The first stage evaluated the following variables: Oven Temp, Fuel Preheat Temp, and Coating. The test was devised utilizing a Box-Behnken response surface statistical design of experiment (SDE). This Box-Behnken test layout out requires 4 tests with the all coatings (6 coatings plus baseline) tested during each of the 4 tests. The purpose of the first stage was to determine which coatings should be used for future endurance testing. The high, medium, and low levels

were chosen as the variables for each test. Owing to test stand capabilities, a single fuel flow rate was chosen. The test stand could only produce fuel flow rates in the laminar Reynolds number region. Higher Reynolds number testing may be possible if fewer specimens are utilized per test.

Table 3.2 shows the SDE test matrix and test conditions. As shown, the fuel and oven temperature were tested at two different conditions, producing a total of four test conditions. The fuel flow rate was kept the same for each specimen. It was originally planned that each test would be 30 hours in duration. After the first SDE test, it was decided that 19.2 hours was sufficient to generate measurable carbon formation rates (see next section for more details). Eight test specimens were tested simultaneously during each of the four tests. Six of the eight specimens had anti-carbon coatings applied while the two remaining were uncoated specimens (see table 3.1). These two uncoated specimens acted as baselines for comparison. Figure 3.2 shows the eight test specimens installed in a single manifold inside the test oven. Each specimen was calibrated to the same flow rate at 25 psi in order to balance the flow rate through each test specimen. In this way the tests are not biased to one specimen.

Test Number	Fuel Temp (°F)	Oven Temp (°F)	Fuel Flow (pph)	Time (Hr)
1	300	800	6.0	19.2
2	300	900	6.0	19.2
3	350	900	6.0	19.2
4	350	800	6.0	19.2

Table 3.2: Devised Test Matrix and Test Conditions

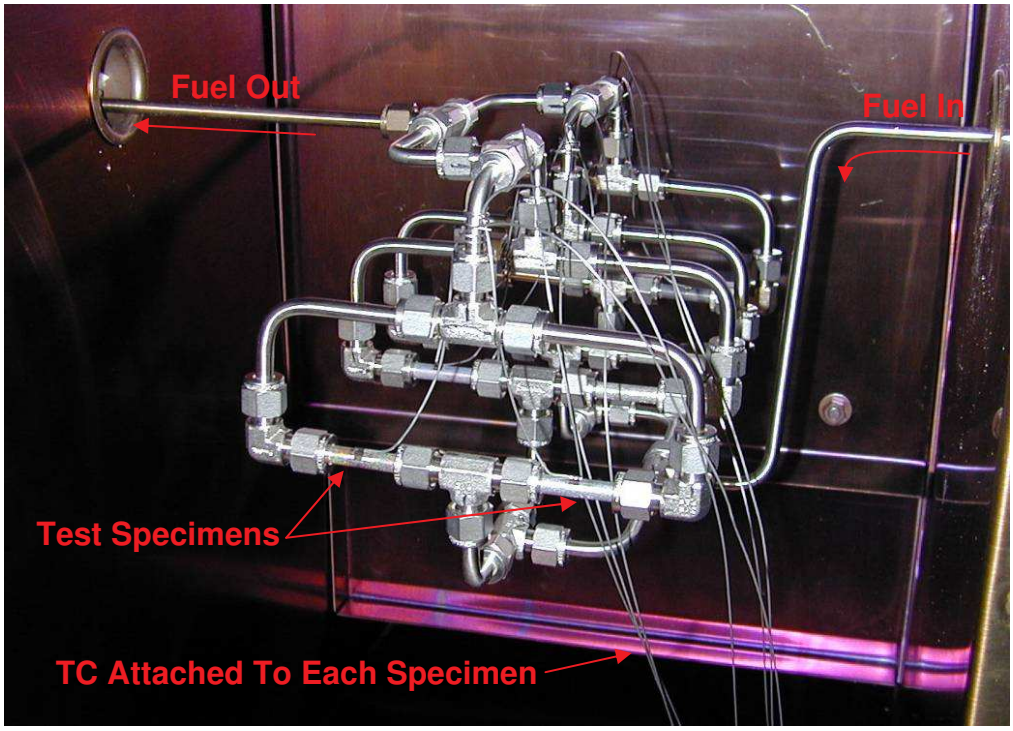

Figure 3.2: Test Specimens Installed In The Test Oven.

This work closed subtask 2.3. It was originally desired that the devised test matrix for coke build-up testing should include fuel velocity as a variable in the test. This was not possible because the system's fuel pump capacity was insufficient for producing the mass flow rates required to achieve desired fuel velocities. Thus, a single fuel flow rate (i.e. velocity) was chosen for the SDE testing.

The next two subtasks completed during this project were:

Task 2.4 Run Coking Tests Using Tube Specimens
Task 2.5 Analyze Test Results and Down-Select the Best Anti-Carbon Coating

Figures 3.3 & 3.4 show some of the typical data collected during the first two SDE Tests (See Table 3.2 for all SDE tests planned). Both tests showed a small glitch in the data collection during the test (6 hour point on test 1 and the 2 hour point on test 2). The potential source of this error was identified as the fuel temperature controller which was refurbished by the manufacturer.

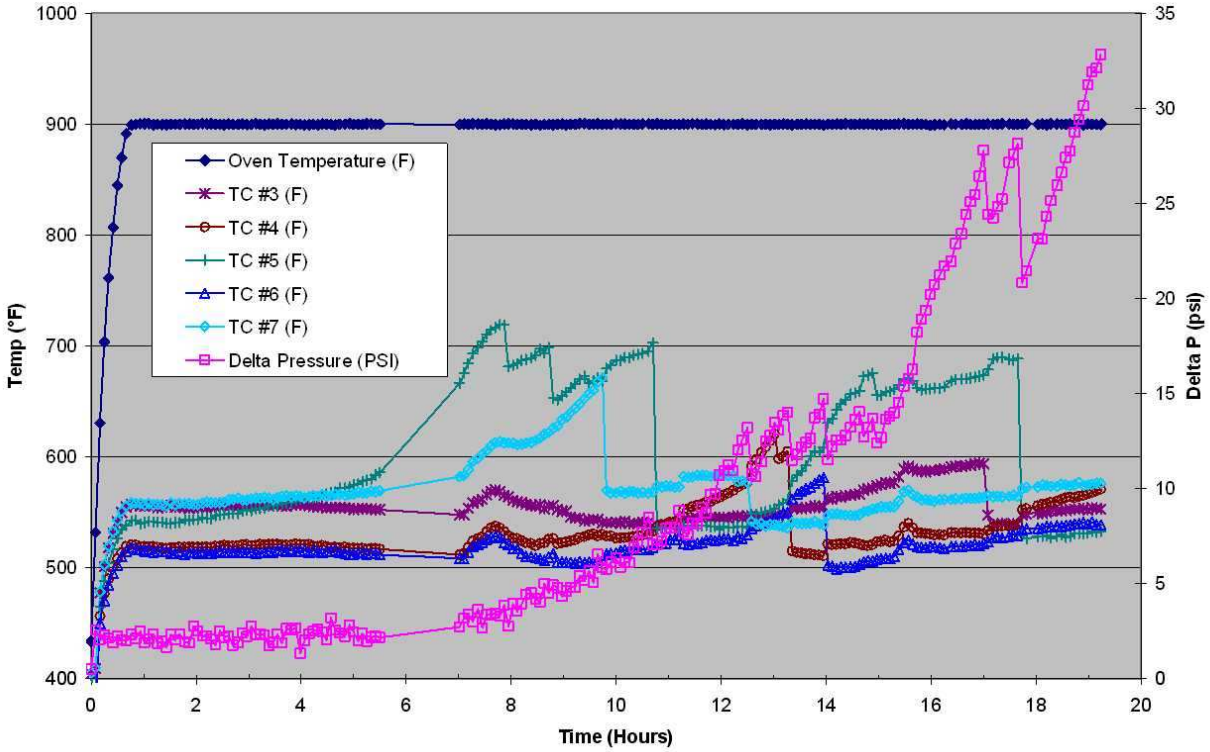

Figure 3.3: SDE Test 1 Data Collection

An interesting point to note is the wall temperature of each specimen. Each specimen has a thermocouple (TC) attached to the outside wall. This TC monitors the outside wall temperature of the test specimen. Test 1 shows that the temperature difference (delta T) between each specimen is around 50°F once the oven reached operation temperature. Test 2 shows about an 80°F delta. This delta T was significant cause for concern because it was suspected that wall temp is likely to have a significant effect on carbon formation rate. It was desired that each specimen should have approximately the same initial wall temperature. It was then expected

that this wall temperature would increase with time as carbon formed (acting as insulation) in the test specimen. This increase over time is readily apparent in both Test 1 and Test 2. This large variation is discussed in more detail later on in this section.

An important item to note during Test 1 is the increase in fuel manifold pressure drop (delta P). The original plan was to run the test for 30 hours. However, since the manifold delta P increased above 30 psi, the test was terminated early (~19.25 hrs). This increase in pressure was caused by carbon formation in the test specimens. It was decided to conduct all future tests for this 19.25 hr test duration.

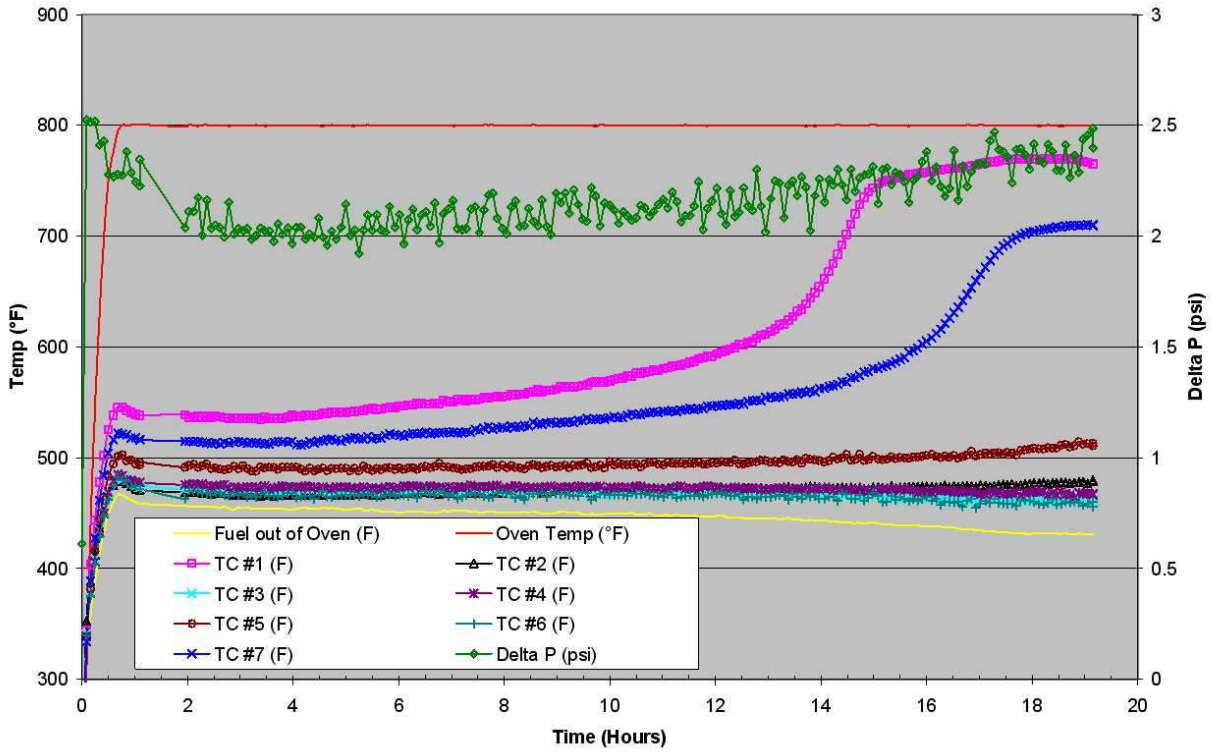

Figure 3.4: SDE Test 2 Data Collection

Coke formation rates from SDE Test 1 and 2 are shown in Table 3.3 and Table 3.4. The carbon formation rates are calculated by measuring the coke thickness on the Test Specimen Rod. The thickness of the carbon is then converted to a formation rate by dividing by the test time. Test 1 shows that anti-carbon formation coating -3 and -4 had the lowest carbon formation rates. However, Test 2 showed that the -2 coating and an uncoated baseline specimen had the lowest carbon formation rate. This uncertainty was attributed to the large variation in initial steady state wall temperature between each test specimen.

	Rate (µm/hr)	TC
-1A	8.43	1
-1B	7.30	7
-2	5.96	2
-3	2.61	3
-4	1.96	6
-5	3.36	4
Baseline (no TC)	7.58	N/A
Baseline (TC)	6.45	5

Table 3.3: Results of SDE Test 1 and TC Numbering.

	Rate (µm/hr)	TC
-1A	0.63	3
-1B	0.63	6
-2	0.00	4
-3	0.69	1
-4	2.34	7
-5	0.89	5
Baseline (no TC)	0.23	N/A
Baseline (TC)	0.69	2

Table 3.4: Results of SDE Test 2 and TC Numbering.

Figure 3.5 is a photograph of typical carbon formation. It shows the carbon that was being deposited (building-up) on the Test Specimen Rod. The carbon formation rates were calculated based upon the thickness of this carbon. Some specimens showed much thicker carbon than Figure 3.5. However, Figure 3.5 is a good representation of the carbon appearance.

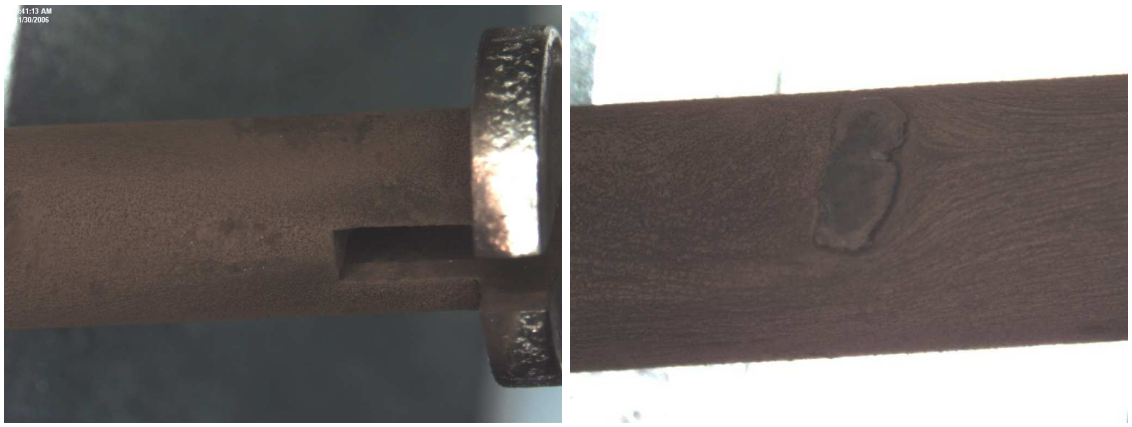

Figure 3.5: Typical Carbon Deposits On The Test Specimen Rod

The first two tests just discussed (of the four test SDE) were completed during Oct - Dec 2006. As previously discussed, it was discovered during the month of December 2006 that there was a large temperature variation between test specimens (wall temperatures). During the SDE Test 2, a greater than 80° F temperature difference was seen between test specimens. This

delta was apparent as soon as steady state was reached (steady state is when the oven and fuel reach desired temperature levels).

To identify the potential source of this large temperature delta, two tests were performed. The first test was to measure the temperature delta inside the oven. Since the oven is a high temperature convection oven it was reasoned that a large temperature delta could exist in the oven depending on the air recirculation zones. The fuel manifold was installed into the oven with TC's attached. However, instead of the TC's being attached to the test specimen wall, the TC was positioned adjacent to the specimen (fuel was not flowing during this test). In this way the air temperature near the specimen would be measured. The oven was then heated to 800° F. Figure 3.6 shows the results of this test.

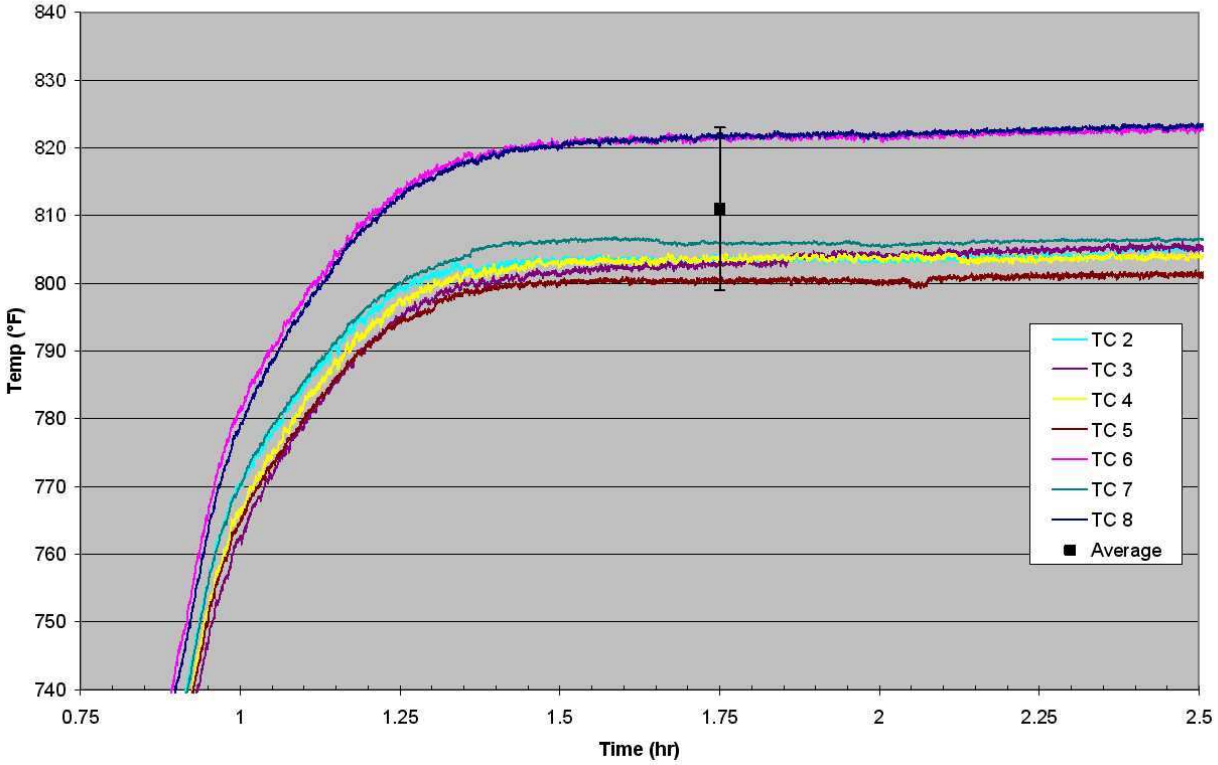

Figure 3.6: Oven Temperature Variation Results.

As seen from Figure 3.6, the average temperature in the oven was 810° F, with the max temperature of 822° F, and a min temperature of 802° F. This shows a variation of approximately 20°F. This is not as large as the 80° detected during SDE test 2 and did not completely explain the problem. Figure 3.7 shows where the TC's were located in the oven. Referencing Figure 3.6 and 3.7 one is able to determine that the highest temp TC's were located near the front of the oven, whereas the lowest temp TC's were located toward the center of the oven. What was possibly occurring is a large recirculation zone setup in the oven by the air circulation fan. The heated air is forced along the bottom of the oven and then upward when it reaches the oven door. The air is forced backwards once it reaches the oven top until being deflected downwards at the oven back and delivered into the blower intake. The upward traveling air would come in contact with the TC's near the door. This may explain why

the TC's in the center of the oven were a little cooler. They are not exposed to this air convection. In order to minimize this effect, a baffle was built and installed around the test manifold. It was concluded that the temperature delta in the oven may be negligible for the anti-carbon coating testing. It was reasoned that if the temperature delta could be kept below ±15° it should not affect the results of the anti-carbon coating test.

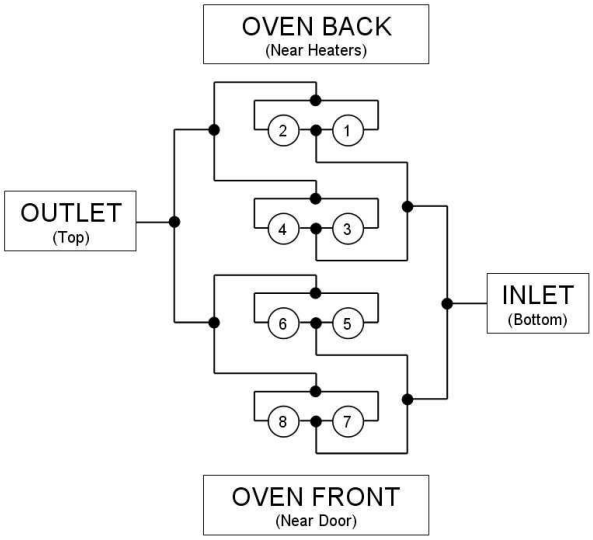

Figure 3.7: TC Location On Manifold

The second test to identify the potential source of the large temperature delta was to check flow rate of the test specimen manifold. It was reasoned that large variations in fuel flow through each specimen could lead to temperature variations during the test. The temperature of the fuel is much lower than the temperature of the oven. If more fuel passed through one specimen versus another, it could significantly impact specimen temperature. Figure 3.8 shows the results of the one of these manifold tests.

As seen from Figure 3.8, there is large flow rate variability between each specimen. This test was accomplished in an ambient environment by flowing 80 pph thru the manifold and catching the fuel flow in separate beakers as the fuel exited each specimen. These beakers were then weighed and compared to each other. It is important to note that the specimens were all calibrated to the same flow rate before this test. As seen from Figure 3.8 the max flow rate is around 11 pph whereas the min is near 5 pph. This is a significant variation and was deemed the root cause of the temperature variation problem.

The first attempt to solve this problem was to change the location of each test sample. Figure 3.9 shows the results of this test. As shown a slight improvement was measured. However, the standard deviation between the flow rates was still high enough to cause concerns. Just changing specimen location was not a satisfactory solution.

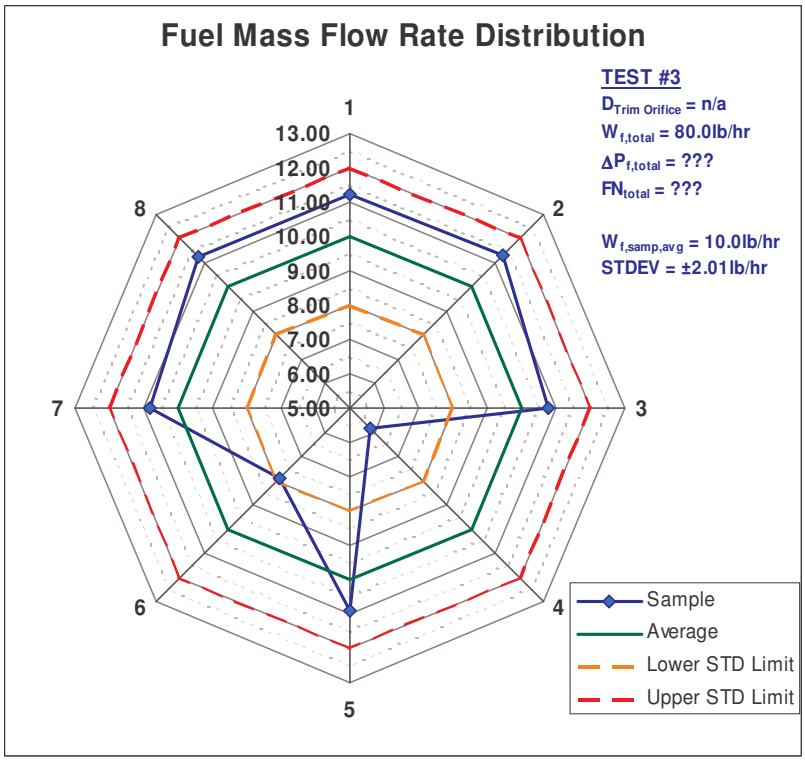

Figure 3.8: Manifold Fuel Flow Distribution Test #3

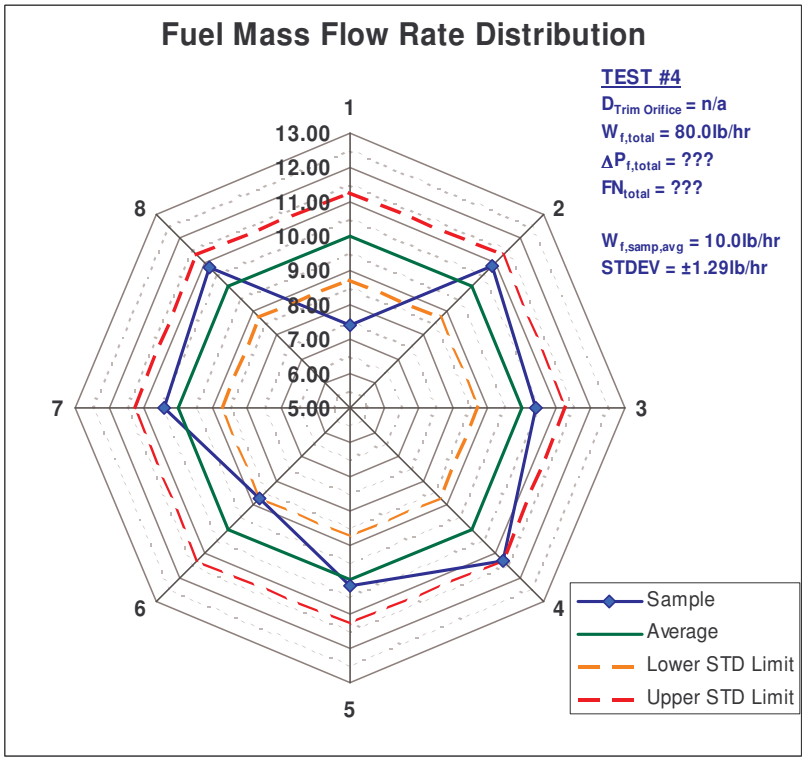

Figure 3.9: Manifold Fuel Flow Distribution Test #4

The next step in creating a uniform flow distribution was the addition of a trim orifice just upstream of each test specimen. The goal was to increase the pressure drop thru each specimen and thus minimize the non-uniform pressure drop thru the manifold. The new pressure drop thru the manifold was increased to 25 psi (was ~ 3 psi). Figure 3.10 and 3.11 show the results of this change. As seen in Figure 3.10 the flow rate distribution standard deviation decreased to approximately .18 pph (was > 1.5 pph). This was a major improvement on the flow distribution. Just to confirm this data was repeatable, the specimen locations where changed in the manifold and the test reran. As shown in Figure 3.11, the standard deviation was repeatable. With this testing completed the coking rig was ready for reassembly and SDE testing could resume.

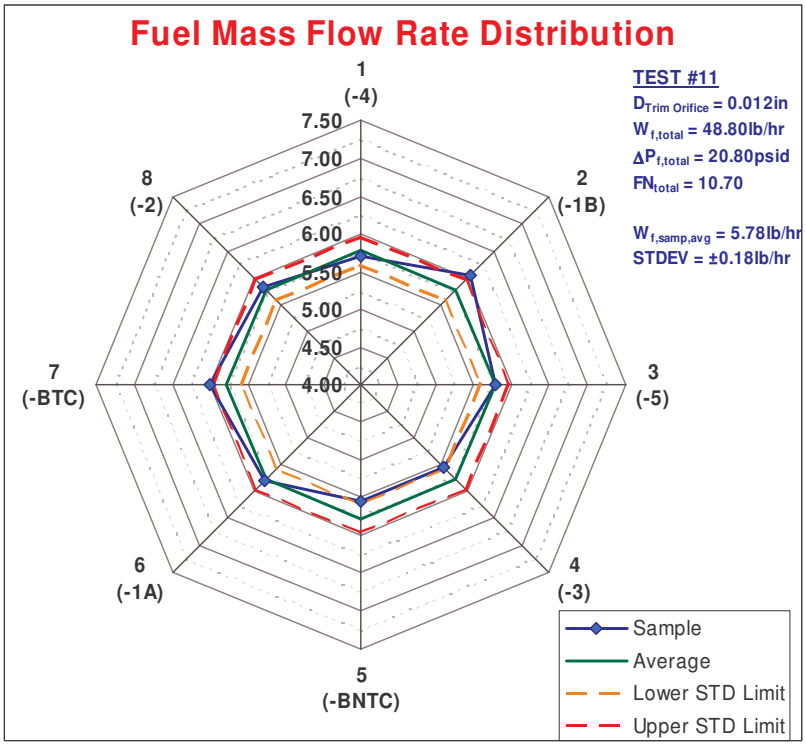

Figure 3.10: Manifold Fuel Flow Distribution Test #11

Test 3 and 4 of the four test Statistical Design of Experiment (SDE) were the next tests completed. Figure 3.12 shows the data collected during test 4 of the SDE (typical of data collected during each SDE test). Test 4 was performed in two steps. As seen from Figure 3.12 this portion of the test lasted approximately 17 hrs. The entire test duration was 45.5 hrs (two tests). The entire test length was longer than the desired 19.25 hours test duration set by test 1 of the SDE. The test was extended because the carbon formation rate of test 4 was significantly decreased. Table 3.5 shows the carbon formation rate of this test. It was expected that the average carbon formation rate of test 4 would be slightly greater than test two (above .23 µm/hr). However, after the first portion of testing it was apparent that the formation rate was almost 10 times less.

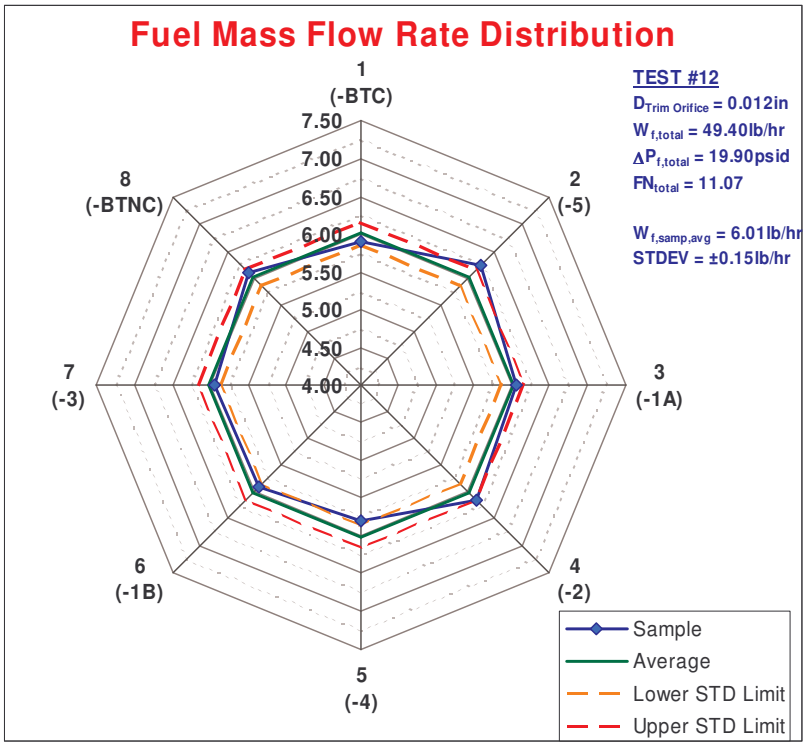

Figure 3.11: Manifold Fuel Flow Distribution Test #12

	Test Conditions			Carbon Growth Rate (µm/hr)						
Test #	Fuel Temp	Oven Temp	Fuel Flow	-1A	-1B	-2	-3	-4	-5	Baseline
2	300° F	800° F	6 pph	0.63	0.63	0	0.69	2.34	0.89	0.23
3	300° F	900° F	6 pph	0.4	0.56	0.38	0.56	0.63	0.23	0.37
1	350° F	900° F	6 pph	8.43	7.3	5.96	2.61	1.96	3.36	7.58
4	350° F	800° F	6 pph	0.02	0.05	0	0.04	0	0.05	0.102

Table 3.5: SDE Growth Rate Summary to Date[2&3]

A review of all four tests was completed to understand the possible reasons for such a large decrease in carbon formation rate. It was determined that the most likely candidate for this decrease in carbon formation rate was a change in diesel fuel. The fuel used for all four tests was Off Road Ultra Low Sulfur Diesel No. 2. However, test 1 thru 3 was fuel purchased from Barton Solvents (BARSOL). A vendor change was required and the diesel used in test 4 was purchased from Keck Oil. This change in vendors was thought to be a negligible change to the fuel. However, the change in carbon formation rate was far from negligible. A review of ASTM D975-07 suggests that there can be a large variation between fuels even though they are the same grade. For example, No. 2 fuel only needs to have a Ramsbottom carbon residue number of less than .35. The carbon residue (Ramsbottom number or Conradson number) of a petroleum product serves as an indication of the likelihood of that product to form thermal coke under the influence of heat. There are many other factors that can lead to thermal coke formation but the Ramsbottom number can be a general guide. Engine Components wanted to send each fuel out for testing to determine the actual Ramsbottom number. However, a

[2] Test #1 has increased uncertainty because of lessons learned during test 2 thru 4.
[3] Test #4 utilized a new batch of diesel fuel from a second vendor.

specimen of the fuel used in test 1 thru 3 was not retained. A specimen of the fuel used in test 4 was tested but unfortunately the results cannot be compared to the fuel used in tests 1 thru 3.

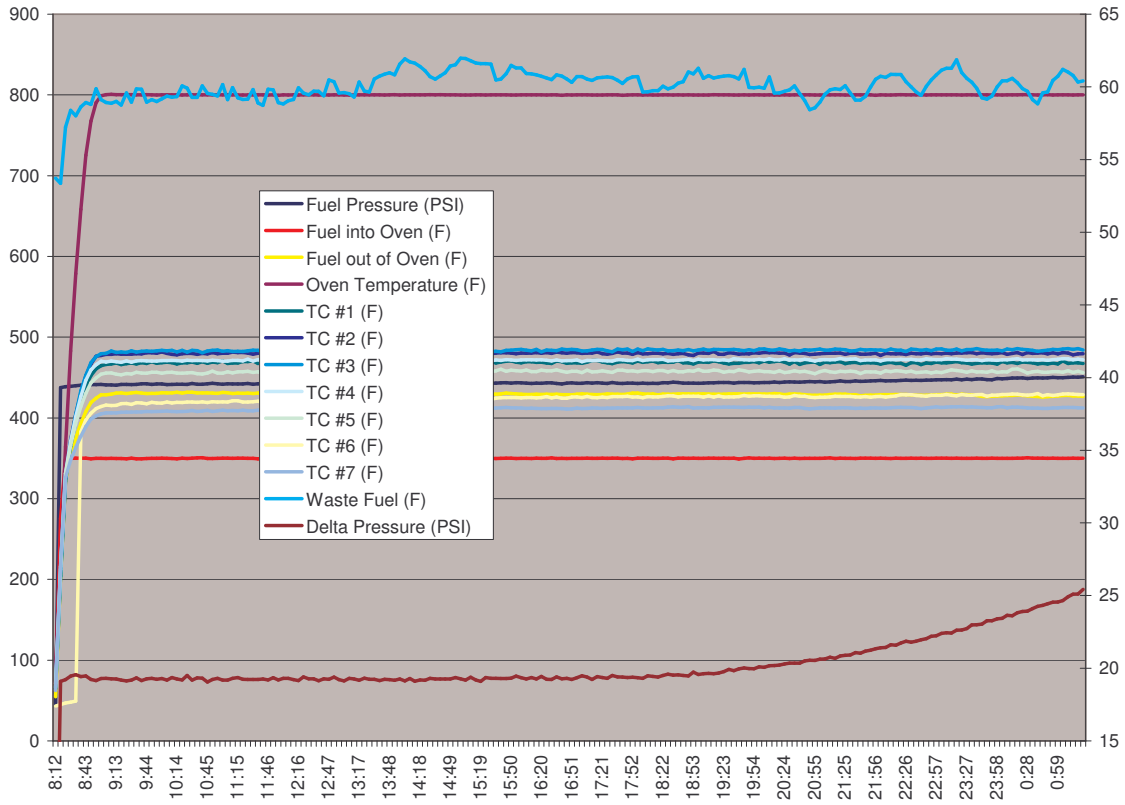

Figure 3.12: SDE Test 4 Data Collection

Despite the change in carbon formation rates, a comparison between anti carbon coating performance could still be made. Figure 3.13 shows the overall ranking of the coatings based upon the average of three ranking techniques. The first ranking technique was specimen weight change. The specimens were ranked 1 thru 7 based upon how much weight was gained during the test (1 being the best or least weight gain). The weight increase was attributed to the amount of carbon present on the test specimen. The second ranking technique was specimen width increase. The specimen width was measured prior to testing and after each test. The width increase was attributed to carbon formation. The third ranking was based upon visual observations. The carbon often formed in very uneven patterns. Thus, the visual technique was used to rank the specimens by which ones looked the cleanest and most carbon free.

Figure 3.13 shows the individual test rankings as single line curves. The overall ranking average is shown as a bar graph. Keep in mind that the lower the rank the better the coating performance. It is apparent that the data has large variations between each test, especially when comparing Test 1. Test 1 was completed before the oven specimen temperature was uniformly controlled and before a trim orifice was used to control the flow thru each specimen. Because of this, the Test 1 data is suspect of being inaccurate. Thus, an overall average is

shown in Figure 3.13 that doesn't include Test 1 (Salmon colored bar chart). As seen from Figure 3.13, coatings -1A and -2 stand out as the best performers. Coating -1A and -2 were down selected for the final specimen test. Coating -1B showed good results as well but did not stand out as much as -1A and -2. -1B was also chosen for the final back to back specimen test. Table 3.6 shows the conversion between dash numbers and actual coatings.

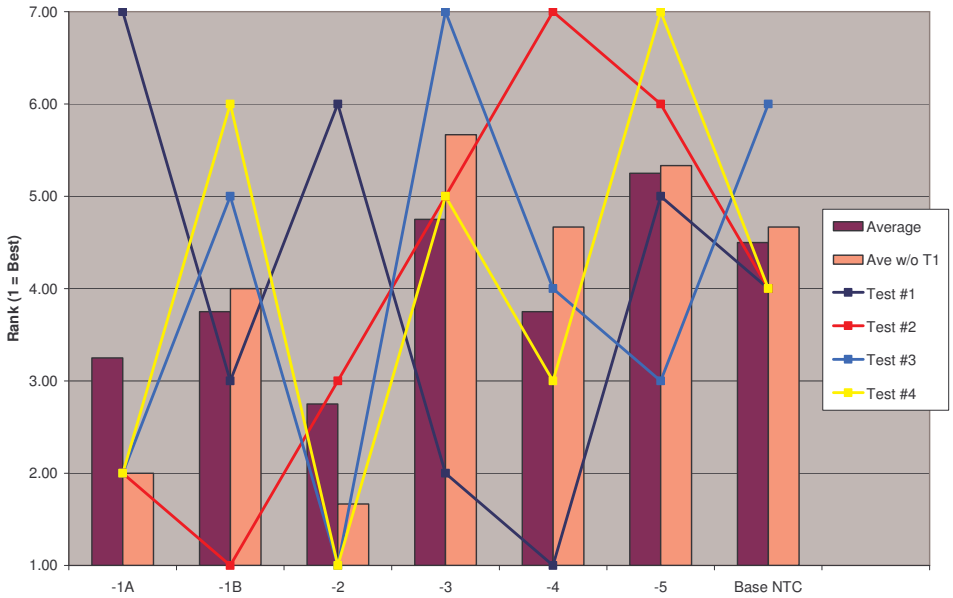

Figure 3.13: Overall Ranking of All Four Tests (Weight, Visual, & Width)

Dash #	Coating Vendor	Coating Type	Application Technique
-1A	AMCX	Inertium	Diffusion Bonded
-1B	AMCX	AMC26	Diffusion Bonded
-2	Restek	Silcosteel AC	Chemical Vapor Deposition

Table 3.6: Anti-Carbon Coating Down Selected For Final Testing.

After the down selection to these three coatings, the test specimens were sent out for a detailed scanning electron microscope (SEM) analysis. Figure 3.14 thru 3.17 show some of the results from this analysis. These figures show results from test 4. Test 4 had an 800°F oven temperature, a 350°F fuel preheat, and a 6 pph fuel flow rate per sample. Figure 3.14 shows the carbon build up on the Inertium coating. The picture was obtained by sectioning the sample after it had been encapsulated in epoxy. The carbon layer was about 3.75µm thick. Figure 3.15 shows the material maps of this same area. The material maps show the amount of carbon, silicon, chromium, iron, and nickel present in the sample area. The presence of carbon is the top left map in Figure 3.15. As expected the layer of material trapped between the metal sample and the epoxy had very high carbon content.

Figure 3.16 and 3.17 are the same type of images but of the Restek coated sample. The item to note in Figure 3.16 is very little carbon seems to be present. The epoxy did not bond to the Restek coating and pulled away during the sectioning and polishing process. This can be seen

by the gap between the coating and the epoxy. It appears from Figure 3.17 (map center top) that there is silicon present in the Restek coating. This is expected since the Restek coating is advertised as a silicon base coating. In summary, the SEM analysis suggests that the Restek coating demonstrated the most resilience to carbon formation and build up during the first four multiple sample anti-carbon coating tests. This SEM analysis was also completed on the final back-to-back testing mentioned above.

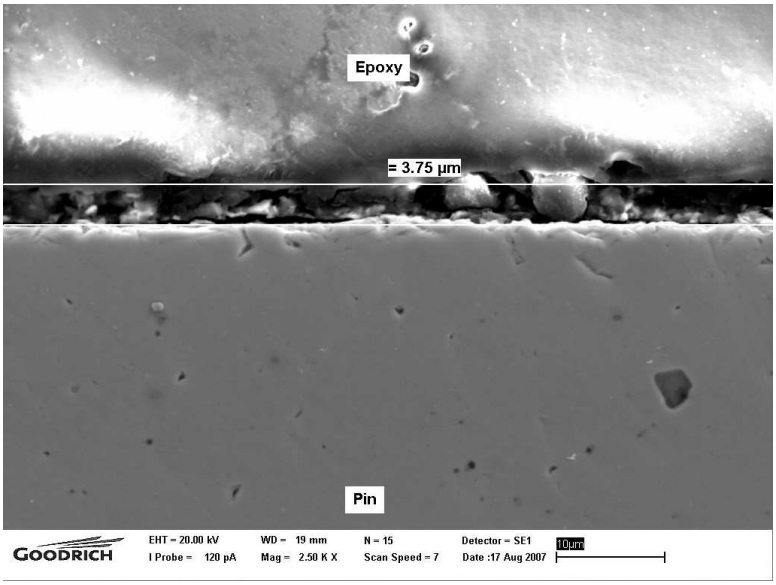

Figure 3.14: Carbon Formation on Inertium Coating (Test 4)

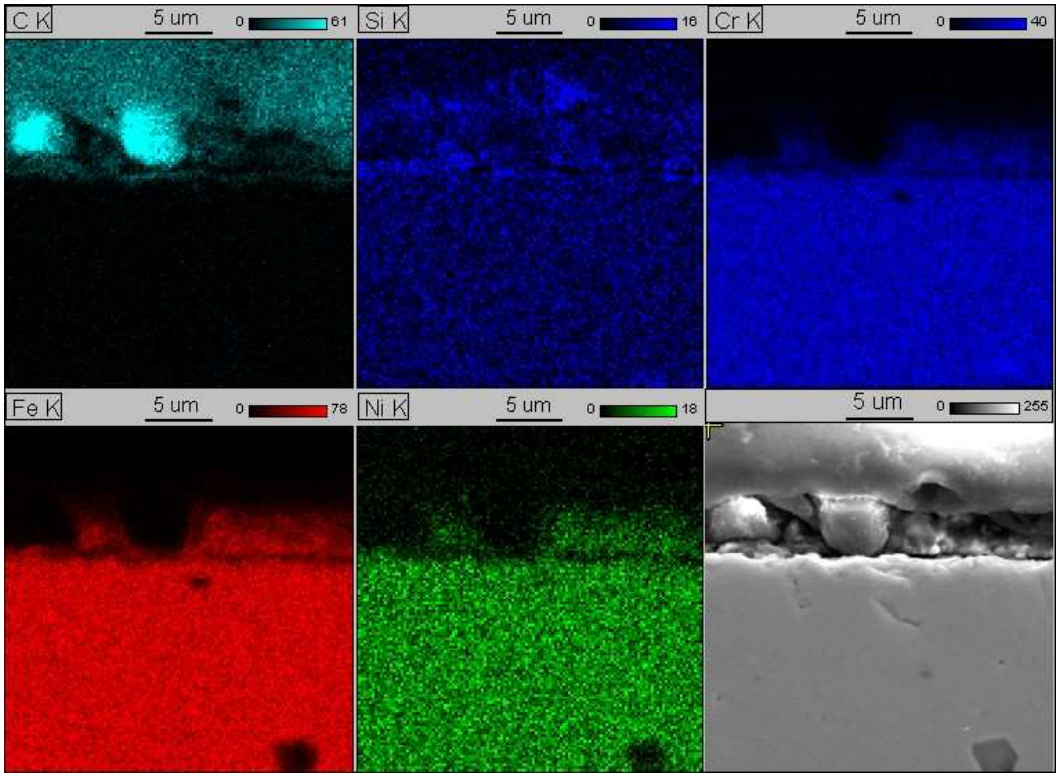

Figure 3.15: Material Maps on Inertium Coating (Test 4)

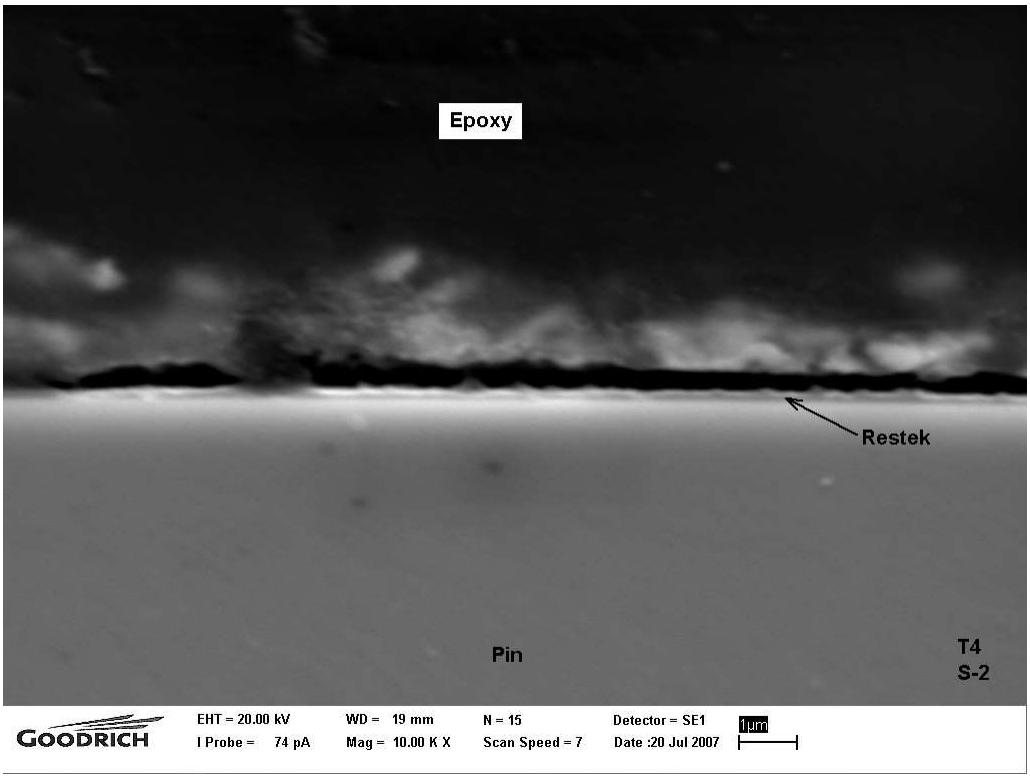

Figure 3.16: Lack of Carbon Formation on Restek Coating (Test 4)

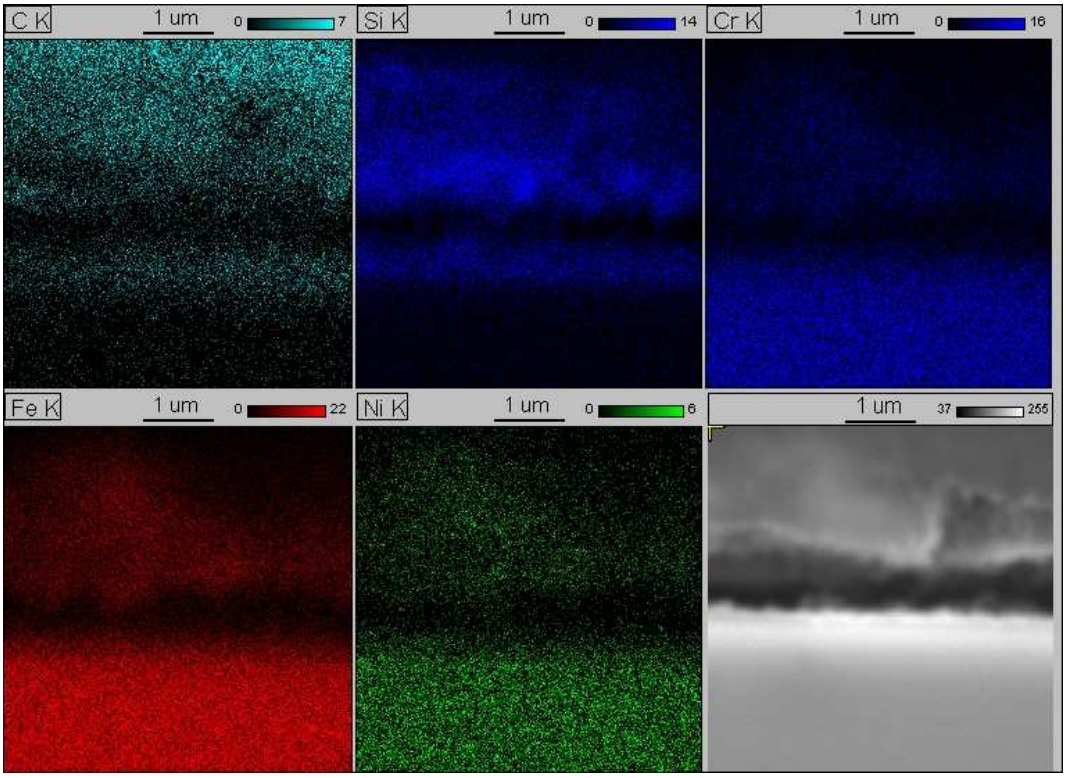

Figure 3.17: Material Maps on Restek Coating (Test 4)

The next subtask of Milestone 3.0 that was completed during this project was:

Task 2.6 Apply the Selected Coating to a Fuel Injector Cartridge

Four injector cartridge assemblies were created using 347 stainless steel material. Three of these cartridges had anti-carbon coatings applied and one remained an uncoated baseline. Figure 3.18 shows the model of this injector cartridge. It is modeled after the actual fuel injector cartridge that will be used in the preheating injector. There was a 3 to 4 week turn around for the coating application.

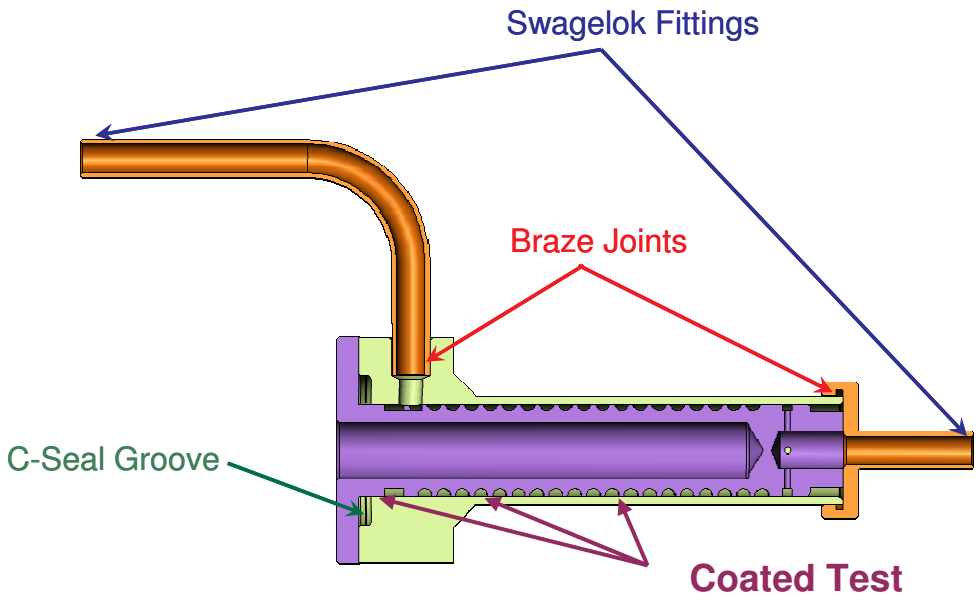

Figure 3.18: Final Nozzle Assembly for the Coking Rig Test

Figure 3.19 shows the four coated and uncoated test specimens (Restek, AMC26, Inertium, and an uncoated baseline). A small portion of each specimen was removed. This portion was used for coating comparison after the test was completed. It was anticipated that this before and after comparison would provide insight on any coating degradation and how carbon is forming on the specimen. It is interesting to note that the Restek and the Inertium coatings have a rainbow appearance. This change in color is used by the manufacturer to determine coating thickness.

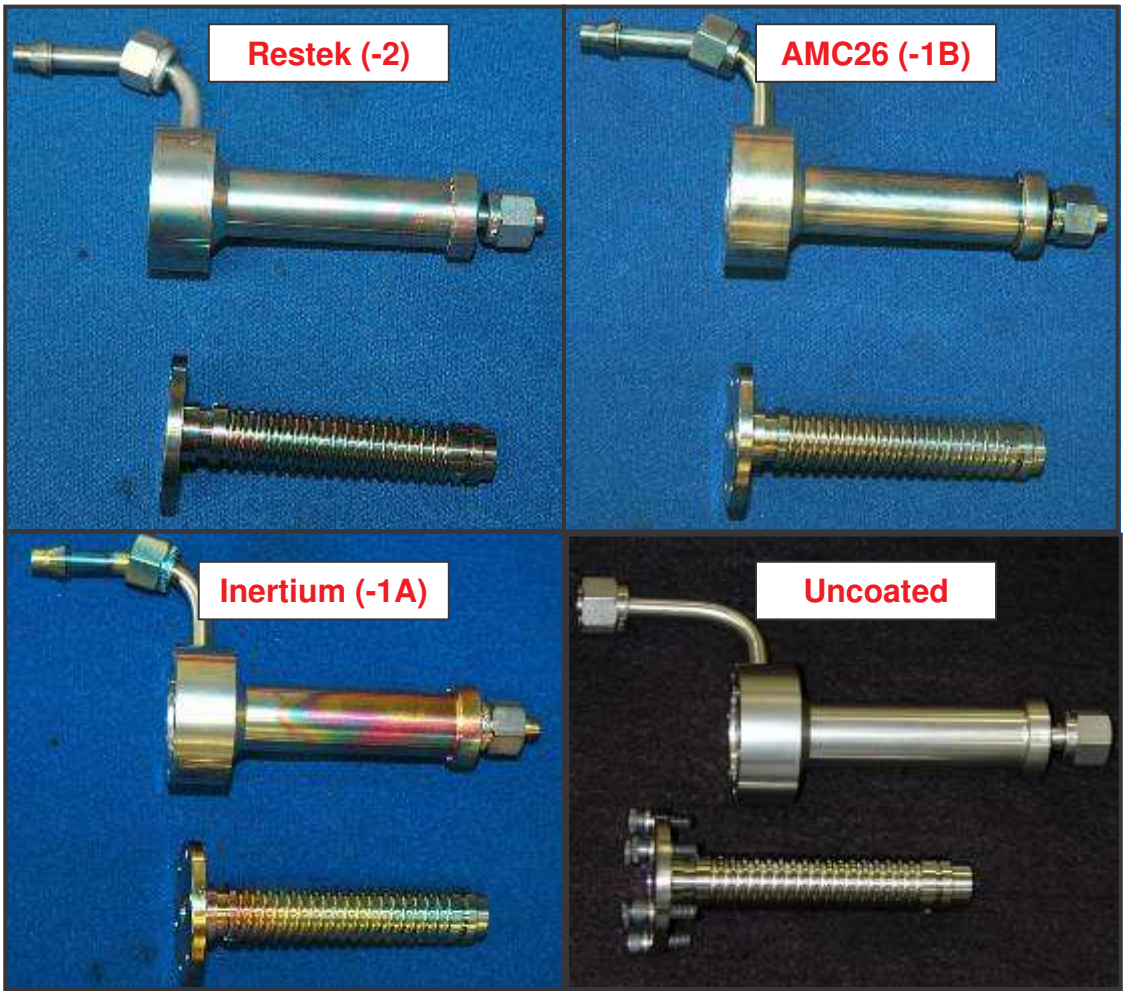

Figure 3.19: Anti-Carbon Coating Down Selected for Final Testing.

The next sub task of Milestone 2.0 completed was:

Task 2.7 Conduct Endurance Tests for a Back-to-Back Comparison Between a Coated and a Non-Coated Injector

Table 3.7 shows the original test conditions planned for this final test. Each specimen was to be tested at the same test condition. The oven was set at 900°F and the fuel flow rate was set at 6 pph. The fuel was to be heated above 400° F at the exit of the test specimen. Each specimen was to be tested separately in the test rig (i.e. “back-to-back”) in order to minimize uncertainties during the test due to inconsistent fuel flow rates and wall temperatures. This final set of tests began during the month of May.

The first specimen (uncoated baseline) completed the first 30 hours of a projected 50 hour test. The test was interrupted because of a thermocouple (TC) braze joint failure. The failure was on a TC that measured the temperature of the fuel exiting the test specimen. This joint is inside the oven. The failure allowed the TC to back out of position allowing fuel to spill directly into the 900°F oven. The oven is N_2 purged which minimized the risk of a fire. The smoke produced from this event was effectively vented, reducing the risk to equipment and personnel.

The rig was shut-down within 15 minutes of the failure with no damage to equipment or injuries to personnel.

	Test Conditions			Carbon Growth Rate (µm/hr)
Test #	Fuel Temp	Oven Temp	Fuel Flow	
Baseline	400° F	900° F	6 pph	
-1A	400° F	900° F	6 pph	
-1B	400° F	900° F	6 pph	
-2	400° F	900° F	6 pph	

Table 3.7: Final Anti-Carbon Coating Back to Back Test Plan

Several rig related operation items were learned from this event. For example, the hydrocarbon sensor on the test rig detected the fuel leak. However, this detection did not shut the rig down. Operator intervention was required to shut the rig down. This item was debugged, fixed, and tested for future rig operations. Other items were also corrected in the software and hardware to allow for a faster and more automatic rig shut down response. The rig was cleaned, tested, and was again readied for continued testing.

The braze joint on the TC that failed was critically reviewed. It was determined that the TC size and braze joint was not robust enough for the conditions inside the oven. The TC was replaced with a thicker sheath wall TC and the braze joint was replaced with a compression locked fitting. This type of joint reduces the likelihood of the TC backing out of joint. Should the joint leak, it would be at a significantly reduced fuel flow rate over a backed out TC. As seen in Figure 3.20, this redesigned joint was implemented into the rig and testing began again. In addition to the new sealing method, a thin metal shim was used as a strap and placed over the TC sheath and spot welded to the t-fitting in which the TC is inserted. This feature prevents the TC from completely backing out of the fitting in the event of a joint failure.

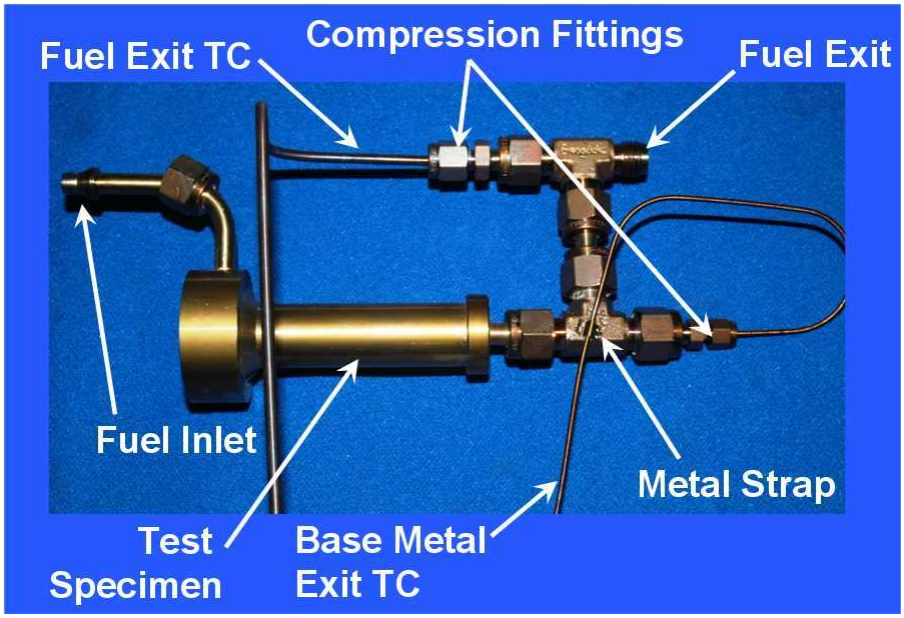

Figure 3.20: Test specimen set-up

Since the test stalled, this gave the opportunity to examine the test specimen for carbon growth. Figure 3.21 is a picture of the coiled fuel path insert at the 30 hour test point. As shown, very little carbon is present. There is a slight varnishing on the part but not the carbon growth desired. This fuel path insert was reassembled into the test piece and completed the 50 hour test. At the 50 hour point the test was again evaluated to determine if more time was required to grow carbon. It was determined that more time was needed so another 20 hours was added to the test with the fuel being preheated to 170° F.

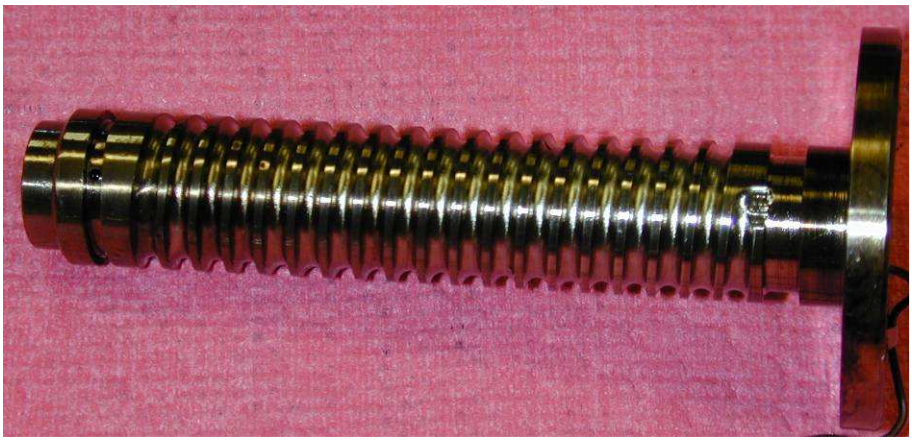

Figure 3.21: Fuel Path Insert at 30hrs of Testing.

At completion of the baseline specimen testing (70 hours of testing), the specimen appeared to have carbon growth. Based on the baseline test, the final test parameters for the remaining specimens were identified. As a summary, four test specimens (Restek, AMC26, Inertium, and an uncoated baseline) were tested in a final back-to-back test. The conditions of this test are:

Step 1: (50 hrs)
- 900°F Oven Temp
- Fuel at ~70°F (ambient no preheat)
- 6 pph Fuel Flow Rate
- 450 psi Fuel Back Pressure

Step 2: (20 hrs)
- 900°F Oven Temp
- Fuel preheated to 170°F
- 6 pph Fuel Flow Rate
- 450 psi Fuel Back Pressure

Figure 3.22 and Figure 3.23 show the fuel cartridge insert of the test specimen after the 70 hour test. Figure 3.22 shows the baseline specimen and Figure 3.23 shows the Restek coated specimen. As seen from Figure 3.22 and Figure 3.23, the heaviest carbon deposits are on the left side of the fuel cartridge. This is caused by the higher fuel and metal temperature on the left side of the fuel cartridge. The fuel temperature increases as it passes thru the helical passage of the fuel cartridge. The left side of the cartridge is near the test specimen exit and is the hottest part of the fuel cartridge (this carbon formation is shown and discussed in more detail later in this section). The circle shown in Figure 3.23 is the area that was examined close up for carbon deposits (see detailed pictures in Figures 3.24 thru 3.31).

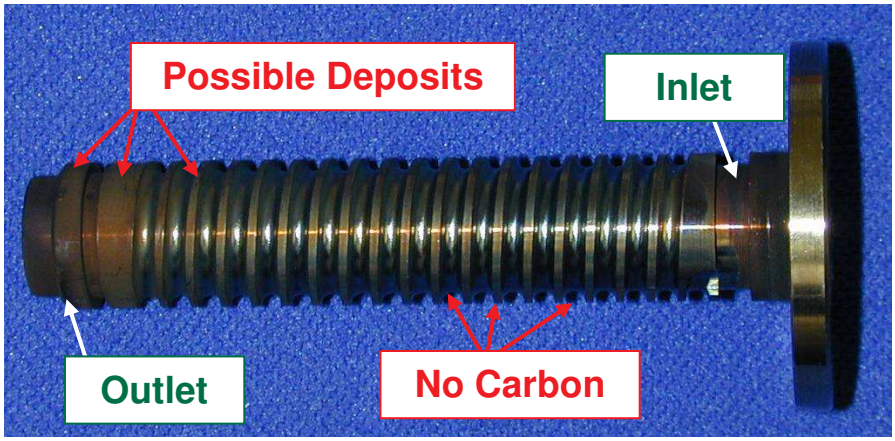

Figure 3.22: Baseline Fuel Cartridge Insert after 70 hrs of Testing.

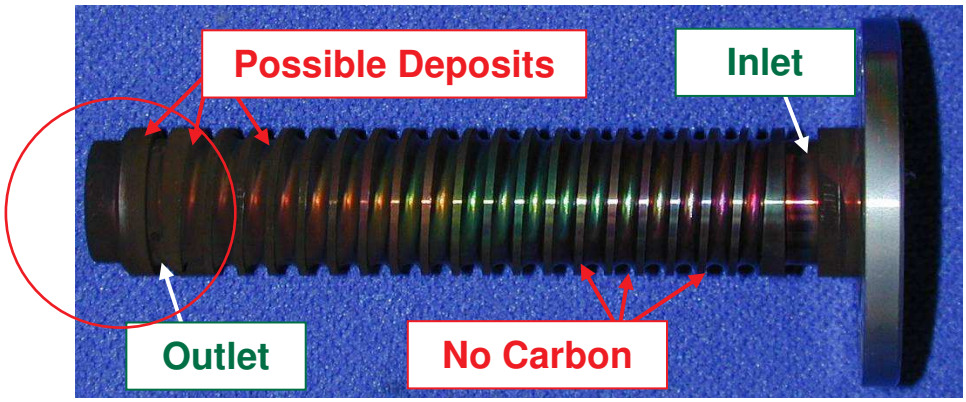

Figure 3.23: Restek Coated Fuel Cartridge Insert after 70 hrs of Testing.

Figures 3.24 and 3.25 show a close up of the Fuel Cartridge Insert of the baseline test specimen after the 70 hour test. As seen the material deposits or material discoloration is just beginning to occur on the baseline test specimen. This discoloration was a little less than desired but thought to be enough to show the differences between possible carbon formation rates between each specimen. The carbon formation rates are discussed in more detail later on in this section when the SEM analysis is presented.

Figures 3.26 and 3.27 show a close up of the Fuel Cartridge Insert of the Silcosteel AC specimen after the 70 hr test. Although the results had not been quantified, it was apparent that the discoloration did not improve compared to the baseline specimen. There is clearly more discoloration on this specimen than on the baseline.

Figures 3.28 and 3.29 show a close up of the Fuel Cartridge Insert of the Inertium coated specimen after the 70 hr test. Although the results had not been quantified, it was apparent that the discoloration did improve compared to the baseline specimen. There were clearly less deposits formed on this specimen than on the baseline. The rainbow pattern from the coating was still apparent through the possible carbon formation or discoloration.

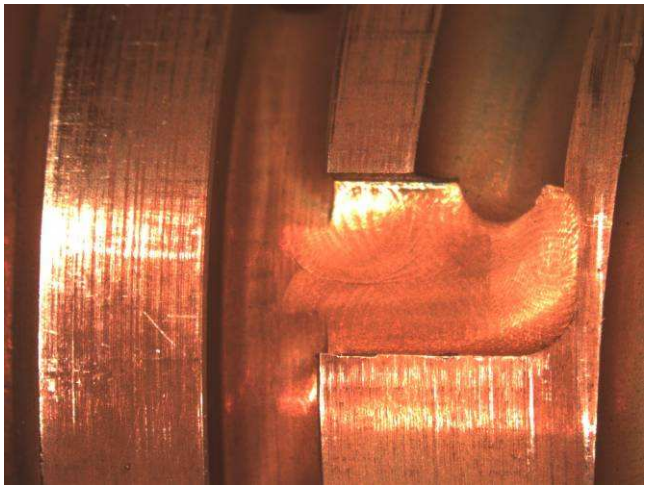

Figure 3.24: Close Up of Baseline Uncoated Test Specimen

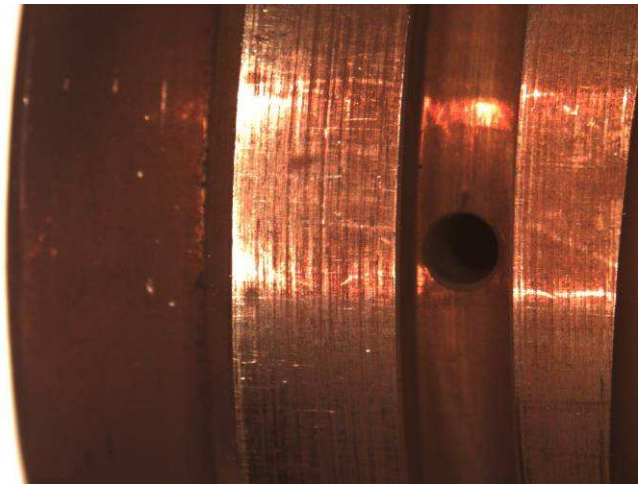

Figure 3.25: Another Close Up of Baseline Uncoated Test Specimen.

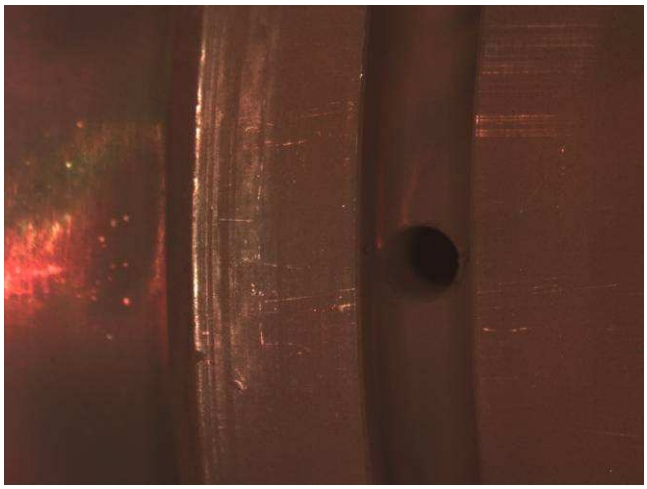

Figure 3.26: Close Up of the Silcosteel AC Coated Test Specimen

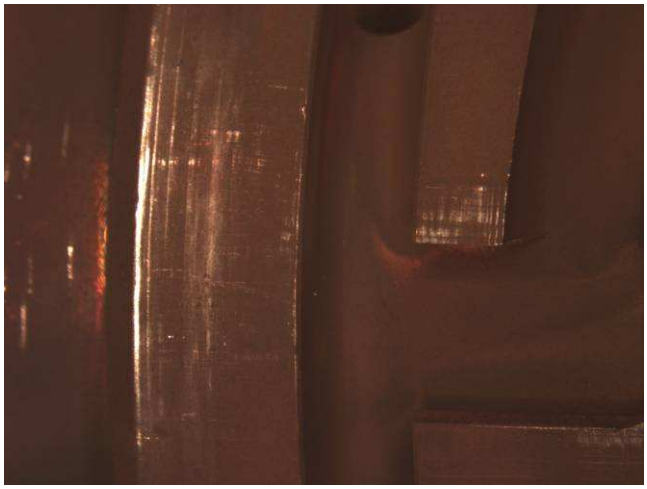

Figure 3.27: Another Close Up of the Silcosteel AC coated Test Specimen

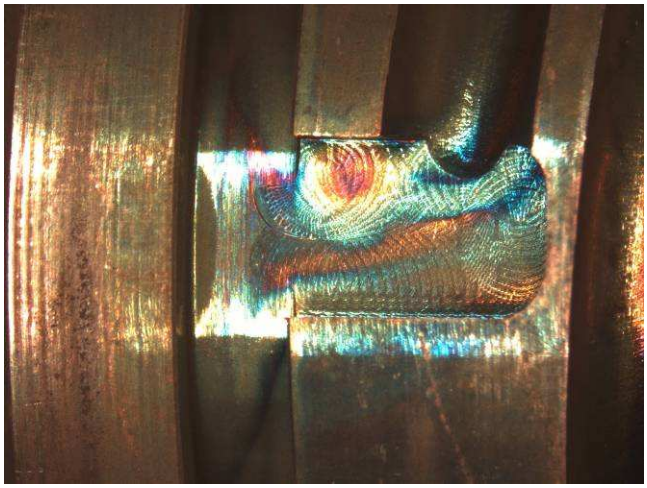

Figure 3.28: Close Up of the Inertium Coated Test Specimen

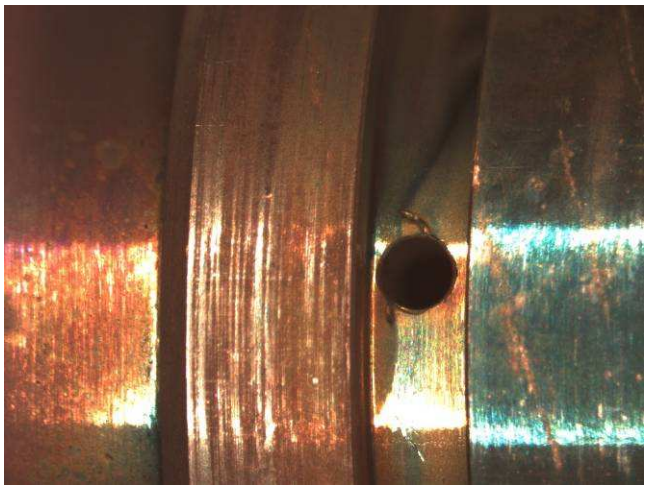

Figure 3.29: Another Close Up of the Inertium Coated Test Specimen

Figures 3.30 and 3.31 show a close up of the Fuel Cartridge Insert of the AMC26 coated specimen after the 70 hr test. Again, there is clearly less discoloration on this specimen than on the baseline. It was questionable if the AMC26 showed less discoloration than the Inertium specimen. The SEM analysis later in this section discusses the carbon formation rates. Based upon visual appearance only, the AMC26 had the best visual look and resisted discoloration.

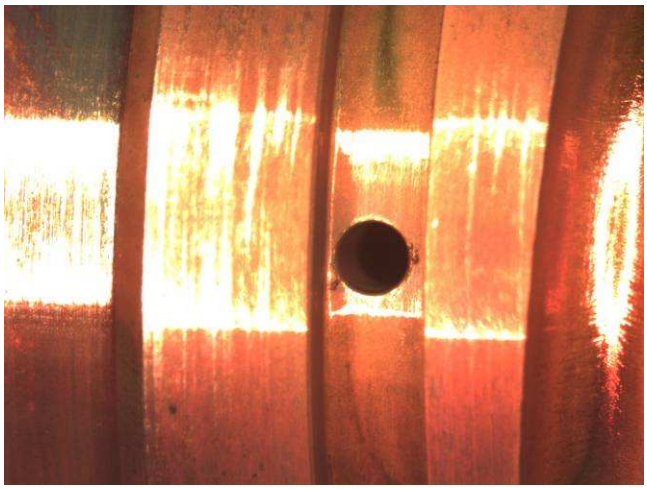

Figure 3.30: Close Up of the AMC26 Coated Test Specimen

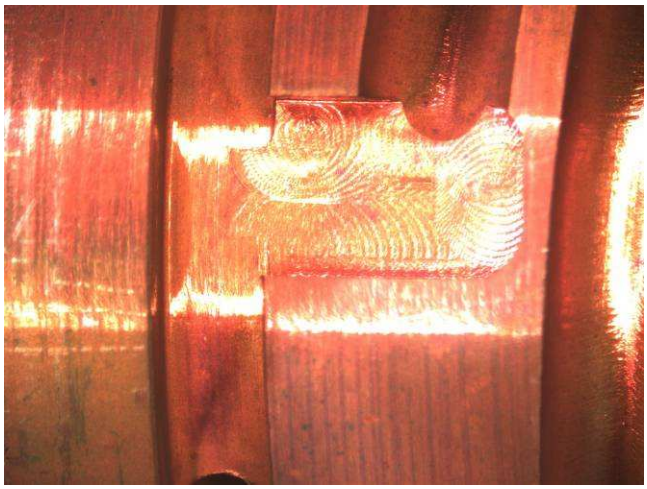

Figure 3.31: Another Close Up of the AMC26 Coated Test Specimen

The four specimens discussed above (Restek Silcosteel AC, AMCX AMC26, AMCX Inertium, and an uncoated baseline) were sent out for a detailed scanning electron microscope (SEM) analysis. As mentioned above, based upon visual appearance, the AMCX's AMC26 test specimen looked like it had the greatest resistance to carbon formation over the non-coated specimen. The SEM analysis was unable to confirm these visual results.

Previous Figure 3.23 showed the Fuel Cartridge Insert of the uncoated baseline specimen after the seventy hour test. As seen from Figure 3.23, there appeared to be carbon deposits on the left side of the fuel cartridge. This was expected since there are higher fuel and metal

temperatures in that region. The fuel temperature increases as it passes thru the helical passage of the fuel cartridge; the left side of the cartridge is near the test specimen exit and is the hottest section of the fuel cartridge. The SEM analysis was completed in the region circled in red shown in Figure 3.23. All four specimens were sectioned and tested in the same way.

Figures 3.32 through 3.45 are the results of the SEM analysis provided by our sister division (Sensors and Integrated Systems). Figures 3.32 and 3.33 show a 3000 X magnification of the interface between the baseline metal and the potting epoxy. Figure 3.32 is the Fuel Insert outer diameter (OD) (Figure 3.23 shows this Fuel Insert) whereas Figure 3.33 is the Fuel Tube Inner Diameter (ID) near the same location. The epoxy is used to hold carbon or any surface particles in place so it can be analyzed. As shown from Figures 3.32 and 3.33 there are no visible foreign material particles present. This was very surprising since the surface of the baseline part showed significant discolorations of the base metal. The zero foreign material and thus zero carbon formation was also confirmed by completing a Material Map on the test specimen. This Material Map can be seen in Figure 3.34. As seen in this figure, the test specimen was analyzed for the presence of the following elements: Carbon (top left), Silicon (top center), Chromium (top right), Iron (bottom left), and Nickel (bottom center). The carbon material map can be some what misleading. As shown, there appears to be carbon present in the test sample. This carbon is actually the carbon that is in the epoxy. Had there been carbon forming on the test specimen there would have been a much higher concentration of carbon at the metal and epoxy interface. This is not the case. The lack of carbon formation will be discussed in more detail at the end of this section.

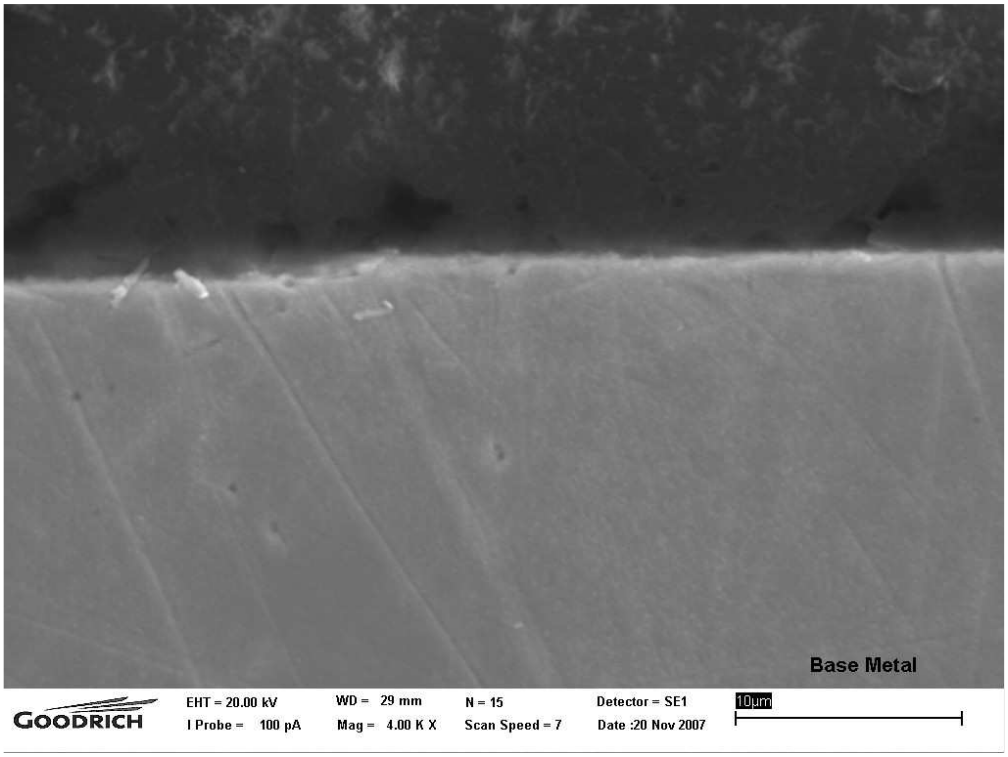

Figure 3.32: Baseline Fuel Insert OD

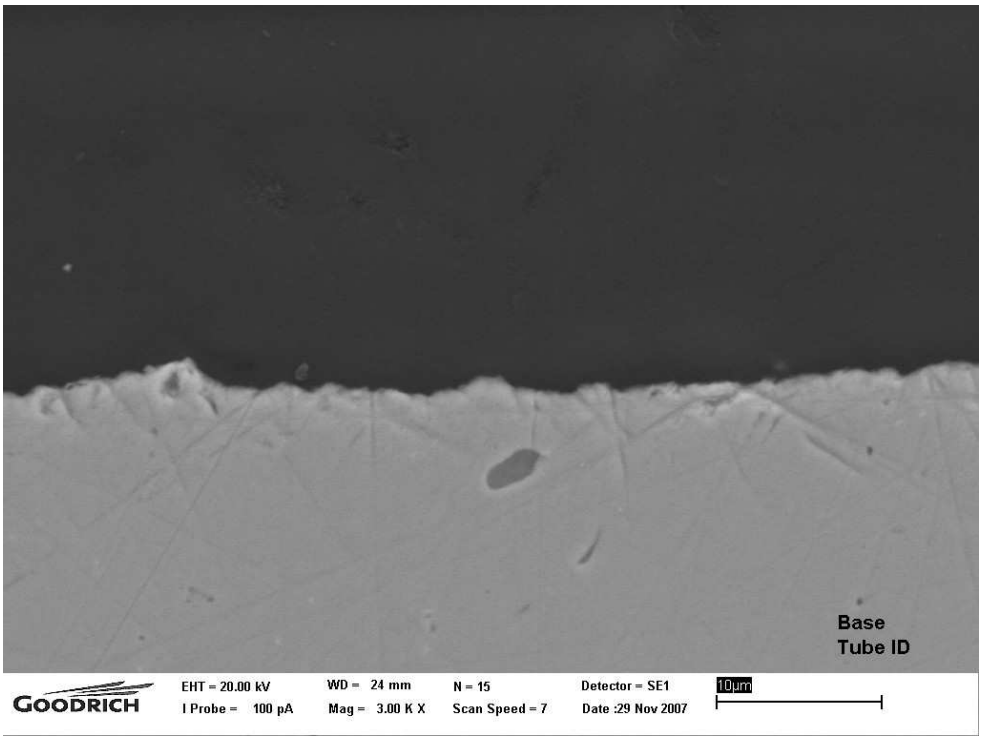

Figure 3.33: Baseline Fuel Tube ID

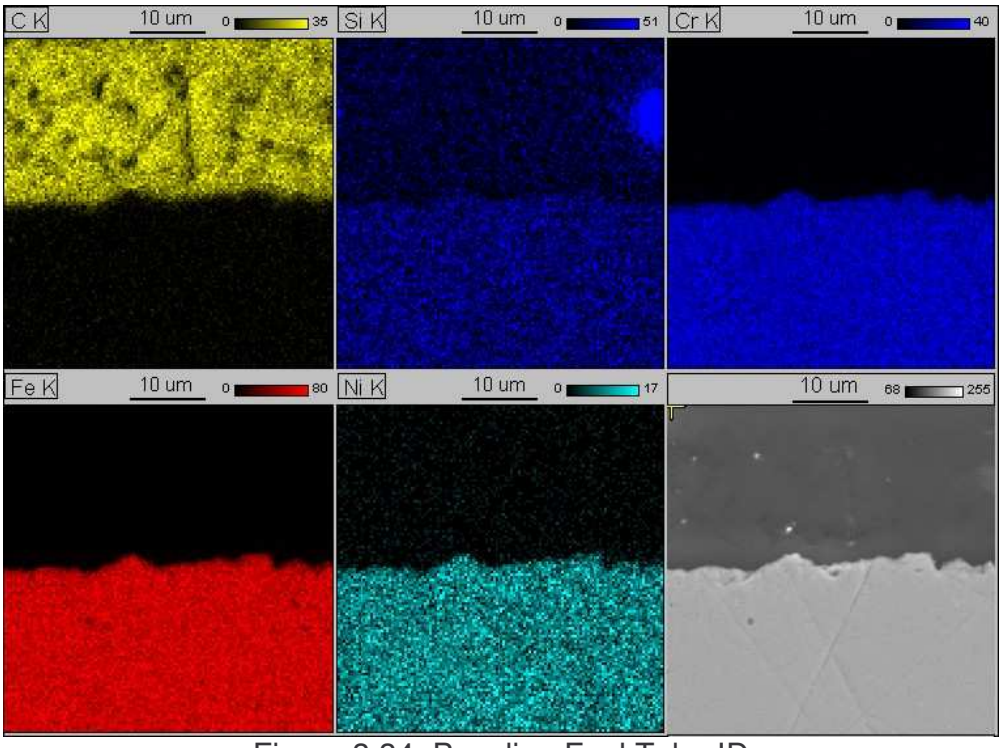

Figure 3.34: Baseline Fuel Tube ID

As expected the Silicon levels are very low. This is the baseline specimen (no coating) and there should be no Silicon at the metal epoxy boundary. The Chromium, Iron, and Nickel levels are typical of what you would expect from a stainless steel specimen.

Figures 3.35 thru 3.38 are the SEM results for the AMC26 coated test specimen. Figures 3.35 and 3.36 show a 3000 X magnification of the interface between the baseline metal and the epoxy. Figure 3.36 is the Fuel Insert outer diameter (OD) whereas Figure 3.35 is the Fuel Tube Inner Diameter (ID) near the same location. As shown from Figure 3.35 and 3.36 there are no visible foreign material particles present. This was not as surprising since it was already discovered that no carbon was present on the baseline test specimen. The zero carbon result was also confirmed by completing a Material Map on the test specimen.

The Material Maps of the Fuel Insert OD can be seen in Figure 3.37 and the Material Maps of the Fuel Tube ID can be seen in Figure 3.38. As seen from Figures 3.37 and 3.38 the test specimen was analyzed for the presence of the following elements: Carbon, Silicon, Chromium, Iron, Nickel, with the addition of Aluminum and Germanium. Had there been carbon present on the test specimen there would have been a much higher concentration of carbon at the metal and epoxy interface, which is not the case. The lack of carbon formation will be discussed in more detail at the end of this section.

There appears to be very slight traces of Silicon at the interface boundary. This is likely caused by the Silicon that may present in the anti-carbon coating. It also appears that Germanium is a component of the anti-carbon coating. The Silicon and Germanium are only present on the Fuel Insert test piece. The Fuel Tube does not show these elements. It is possible that the anti carbon coating was not applied uniformly to the test specimen. The Chromium, Iron, and Nickel levels are typical of what you would expect from a stainless steel specimen.

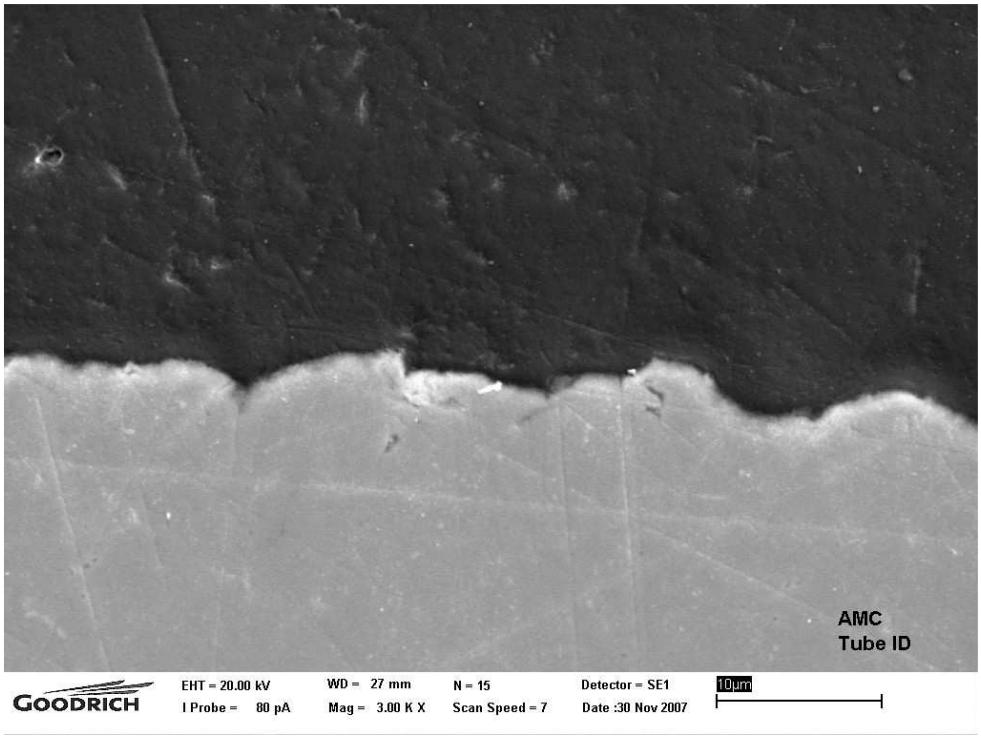

Figure 3.35: AMC26 Coating Outer Fuel Tube ID

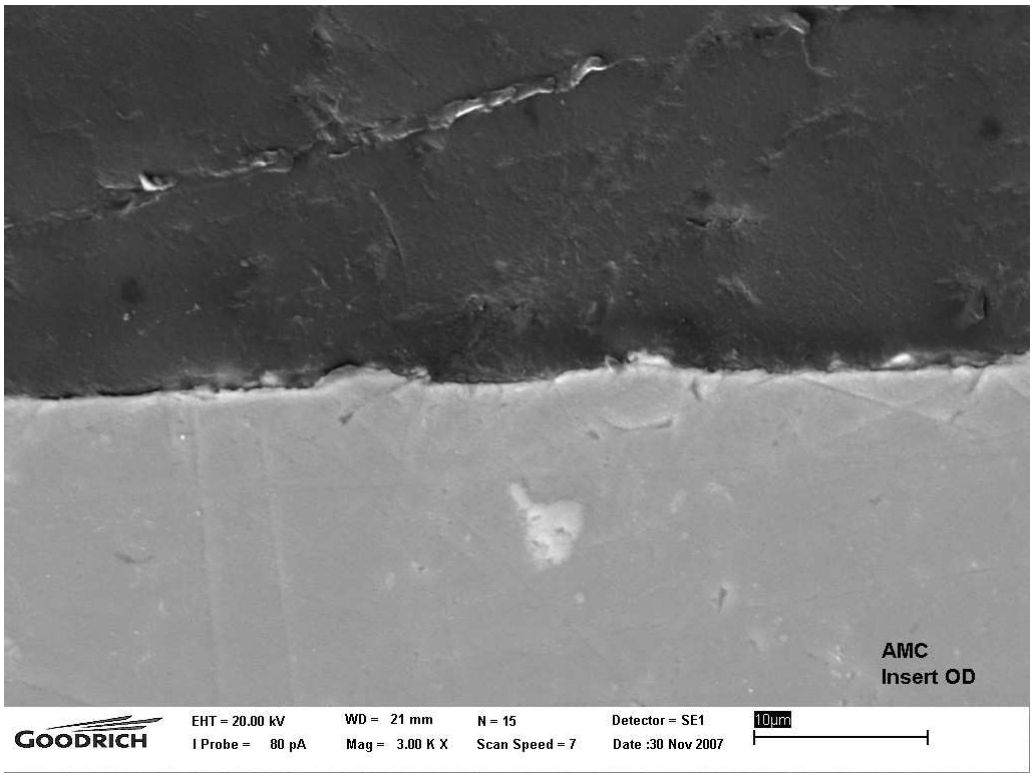

Figure 3.36: AMC26 Coating Fuel Insert OD

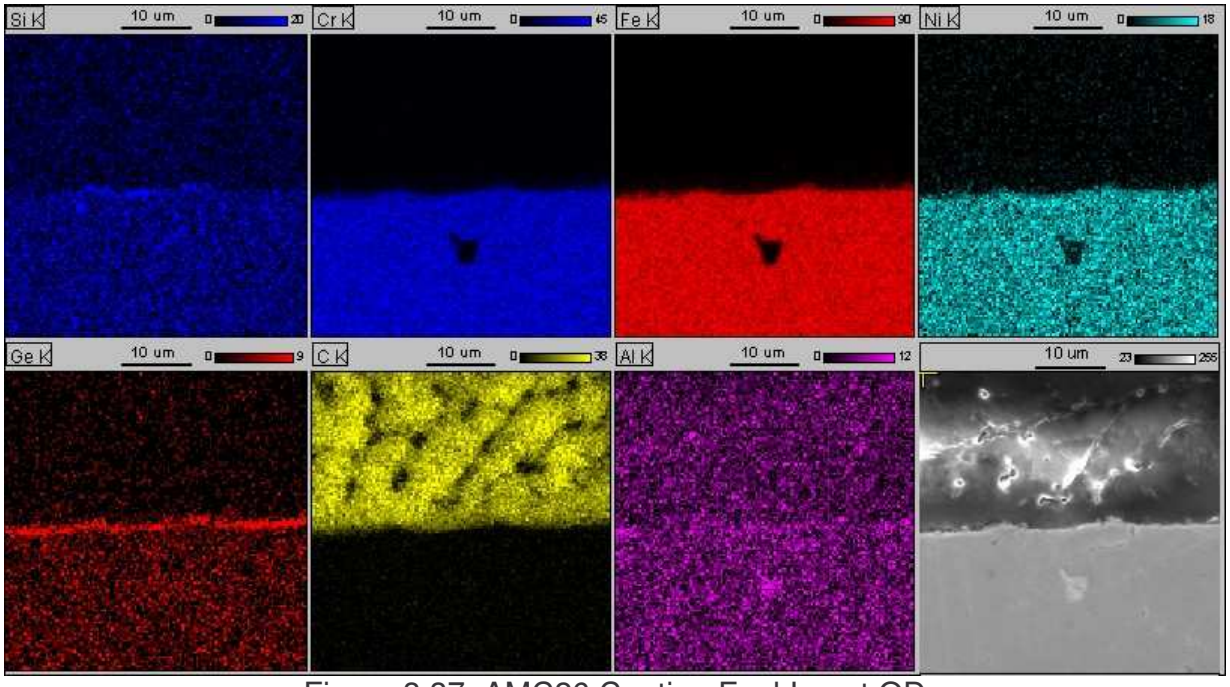

Figure 3.37: AMC26 Coating Fuel Insert OD

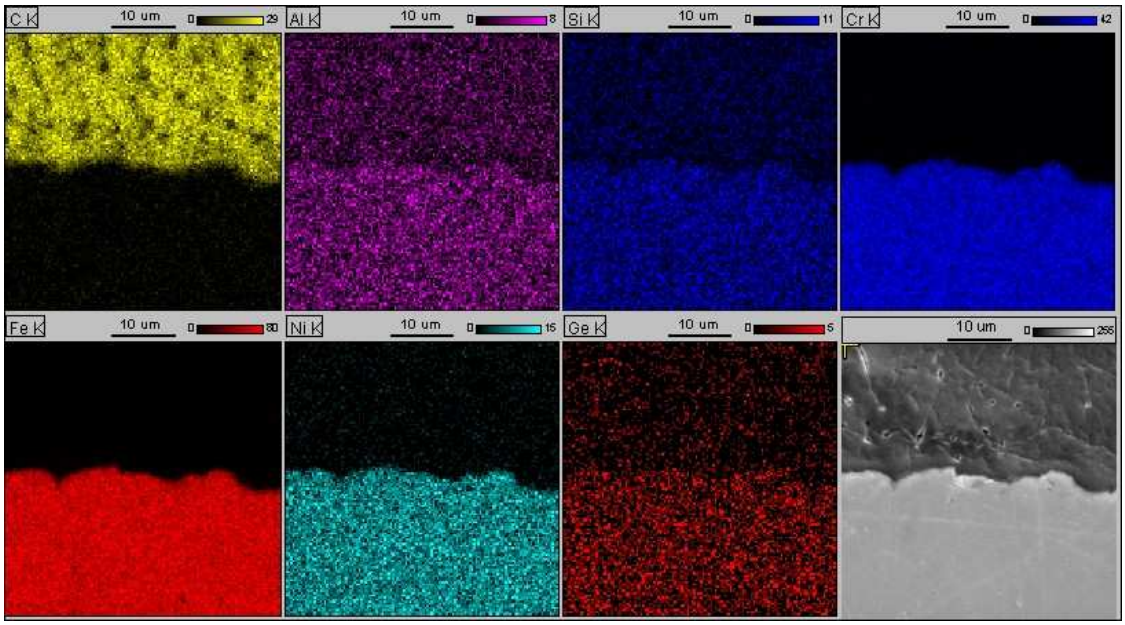

Figure 3.38: AMC26 Coating Fuel Tube ID

Figures 3.39 thru 3.41 are the results for the Inertium coated test specimen. Figures 3.39 and 3.40 show a 3000 X magnification of the interface between the baseline metal and the epoxy. Figure 3.39 is the Fuel Insert outer diameter (OD) whereas Figure 3.40 is the Fuel Tube Inner Diameter (ID) near the same location. As shown from Figure 3.39 and 3.40 there are no visible foreign material particles present. This was not as surprising since it was already discovered that no carbon was present on the previous two test specimens. The zero carbon result was also confirmed by completing a Material Map on the test specimen.

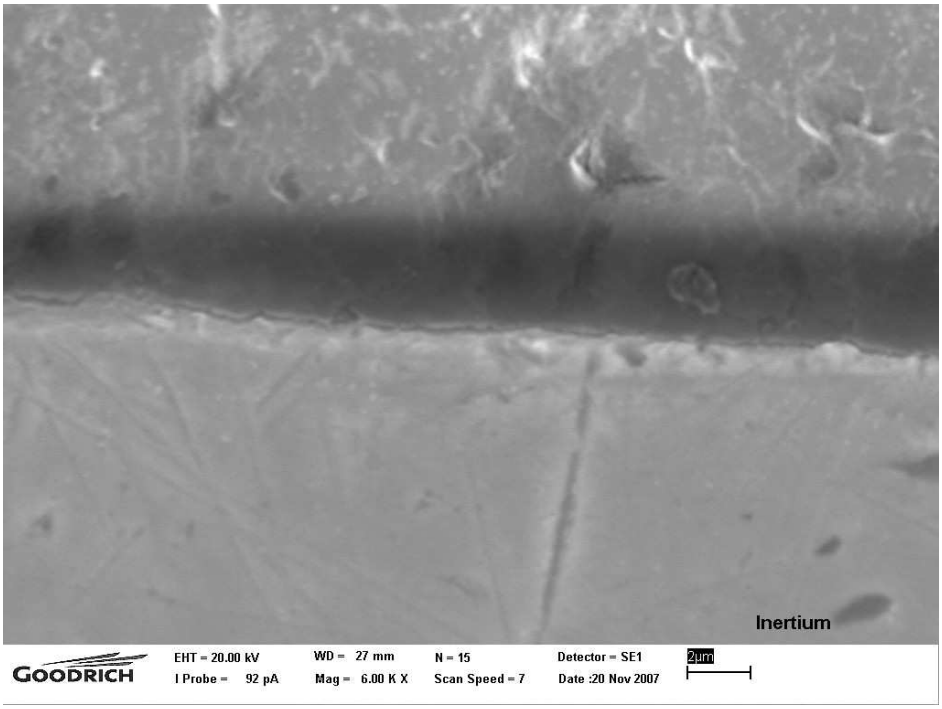

Figure 3.39: Inertium Coating Fuel Insert OD

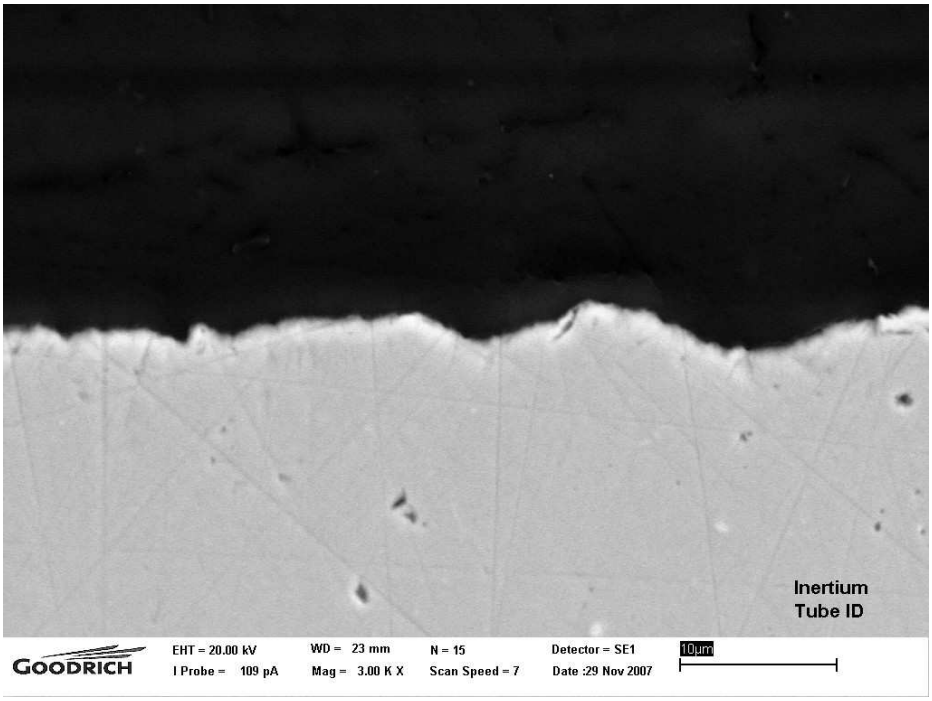

Figure 3.40: Inertium Coating Fuel Tube ID

The Material Map of the Fuel Tube ID can be seen in Figure 3.41. As seen from Figure 3.41 the test specimen was analyzed for the presence of the following elements: Carbon, Silicon, Chromium, Iron, and Nickel. Had there been carbon present on the test specimen there would have been a much higher concentration of carbon at the metal and epoxy interface. Again, the lack of carbon formation will be discussed in more detail at the end of this section.

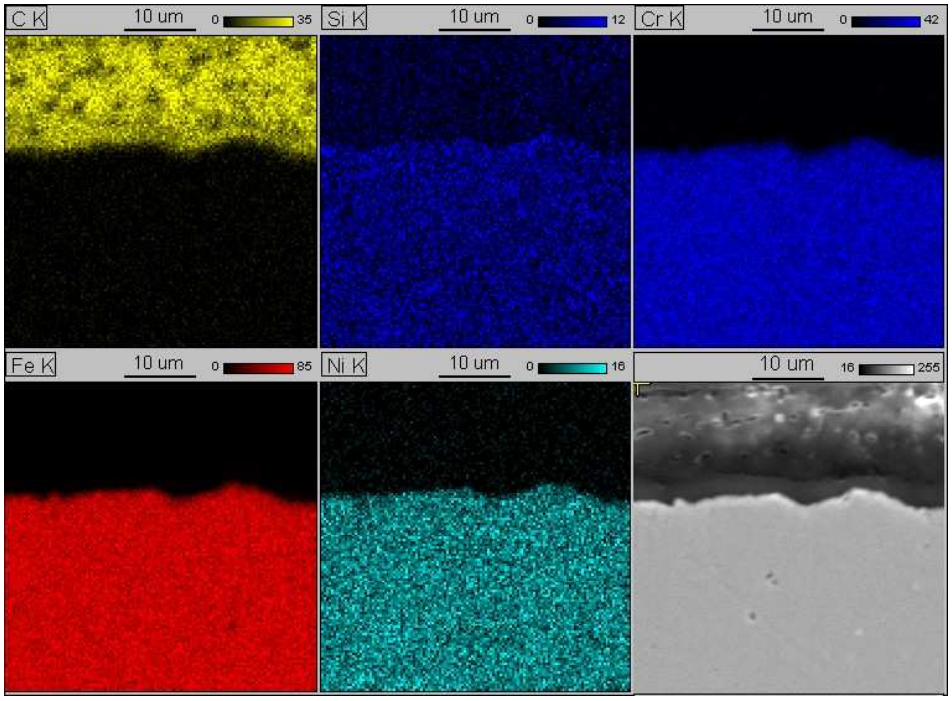

Figure 3.41: Inertium Coating Fuel Tube ID

There appears to be no trace of Silicon at the interface boundary. This implies that the Inertium coating is not a Silicon based coating. Germanium (not shown in the map) which was present in the previous specimen was not present in this anti-carbon coating. The Chromium, Iron, and Nickel levels are typical of what you would expect from a stainless steel specimen.

Figures 3.42 thru 3.45 are the results for the Restek coated test specimen. Figures 3.42 and 3.43 show a 3000 X magnification of the interface between the baseline metal and the epoxy. Figure 3.42 is the Fuel Insert outer diameter (OD) whereas Figure 3.43 is the Fuel Tube Inner Diameter (ID) near the same location. As shown from Figure 3.42 and 3.43 there are no visible foreign material particles present. This was not as surprising since it was already discovered that no carbon was present on any of the previous test specimens. The zero carbon result was also confirmed by completing a Material Map on the test specimen.

The Material Maps of the Fuel Insert OD can be seen in Figure 3.44 and the Material Maps of the Fuel Tube ID can be seen in Figure 3.45. As seen from Figures 3.44 and 3.45 the test specimen was analyzed for the presence of the following elements: Carbon, Silicon, Chromium, Iron, and Nickel. Had there been carbon present on the test specimen there would have been a much higher concentration of carbon at the metal and epoxy interface. This is not the case. The lack of carbon formation will be discussed in more detail at the end of this section.

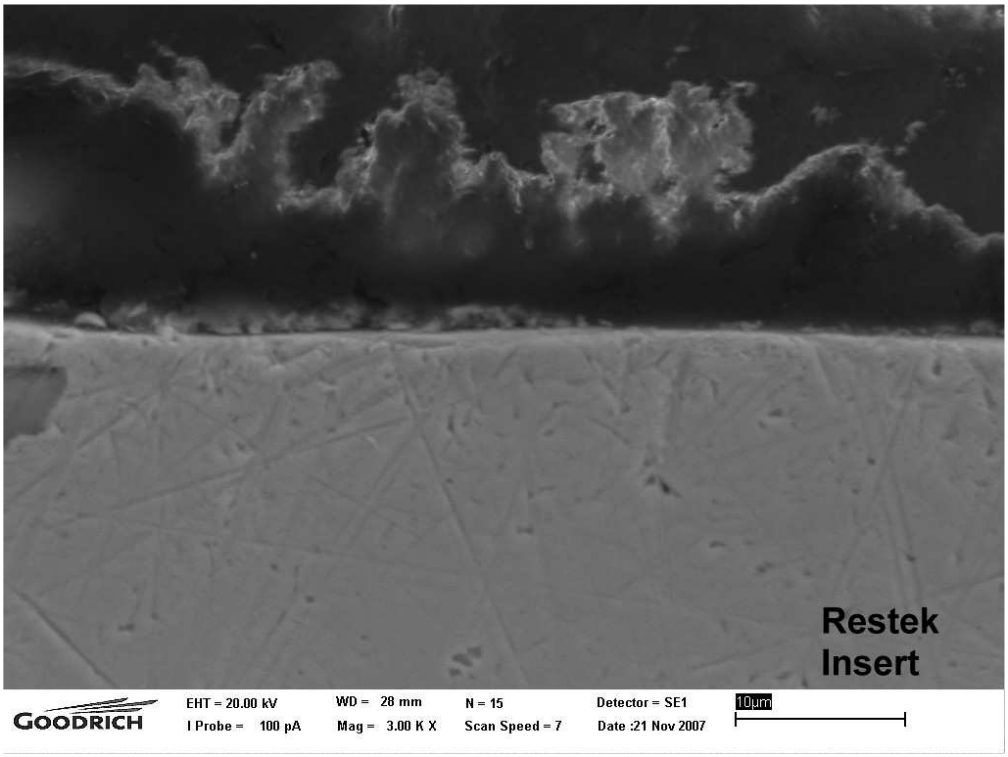

Figure 3.42: Restek Coating Fuel Insert OD

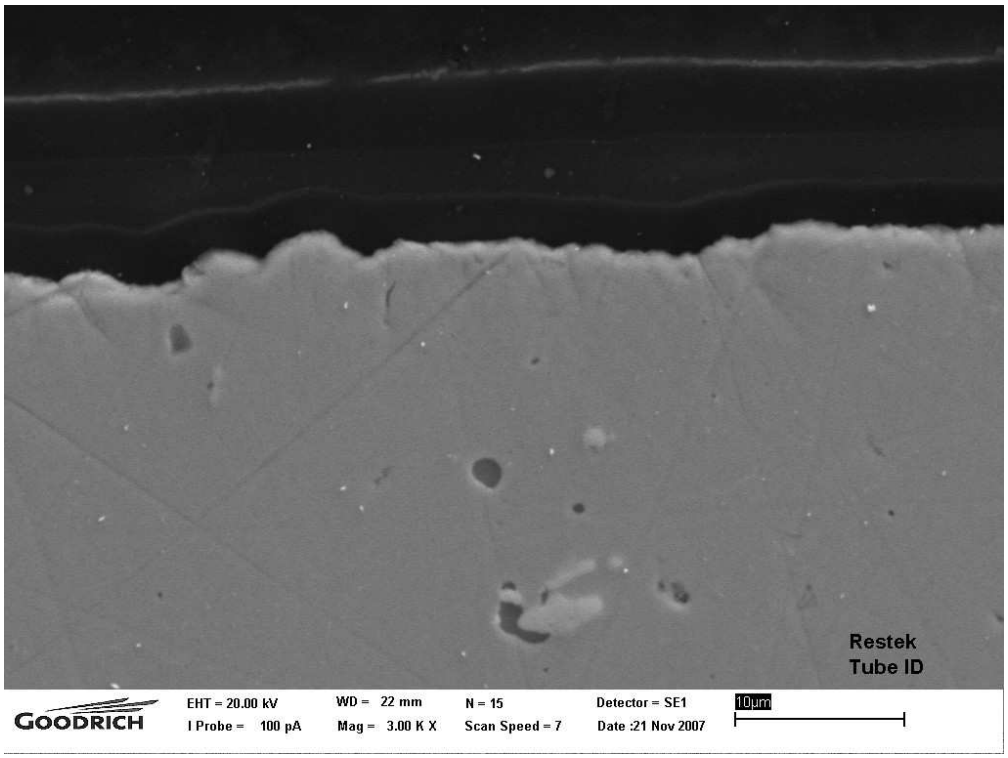

Figure 3.43: Restek Coating Fuel Tube ID

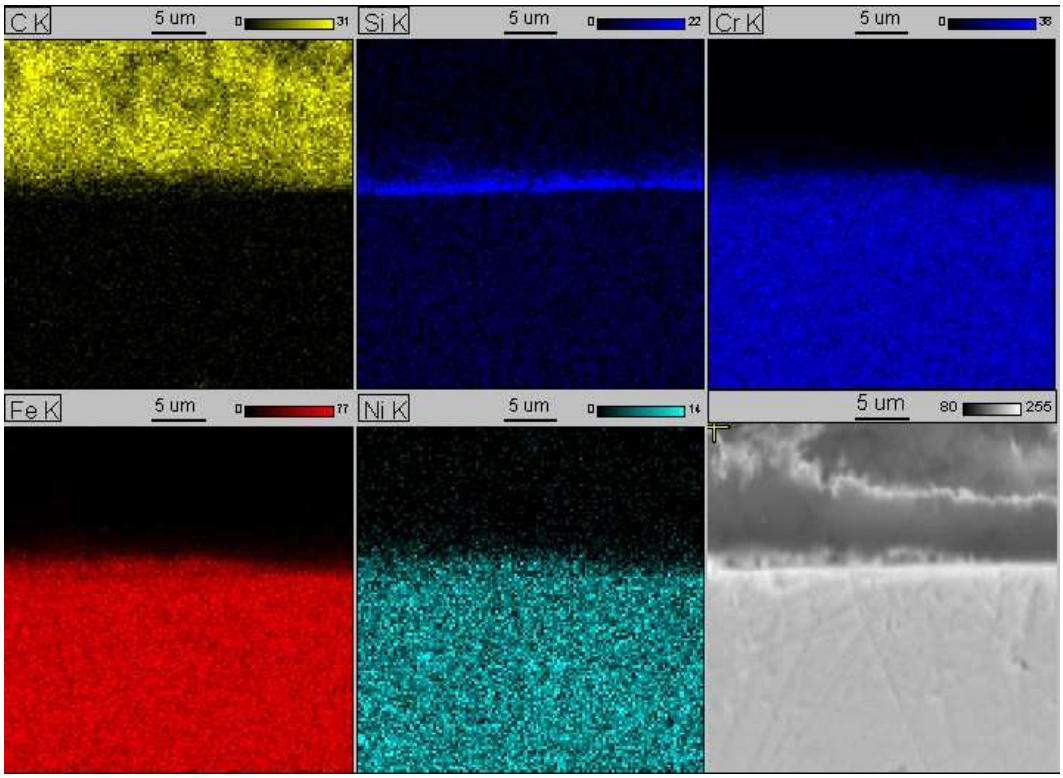

Figure 3.44: Restek Coating Fuel Insert OD

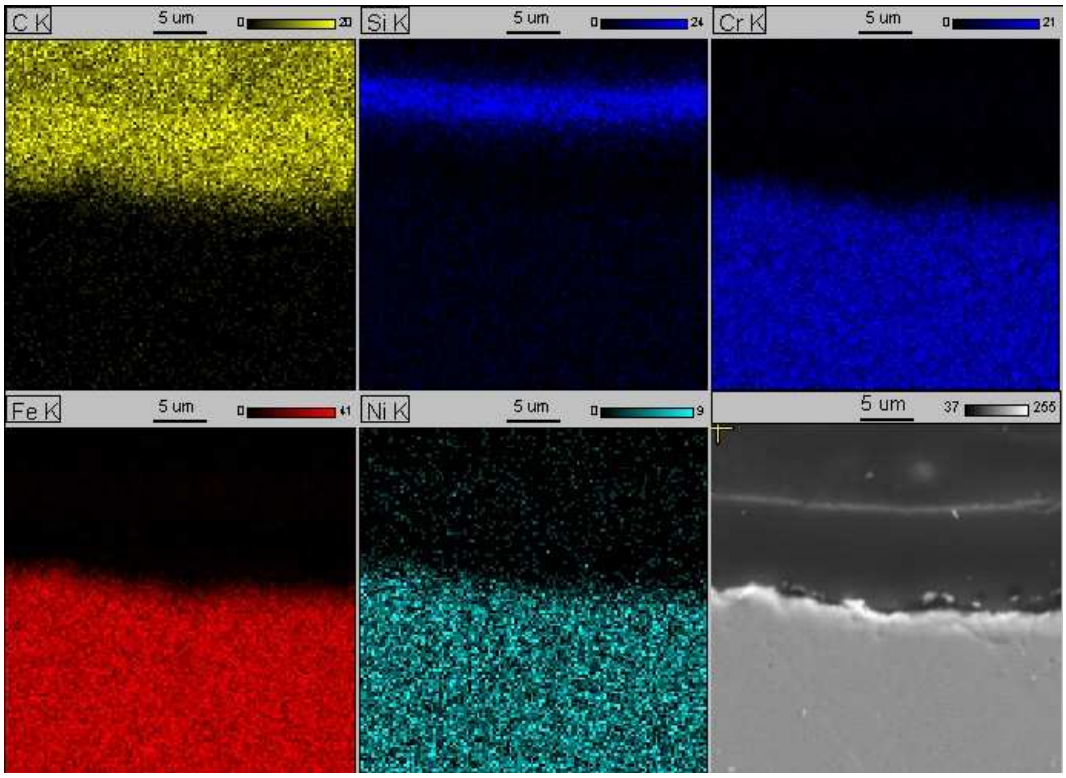

Figure 3.45: Restek Coating Fuel Tube ID

There appears to be significant amounts of Silicon at the interface boundary. This implies that the Restek coating is a Silicon based coating. It is interesting to see the differences in Silicon location between Figures 3.44 and 3.45. In Figure 3.44 the Silicon is at the epoxy interface. In figure 3.45 the Silicon is raised off of the base metal. It is theorized during test specimen handling or the SEM analysis process, the anti-carbon coating detached from the surface of the Fuel Tube ID. The epoxy then encapsulated the Restek anti-carbon coating and held it in the raised position. The Chromium, Iron, and Nickel levels are typical of what you would expect from a stainless steel specimen.

The discovery that no carbon was present on any of the test specimens was extremely disappointing. The leading theory for why no carbon was generated is a fuel change prior to the testing of the final four specimens. To help explain this theory a review of the first anti-carbon coating test needs to occur. Table 3.8 is a summary of the growth rates from the preliminary tests of the various anti-carbon coatings. Table 3.9 is a summary of the final down selected anti-carbon coatings.

	Test Conditions			Carbon Growth Rate (µm/hr)						
Test #	Fuel Temp	Oven Temp	Fuel Flow	-1A	-1B	-2	-3	-4	-5	Baseline
2	300° F	800° F	6 pph	0.63	0.63	0	0.69	2.34	0.89	0.23
3	300° F	900° F	6 pph	0.4	0.56	0.38	0.56	0.63	0.23	0.37
1	350° F	900° F	6 pph	8.43	7.3	5.96	2.61	1.96	3.36	7.58
4	350° F	800° F	6 pph	0.02	0.05	0	0.04	0	0.05	0.102

Table 3.8: SDE Growth Rate Summary to Date

Dash #	Coating Vendor	Coating Type	Application Technique
-1A	AMCX	Inertium	Diffusion Bonded
-1B	AMCX	AMC26	Diffusion Bonded
-2	Restek	Silcosteel AC	Chemical Vapor Deposition

Table 3.9: Anti-Carbon Coating Down Selected For Final Testing.

The fuel used for tests 1 thru 3 shown in Table 3.8 was Off Road Ultra Low Sulfur Diesel No. 2 purchased from Barton Solvents (BARSOL). A vendor change was required and the diesel used in test 4 was purchased from Keck Oil (Off Road Ultra Low Sulfur Diesel No. 2). It was originally thought that this change in vendors was a negligible change to the fuel. However, as seen there was a significant change in carbon formation rate. To eliminate this concern or variable in the final back-to-back test, two new barrels were purchased. Therefore, the last four tests were performed using fuel from the same lot, eliminating any inconsistencies due to variations in the fuel. As seen in the first round of testing, the fuel has a significant impact on carbon formation rate. Thus, the two new barrels of fuel used in the final test decreased the carbon formation rate to the point that carbon would not form during the seventy hour test.

Despite the disappointing carbon formation results Milestone 2.0 was completed. At this time the results do not point to a single top performing anti-carbon coating but it has been demonstrated that AMCX Inertium, AMCX AMC26, and Restek Silcosteel AC have shown improved performance over an uncoated baseline specimen. If this atomizer and mixing assembly were to continue in production, it is recommended that one of these coatings be selected for coating of the entire fuel circuit. A good way to decide between the three coatings could be cost and coating lead time.

It should be noted that these test results are at best preliminary. Sound conclusions could only be reached if the test results were found to be repeatable. Despite all efforts to conduct each test under identical conditions, a number of unexpected scenarios may have skewed the results. The Restek sample, for example, experienced a number of unplanned shutdowns in which stagnant fuel remained in the test specimen in the heated environment until it could be purged or the flow restarted. It is recommended that these tests be repeated and all data reconfirmed.

4.0 Milestone 3.0: Complete Optimized Preheating Simplex Injector

Milestone 3.0 begins the shift away from carbon formation testing to actual Fuel Cell injector build and testing. Engine Components feels that fuel/air stream preparation prior to the reformer or fuel cell is critical to increase fuel cell and reformer life and performance. Because of this, Engine Components proposed a preheating simplex injector that could prepare the fuel and air for reformer injection that could accomplish these goals. The goal of this injector was to increase efficiency by heating the fuel prior to atomization, evenly mixing the fuel and air throughout the injector mixing chamber exit, and decreasing the fuel and air pressures as low as possible so that low cost solutions could be utilized to supply the fuel and air. This section summarizes the work and testing that was accomplished in developing a Preheating Simplex

Injector. As a side note, a simplex injector is a pressure atomizer where fuel line pressure is used to produce atomization of the fuel.

Milestone 3 work began during the second quarter of this six quarter project and was not fully completed until the fifth quarter of the project. The first Sub Task that was completed (during the second quarter) was:

Task 3.1 Define Operation and Performance Requirements for the Injector/Mixer System

The following three tables show the defined operation and performance requirements for the injector. Table 4.1 shows the comparison between operation points if the fuel cell has a 40% efficiency versus a 20% efficiency. The goal of the fuel cell is to have a 40% thermal efficiency. However, after speaking with Cummins it was determined that a 20% thermal efficiency would be more appropriate for preliminary testing. Thus, the flow rates were calculated at the two efficiency points.

Fuel Flow	40% Thermodynamic Efficiency			20% Thermodynamic Efficiency		
	Min Flow	Max Flow		Min Flow	Max Flow	
Electrical Power Output	2	10	kW	2	10	kW
Thermal Efficiency	40.0%	40.0%	*	20.0%	20.0%	*
Diesel fuel power requirement	5	25	kW	10	50	kW
Diesel energy content (LHV)	42.6	42.6	MJ/kg	42.6	42.6	MJ/kg
Diesel Specific Gravity	0.835	0.835		0.835	0.835	
Fuel flow required	0.4225	2.1127	kg/hr	0.8451	4.2254	kg/hr
Fuel flow required	0.9315	4.6576	pph	1.8631	9.3153	pph
Flow Number (Cal. fluid)	0.90	0.90	*	1.80	1.80	*
Flow Number (Diesel)	0.94	0.94	*	1.88	1.88	*
Fuel pressure required	0.98	24.42	psig	0.98	24.42	psig
Air Flow						
Air/Fuel Ratio-mass	5.015	5.015	*	5.015	5.015	*
Fuel flow rate	0.932	4.658	pph	1.863	9.315	pph
Air mass flow rate	4.672	23.358	pph	9.343	46.716	pph
Air mass flow rate	0.000589	0.002943	kg/s	0.001177	0.005886	kg/s
Air Pressure	0.120	3.000	" H2O	0.120	3.000	" H2O
Air Pressure	29.8	746.5	Pa	29.8	746.5	Pa
Air Temperature	463.7	463.7	K	463.7	463.7	K
Air Effective Flow Area	0.1350	0.1350	sq.in.	0.2710	0.2710	sq.in.
Air Velocity	8.9	44.2	m/s	8.9	44.2	m/s

Table 4.1: Operation Points 40% vs. 20% Efficiency

In Table 4.1 the maximum air pressure drop through the nozzle was set at 3.0 inH_2O. Engine Components has been requested to drive the air pressure delta as low as possible. Engine Components realizes that the resultant air effective area may be too large to generate the desired swirl needed for proper mixing. With this in mind Engine Components generated multiple options for this flow point. Table 4.2 shows these alternate options which include an 11.0 inH_2O and a 25.0 inH2O of air delta P. Engine Components feels that these two points are more likely to show the desired atomization and mixing characteristics needed for a fuel cell application. However, the goal is to decrease the air delta P to the lowest possible point and still generate proper atomization and mixing.

Fuel Flow	Medium High Air Pressure 20% Thermodynamic Efficiency Min Flow	 Max Flow		High Air Pressure 20% Thermodynamic Efficiency Min Flow	 Max Flow		
Electrical Power Output	2	10	kW	2	10	kW	
Thermal Efficiency	20.0%	20.0%	*	20.0%	20.0%	*	
Diesel fuel power requirement	10	50	kW	10	50	kW	
Diesel energy content (LHV)	42.6	42.6	MJ/kg	42.6	42.6	MJ/kg	
Diesel Specfic Gravity	0.835	0.835		0.835	0.835		
Fuel flow required	0.8451	4.2254	kg/hr	0.8451	4.2254	kg/hr	
Fuel flow required	1.8631	9.3153	pph	1.8631	9.3153	pph	
Flow Number (Cal. fluid)	0.90	0.90	*	1.80	1.80	*	
Flow Number (Diesel)	0.94	0.94	*	1.88	1.88	*	
Fuel pressure required	3.91	97.70	psig	0.98	24.42	psig	
Air Flow							
Air/Fuel Ratio-mass	5.015	5.015	*	5.015	5.015	*	
Fuel flow rate	1.863	9.315	pph	1.863	9.315	pph	
Air mass flow rate	9.343	46.716	pph	9.343	46.716	pph	
Air mass flow rate	0.001177	0.005886	kg/s	0.001177	0.005886	kg/s	
Air Pressure	0.439	11.000	" H2O	0.996	25.000	" H2O	
Air Pressure	109.3	2737.3	Pa	247.8	6221.1	Pa	
Air Temperature	463.7	463.7	K	463.7	463.7	K	375.0
Air Effective Flow Area	0.1414	0.1414	sq.in.	0.0939	0.0939	sq.in.	
Air Velocity	17	84	m/s	25	125	m/s	

Table 4.2: Operation Points 20% Efficiency With Higher Delta P

The final flow conditions are shown in Table 4.3. This table shows the effect of high temperature air on the air effective area of the nozzle. The final fuel cell atomizer is going to utilize high temperature air (400° C or above), which will have an effect on the air effective area. As shown, the effective area would need to increase to maintain the desired air mass flow rate and maintain a delta P of 3.0 inH_2O. This table is used for reference when testing the atomizer at ambient conditions.

Fuel Flow	Initial Air Temperature (190.5 C) 20% Thermodynamic Efficiency Min Flow	 Max Flow			High Air Temperature (400 C) 20% Thermodynamic Efficiency Min Flow	 Max Flow		
Electrical Power Output	2	10	kW		2	10	kW	
Thermal Efficiency	20.0%	20.0%	*		20.0%	20.0%	*	
Diesel fuel power requirement	10	50	kW		10	50	kW	
Diesel energy content (LHV)	42.6	42.6	MJ/kg		42.6	42.6	MJ/kg	
Diesel Specific Gravity	0.835	0.835			0.835	0.835		
Fuel flow required	0.8451	4.2254	kg/hr		0.8451	4.2254	kg/hr	
Fuel flow required	1.8631	9.3153	pph		1.8631	9.3153	pph	
Flow Number (Cal. fluid)	1.80	1.80	*		1.80	1.80	*	
Flow Number (Diesel)	1.88	1.88	*		1.88	1.88	*	
Fuel pressure required	0.98	24.42	psig		0.98	24.42	psig	
Air Flow								
Air/Fuel Ratio-mass	5.015	5.015	*		5.015	5.015	*	
Fuel flow rate	1.863	9.315	pph		1.863	9.315	pph	
Air mass flow rate	9.343	46.716	pph		9.343	46.716	pph	
Air mass flow rate	0.001177	0.005886	kg/s		0.001177	0.005886	kg/s	
Air Pressure	0.120	3.000	" H2O		0.120	3.000	" H2O	
Air Pressure	29.8	746.5	Pa		29.8	746.5	Pa	
Air Temperature	463.7	463.7	K	375.0	673	673	K	751.7
Air Effective Flow Area	0.2710	0.2710	sq.in.		0.3261	0.3261	sq.in.	
Air Velocity	8.9	44.2	m/s		10.7	53.2	m/s	

Table 4.3: Operation Points 20% Efficiency Utilizing Higher Temperature Air

With task 3.1 complete, Tasks 3.2 thru 3.5 could be worked in parallel. Thus, these tasks are covered in one section. These subtasks are:

Task 3.2 Evaluate New Concepts for Operation and Performance Improvements
Task 3.3 Prepare Solid Models for the Optimized Preheating Simplex Injector
Task 3.4 Prepare Drawings for the Optimized Components
Task 3.5 Fabricate and Assemble Test Hardware for the First Build

Solid models (atomizer layouts) and drawings were created for the Build 1 pre-heating atomizer. Figure 4.4 shows a picture of some of Build 1 components as well as the solid model geometry. A partial view of the Inner Air Swirler can be seen in computer generated model in Figure 4.4. The Inner Air Swirler took longer to manufacture because of a new swirler design being utilized. This new air swirler design requires a little more development but has the potential to reduce part cost while increasing performance. To develop the Inner Air Swirler, wax rapid prototype pieces were constructed and tested (before actual metal components). Some of the testing of the rapid prototype parts can be seen in Figures 4.5 and 4.6.

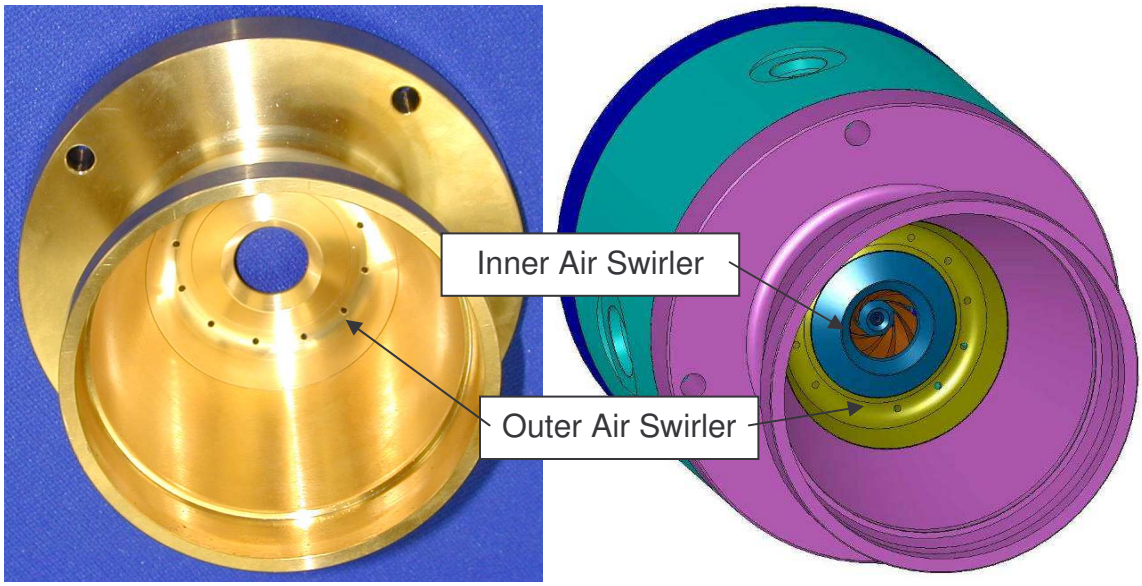

Figure 4.4: Preliminary Components and Models of Build 1.

Figure 4.5 shows the fuel flow field of SK16276-05 (one of the wax rapid prototype parts) at a fuel pressure of 28 psi (9.4pph) with an air pressure of 8 in H_2O (23.8 pph). This point would be the fuel and air required for a 10 kW Fuel Cell with ~20% efficiency. This flow field demonstrates exceptionally fine droplets, even distribution and excellent spray quality.

Figure 4.6 shows the fuel flow field of SK16276-05 (same configuration as Figure 4.5) with a fuel pressure of 8 psi (4.65 pph) and an air pressure of 2 in H_2O (11.41 pph). This point would be the fuel and air required for a 5 kW Fuel Cell with ~20% efficiency. This flow field also looks good, but the fuel mist is beginning to weaken and form larger droplets. This configuration's performance degraded when the fuel pressure was decreased below 5 psi and the air decrease below 1.0 in H_2O (no pictures shown).

Figure 4.5: Photo's Of Prototype SK16276-05 Inner Air Swirler Testing (10 kW test point)

The testing shown in Figure 4.5 and 4.6 was performed without the Outer Air Swirler (See Figure 4.4). Thus, only 50% of the required air is being utilized in this testing. It was anticipated that the increased air from the Outer Swirler will improve the atomization.

Figure 4.6: Photo's Of Prototype SK16276-05 Inner Air Swirler Testing (5 kW test point)

Construction of the pre-heating injector Build 1 was accomplished once the Inner Air Swirler was manufactured. Build 1 parts for the preheating injector were received during the month of January 2007 and the nozzle was assembled. Figures 4.7 thru 4.10 show the completed Build 1 injector. Figure 4.10 shows some of the multiple component configurations.

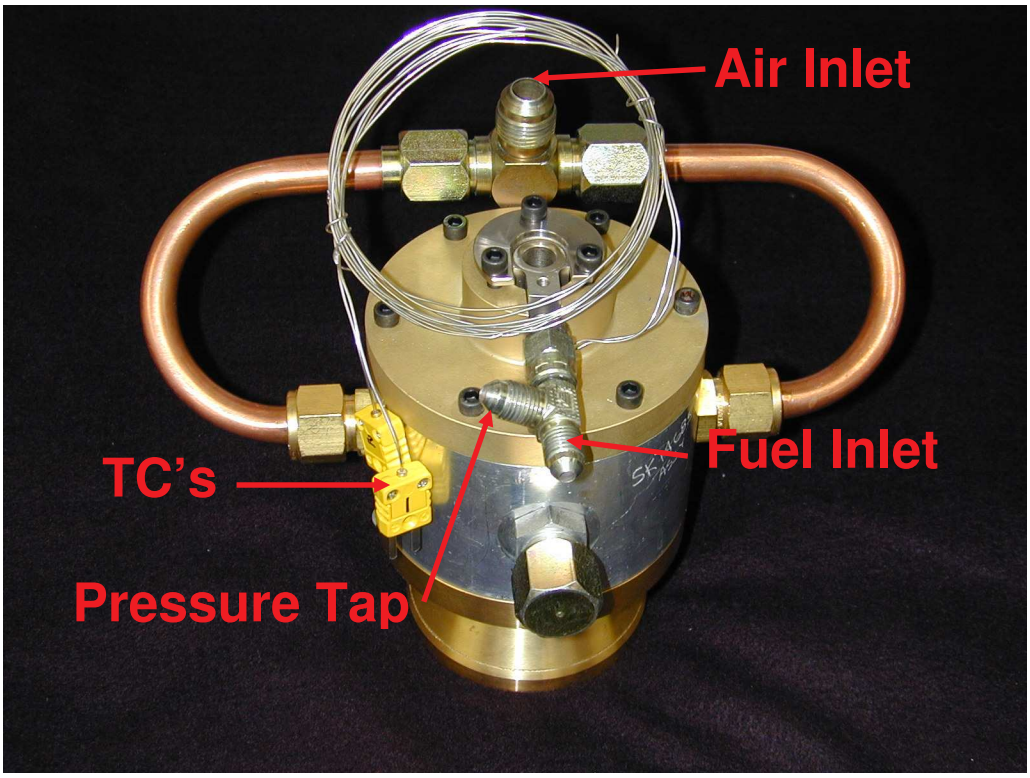

Figure 4.7: Photo Of Build 1 Top View


Figure 4.8: Photo Of Build 1 Side View

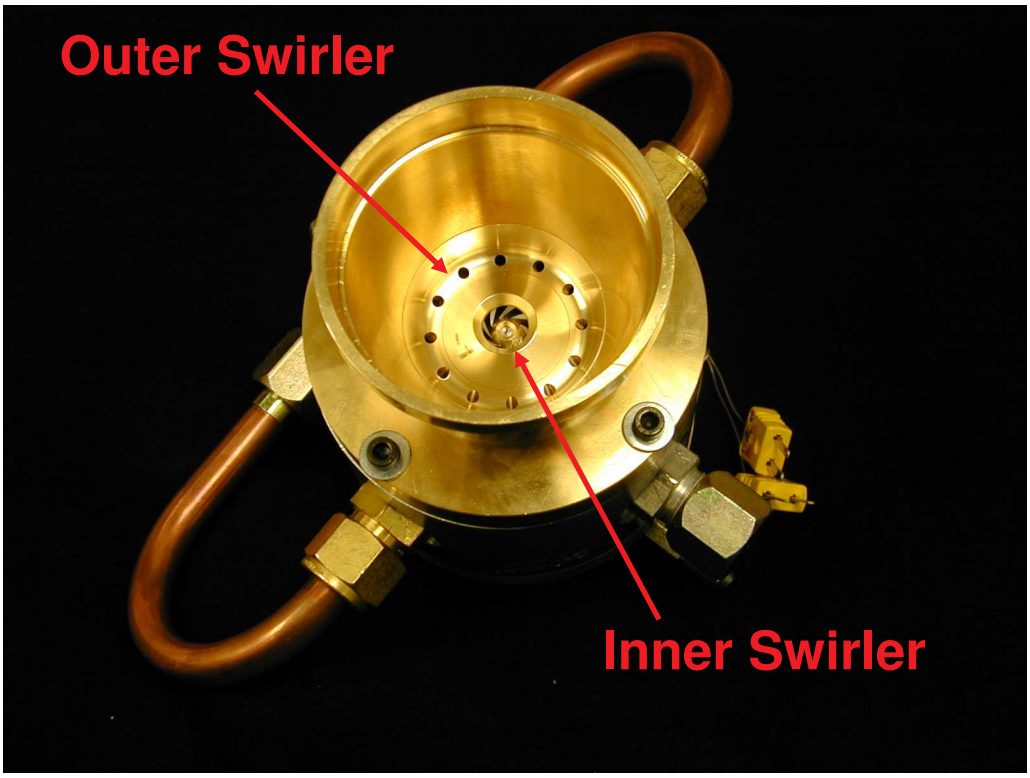

Figure 4.9: Photo Of Build 1 Bottom View.

Figure 4.10: Photo Of Alternate Configurations For Testing

This assembly of the preheating injector Build 1 completes subtask 3.3, 3.4 & 3.5. The next subtask completed of Milestone 3 was:

Task 3.6 Run Injector Tests and Establish Performance Curves for the First Build

Figures 4.11 show a cross section of this Build 1 assembly. Shown in Figure 4.11 are three components which were designed to be removable and replaceable. These components are the Outer Swirler, Diffuser and Air Cap. Other components that could be replaced that are not shown in Figure 4.11 are the Inner Air Swirler and the “Peanut” spray tip. Two configurations were created of each of the Outer Swirler, Air Cap, and “Peanut” spray tip. These alternate configurations can be seen in Figure 4.12 & 4.13.

Figure 4.12 shows the two Air Cap options. Option -01 has a smaller throat area with a larger transition radius than the -02 option. These changes were designed to have no impact on the atomizer air effective area. However, past work has shown that small subtle changes such as these could lead to large effects on the spray distribution.

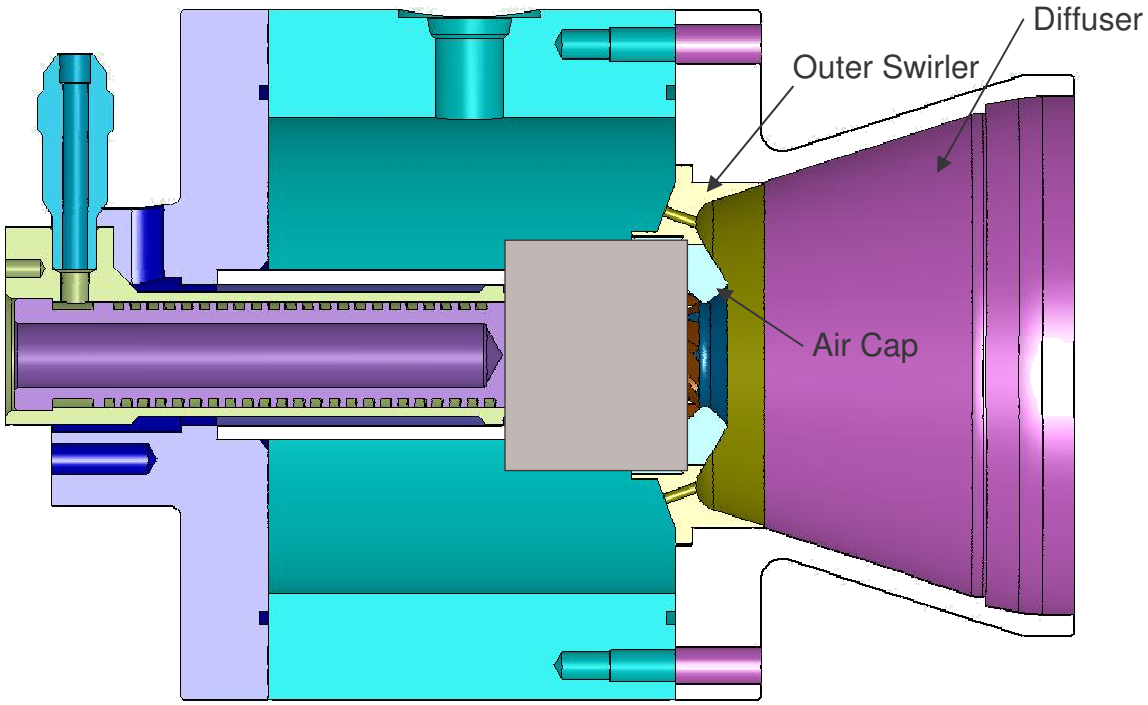

Figure 4.11: Build 1 Air Box Cross Section

Figure 4.13 shows the two Outer Swirler Options. The -01 option was designed to have no tangential air velocity (i.e. no “Swirl”). The idea was to force air into the fuel spray path and improve fuel air mixing. The -02 option had counter rotating air relative to the fuel spray and Inner Air stream. The -02 option also had bi-directional drilled air holes. The hope was to encourage mixing of the fuel as well as create an air boundary layer on the diffuser that could possibly reduce fuel impingement on the diffuser. It was noticed during preliminary testing that the -01 outer swirl had a small fuel/air re-circulation zone near the fuel spray tip. The -02 was designed to reduce this re-circulation zone.

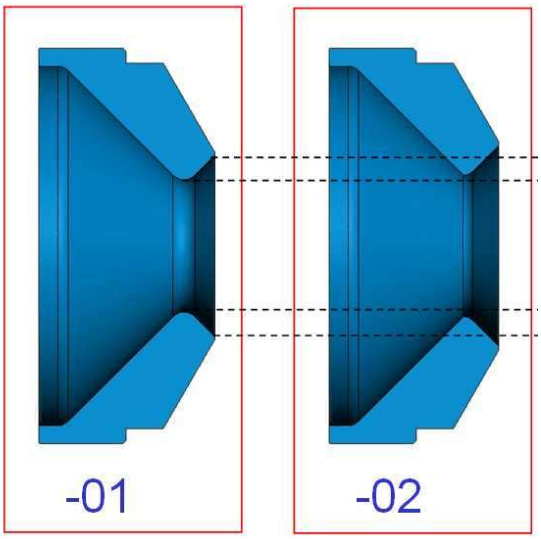

Figure 4.12: Air Cap Options In the Build 1 SDE

The third and final option that was created for Build 1 was two different fuel spray “Peanut” tips. The two “Peanuts” were created with different spray angles (55° & 65°). Spray angle often has a large effect on fuel distribution. These two angles were chosen based upon knowledge of the diffuser angle, diffuser width, and predicted air flow paths.

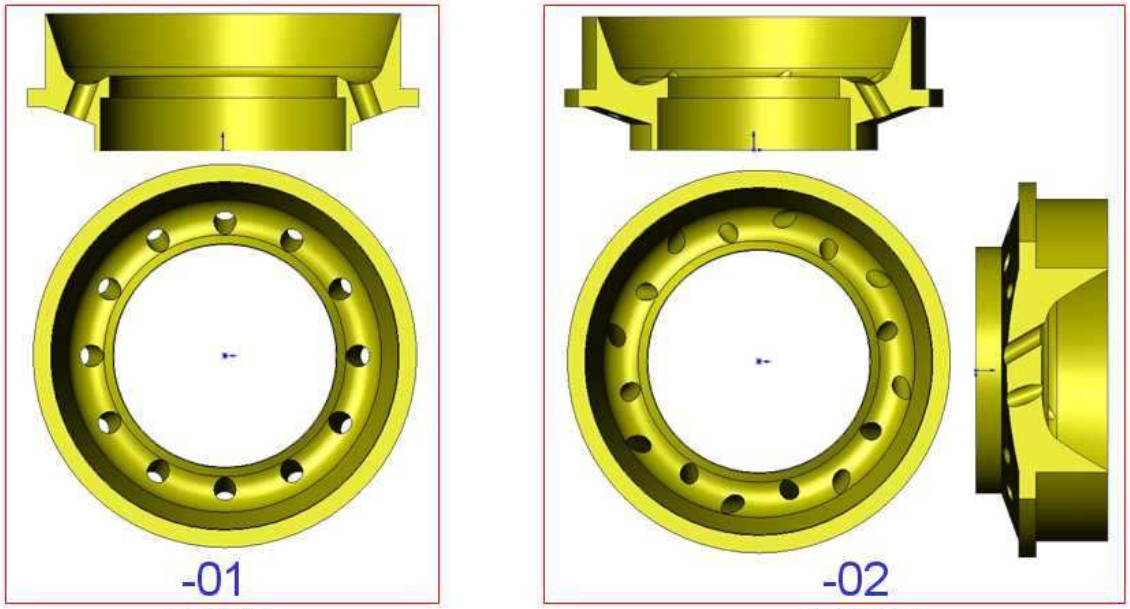

Figure 4.13: Outer Swirler Options In the Build 1 SDE

With these multiple configurations a Statistical Design of Experiment (SDE) was designed and completed on the preheating Build 1 injector. An eight test SDE was created by using the three changeable components with two different component levels. To increase reliability, each test was repeated three times. This generated a 24 test SDE matrix. It was determined that the tests would be performed on Engine Components En’Urga SetScan Optical Patternator. The

Optical Patternator has the ability to collect several useful pieces of information. The two most useful data points provided by the Optical Patternator are the radial distribution of the fuel and the circumferential distribution of the fuel. The latter, when divided into equal segments (often 12), is referred to as patternation. Figures 4.14 and 4.15 are some results that were obtained from the Optical Patternator.

Figure 4.14 shows the fuel spray radial distribution of the Build 1 Assembly. The data shown is a partial set of the SDE test. Figure 4.14 only shows the radial distribution of the 55° spray peanut (actual spray angle of "Peanut" used is ~53°) and how it is affected by the other components. As seen from Figure 4.14, the Outer Swirler and Air Cap had a large effect on the fuel spray distribution. At this time it is not exactly clear what the most desirable radial fuel distribution is. A flat radial distribution would imply a more uniform mixture. A couple configurations show a flatter radial distribution than others. However, these configurations tend to allow more fuel impingement on the diffuser. The diffuser wall location is shown as a grey line in Figure 4.14. The diffuser was not actually used during the SDE testing since the fuel impingement caused large drops of fuel that tended to corrupt the data collection.

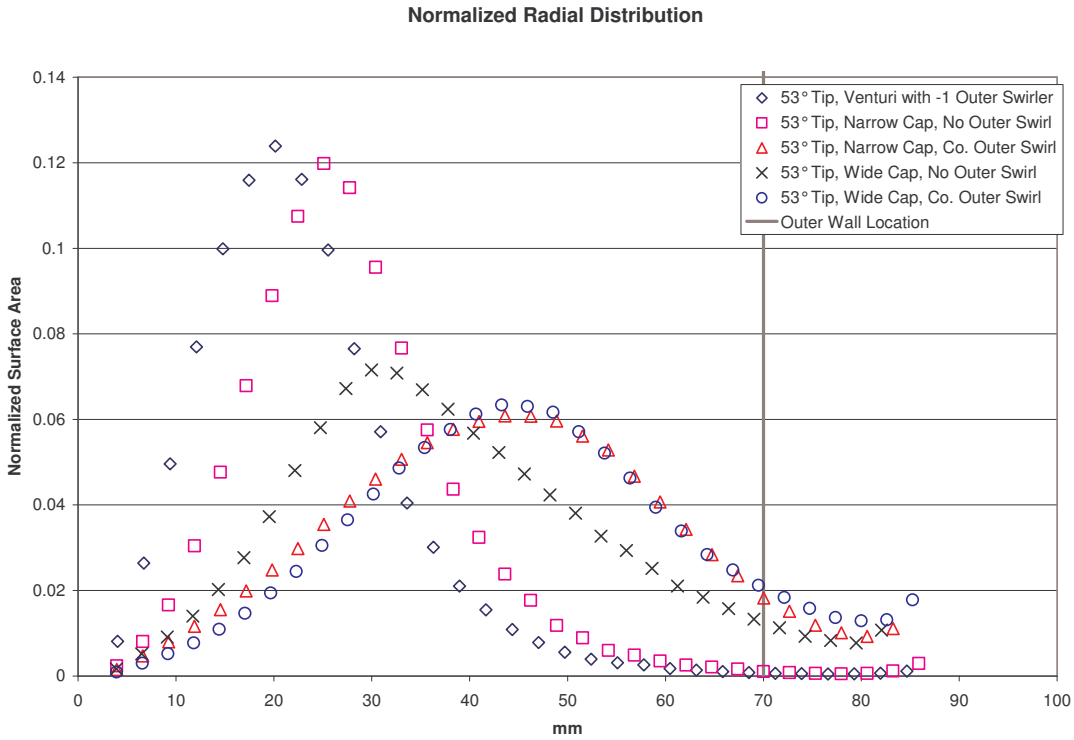

Figure 4.14: Radial Distribution Comparison of Preheating Build 1

Figure 4.14 also contains data from another Build 1 configuration. This configuration, called the "Venturi" (later termed Build 2), was not included in the SDE. A cross section is shown in Figure 4.20. As seen from Figure 4.14 the "Venturi" configuration fuel spray peaks near 20 mm and has the highest fuel concentration ("tallest peak"). The "Venturi" concept was designed to have a majority (>50%) of the available air directed to wipe the diffuser wall. The high peak near the nozzle center line is somewhat expected in the "Venturi" Build 1.

The SDE requires that a single value be used that allows comparison of each radial distribution curve. An equation was developed to compare each curve in Figure 4.14. The equation is:

$$P_C = \frac{P_{MAX} - P_{AVG}}{P_{MAX}}$$

P_{MAX} is the highest point on the curve and P_{AVG} is the average of all points on the curve. This simple equation is used to create a percentage that determines the relative flatness of each curve.

Figure 4.15 is the Surface Contour plot of two of the tests shown in Figure 4.14. Figure 4.15 shows how the fuel is distributed 360° around the nozzle. Heavy fuel concentrations are shown in red whereas light areas are shown in blue. These contours are often used to show the areas of heavy and light fuel concentration. Figure 4.15 also helps explain how the radial distribution data is obtained. The radial distribution shown in Figure 4.14 is an average around this surface at incremental steps from the nozzle centerline (similar to ring averages). Figure 4.15 shows that when the -02 Air Cap ("Wide" Air Cap) is used with the -02 Outer Swirler (counter rotating Outer Swirler) a much wider fuel/air distribution is obtained. In addition, the distribution looks more uniform.

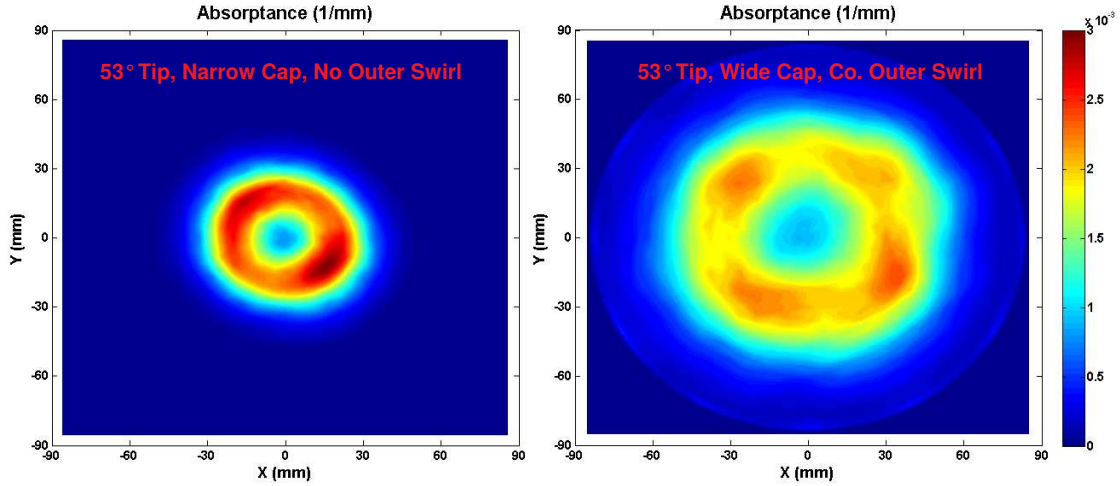

Figure 4.15: Surface Contour of Fuel Spray Distribution

Again, the SDE requires that a single value be used that allows comparison of the circumferential fuel distribution. An equation was developed to compare one surface contour to another. First the contour is divided into 12 different but equal area segments and the absorptance is summed in each segment. These 12 segments are 12 "Pie" like slices of each test point contour. The following equation is then used:

$$S_P = \frac{S_{MAX} - S_{AVG}}{S_{MAX}}$$

S_{MAX} is the highest segment of the 12 segments and S_{AVG} is the average of all segments. This simple equation is used to create a percentage that determines how evenly distributed the fuel is around the spray contour.

With S_P and P_C calculated, the results were tabulated and analyzed using Minitab. Figures 4.16 and 4.17 show the Main Effect plots for 12 Sector Patternation and Radial Distribution. The data shows that the Outer Swirler had the biggest effect on Radial Distribution and Patternation. The -02 Outer Swirler significantly improves circumferential fuel distribution and causes the most uniform radial distribution. The spray angle and Air Cap also have an effect on mixture uniformity but in opposite fashion.

It is important to note that the data shown in Figures 4.16 and 4.17 is very helpful in understanding the interactions between the three components tested. However, the data is somewhat incomplete. Some of the configurations tested demonstrated significant fuel impingement on the diffuser wall. The data shown does not show this impingement, nor does the data address recirculation zones in the fuel/air stream. This data will be used to help improve Build 1 and prepare for Build 2 but will not be the driving factor for final design validation.

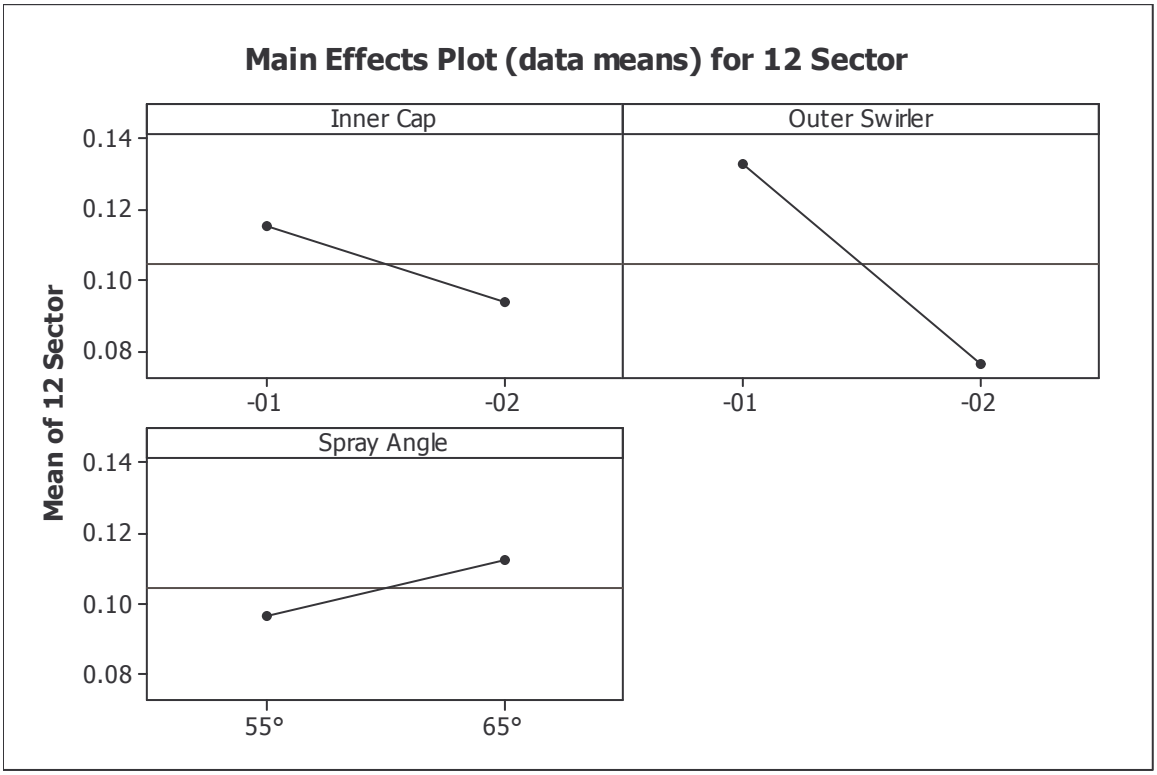

Figure 4.16: Main Effects for 12 Sector Patternation

It is important to note that all the SDE testing performed on Build 1 was done at room temperature and at ambient pressure conditions. The fuel used was Mil-PRF-7024 Type 2 test fluid and the fuel temperature was near 80° F. The air used in this test was at 75° F and was discharge into atmospheric pressure. This SDE test data was used to determine which configurations underwent heated air testing.

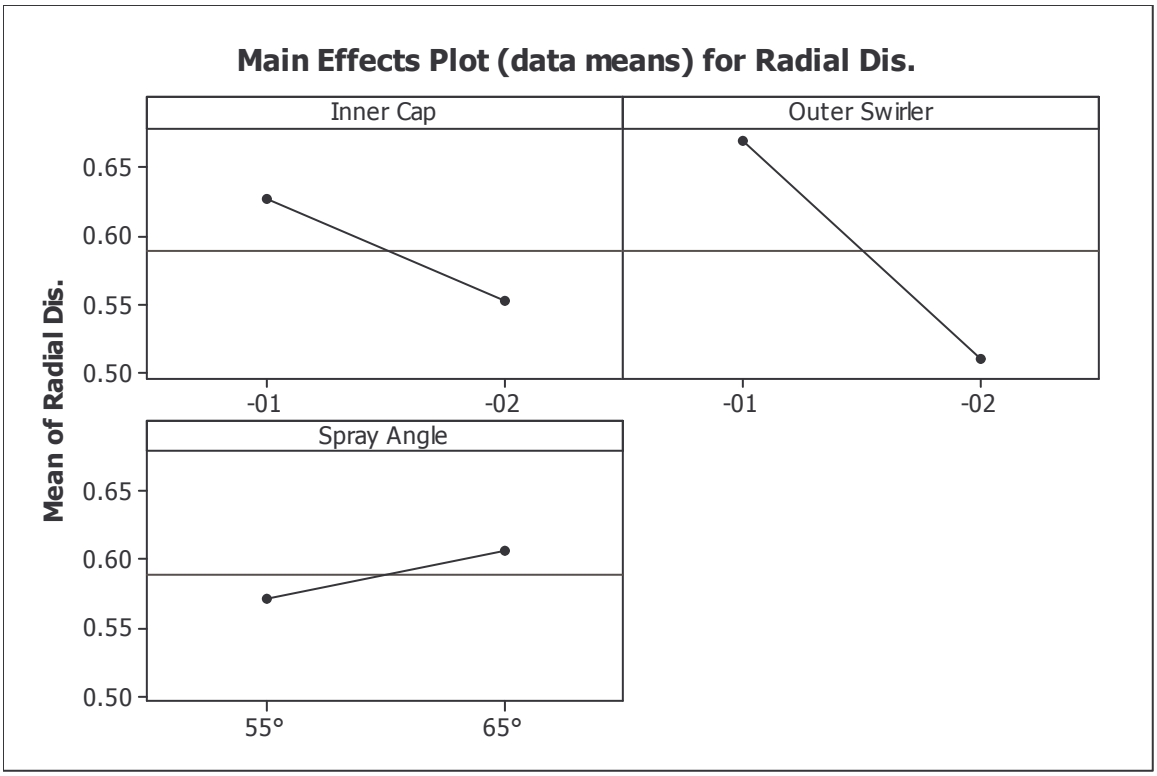

Figure 4.17: Main Effects for Radial Distribution

From the above information, two configurations were selected for heated air testing. The two configurations both utilized a 55° spray angle peanut tip and the -1 Air Cap (see Figure 4.12). The only difference between the two configurations was the Outer Air Swirler (see Figure 4.13). The two Build 1 configurations were installed on the heated air/steam rig and tested for temperature uniformity. This test involves using 8 thermocouples (TC) uniformly spaced around the axis in a single plane down stream of the atomizer exit. Figure 4.18 shows the TC test fixture used for this test. TC 1 thru 4 are equally spaced around a 2.50 inch diameter circle. TC 5 thru 6 are equally spaced around a 1.25 inch diameter circle.

Figure 4.19 shows the results of the two configurations tested. The outer TC's and inner TC's are averaged into two curves for each configuration. As shown the atomizer that utilized the -1 Air Cap, -2 Outer Swirler, and 55° spray tip had the best temperature uniformity. In addition, this configuration had less temperature variation through time as well as a higher temperature (~123°F). This is attributed to better mixing of the -1 Air Cap, -2 Outer Swirler, and 55° spray tip configuration.

The temperature uniformity shown in Figure 4.19 is calculated by using the following equation:

$$U_I = \frac{T_{MAX} - T_{MIN}}{T_{AVG}}$$

Each TC temperature measurement is averaged over the given sample interval. For Figure 4.16 the sample interval was 250 data points. From these average temperatures, a max, min, and average are calculated. T_{MAX} is the highest TC of the selected group, T_{MIN} is the lowest TC

measurement of the selected group, whereas, T_{AVG} is the average of all selected measurements.

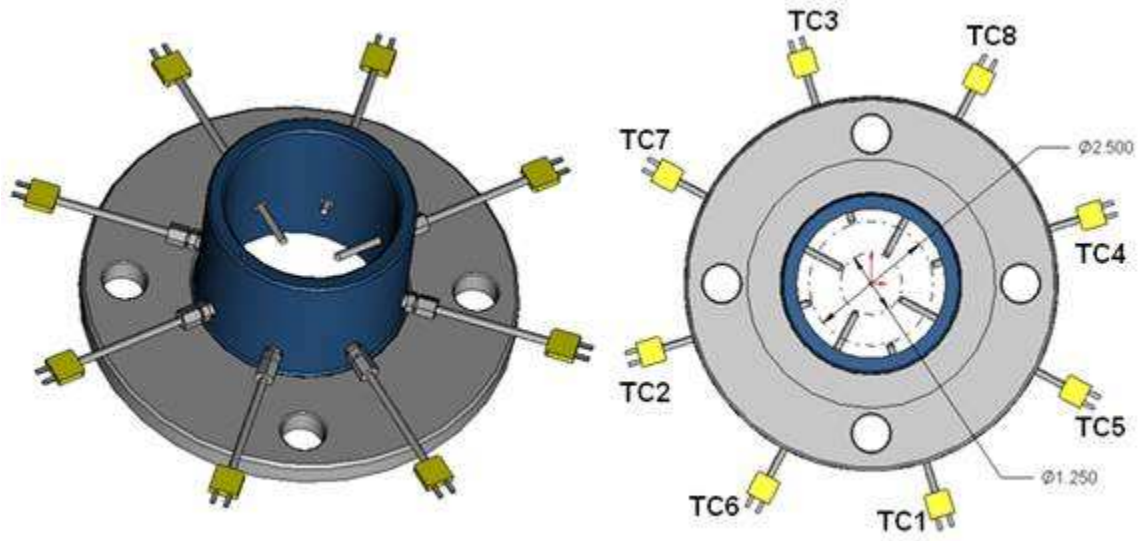

Figure 4.18: Uniformity TC Test Fixture

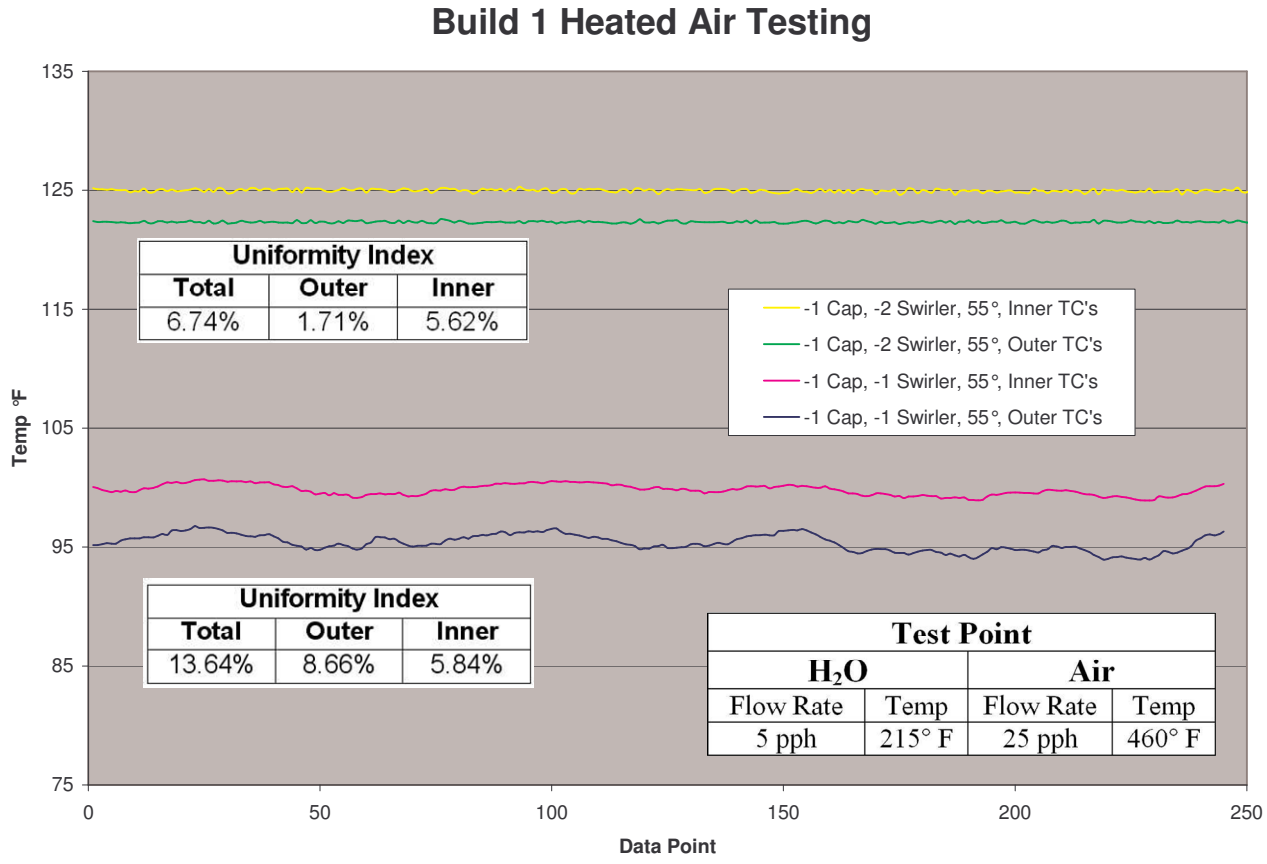

Figure 4.19: Temperature Uniformity Test

The next subtasks completed of Milestone 3.0 were:

Task 3.7 Analyze test results and propose design refinement
Task 3.8 Fabricate and assemble test hardware for the second build
Task 3.9 Run injector tests and establish performance curves for the second build

The preheating "Venturi" injector (Build II) was assembled and first tested on the optical patternator. Figure 4.20 shows the cross section of the "Venturi" injector assembly. Also, shown in Figure 4.20 are several components which were designed to be interchangeable. These components are the Outer Swirler, Diffuser, and Air Cap. Other components that could be exchanged (not shown in Figure 4.20) are the Inner Air Swirler and the "Peanut" spray tip. With these various components a SDE was created to optimize the "Venturi" design.

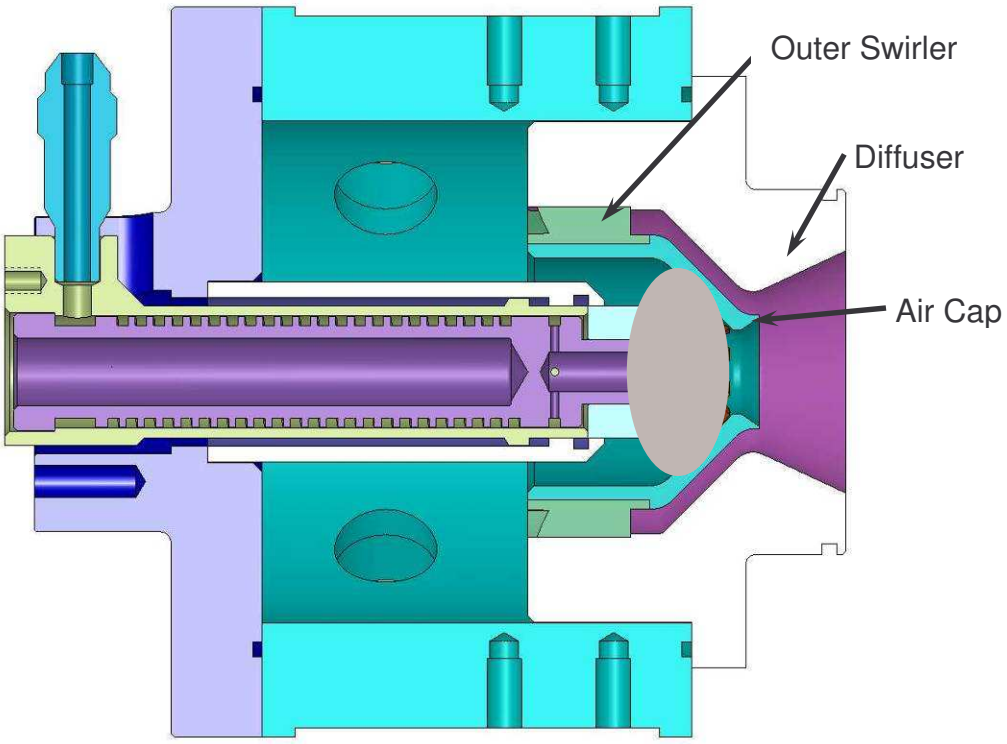

Figure 4.20: "Venturi" Injector Air Box Cross Section

Three components were chosen as part of the full factor SDE. The first component shown (Figure 4.24) is the Outer Air Swirler. As seen the Outer Air Swirler has three versions (-4 thru -5). The only difference between the three versions is the swirler vane angle (lead). The air effective area was design and tested to be the same for each swirler. The vane angle affects the air tangential velocity. The effect of tangential air velocity on the outer air could be examined thru this SDE.

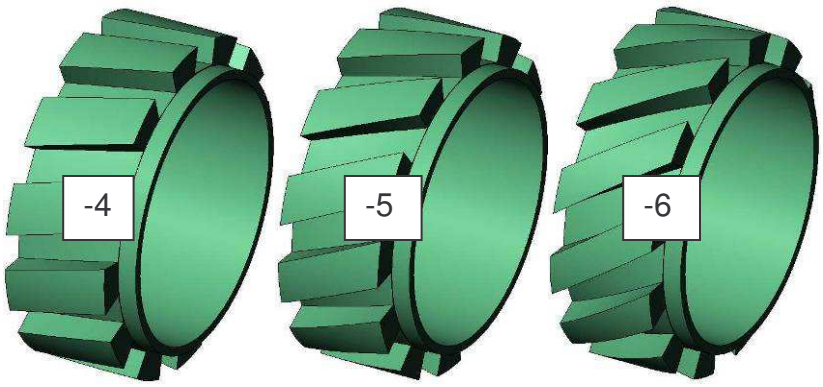

Figure 4.21: Outer Swirler Options

The two other components that were selected as part of this SDE were the Peanut Spray Tip and the Inner Air Swirler. Two configurations of the Peanut Spray Tip were selected and three of the Inner Air Swirler. The two peanut tips have different fuel spray angles, one 55° and the other 65°. The vane angle of the Inner Air Swirler is slightly different for each configuration. With these three components an SDE could be performed in order to optimize the design.

Table 4.4 shows the layout of this SDE. As seen from Table 4.4 a full factor SDE required a minimum of 18 tests based upon the three components and component levels. These 18 tests were replicated 3 times to determine data repeatability. The SDE was performed on the optical patternator. From the optical patternator, a 12 Sector Uniformity and Radial Uniformity could be determined for each test point. This data collection process is discussed in more detail previously in this section. Simply put, the 12 Sector Uniformity is a measure of how evenly the fuel is distributed around the circumference of the atomizer exit (the lower the number the more evenly distributed). The Radial Uniformity is the measure of how evenly the fuel is distributed radially (from nozzle centerline to diffuser wall).

StdOrder	Outer Swirler	Peanut	Inner Swirler	12 Sector Uniformity	Radial Uniformity
1	-4	55	-1	24.4%	70.5%
2	-4	55	-2	12.1%	71.8%
3	-4	55	-3	19.6%	71.5%
4	-4	65	-1	27.3%	71.4%
5	-4	65	-2	16.2%	72.4%
6	-4	65	-3	16.2%	67.6%
7	-5	55	-1	18.9%	66.3%
8	-5	55	-2	15.5%	66.8%
9	-5	55	-3	12.6%	67.8%
10	-5	65	-1	22.0%	67.6%
11	-5	65	-2	15.4%	67.4%
12	-5	65	-3	12.6%	67.6%
13	-6	55	-1	12.2%	65.8%
14	-6	55	-2	10.0%	68.2%
15	-6	55	-3	16.5%	67.4%
16	-6	65	-1	20.2%	68.6%
17	-6	65	-2	19.2%	69.1%
18	-6	65	-3	14.0%	68.9%

Table 4.4: Sample of SDE Collected

Figures 4.22 and 4.23 show the results of this SDE. Figure 4.22 shows the main effect plots for 12 Sector Uniformity whereas Figure 4.23 shows the main effect plots for Radial Uniformity. As seen, all the components had an effect on the 12 Sector Uniformity with the Outer Air Swirler having the largest effect. The Peanut Tip and the Inner Air Swirler did not have a significant effect on the Radial Uniformity. These results are not surprising in that much of Engine Components performance development work is spent focusing on the air swirler since it has a major effect on fuel air distribution. However, from a SDE it is possible to determine how to optimize the design. In this example, the go forward design is the -5 Outer Swirler, -2 Inner Swirler, and a 55° spray Peanut Tip. This configuration yields very good Radial and 12 Sector Uniformity. This optimized injector will be added to a mixing chamber that will also be optimized. In this way an entire injector system will be created that will generate a very uniform hot air and vaporized fuel mixture.

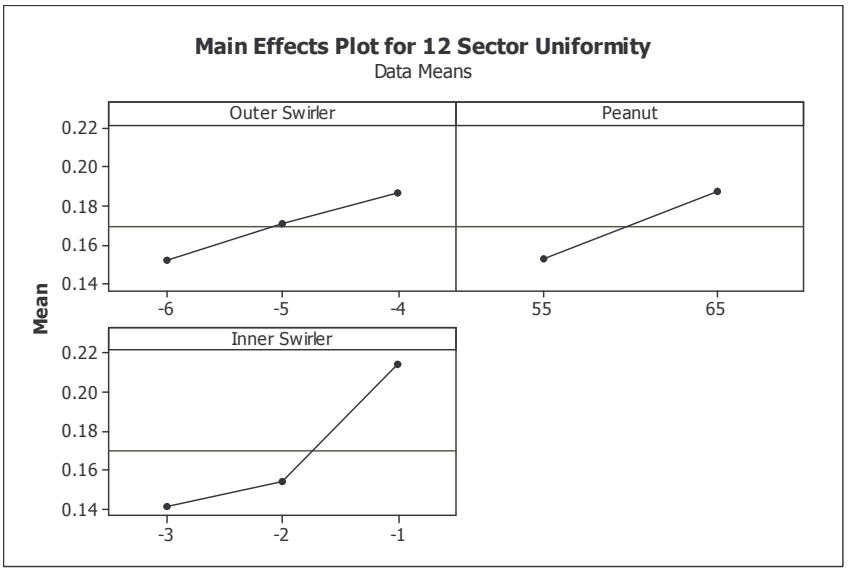

Figure 4.22: 12 Sector Uniformity Mean Effects Plot

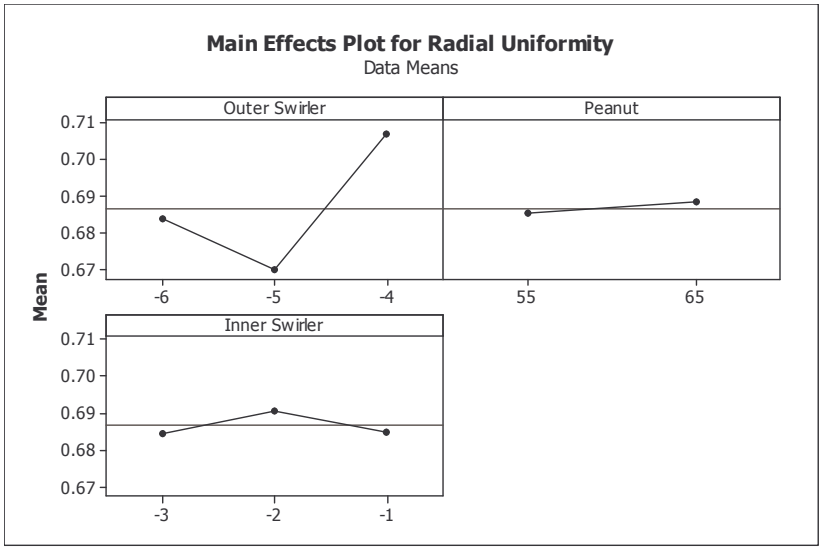

Figure 4.23: Radial Uniformity Mean Effects Plot

Figure 4.24 shows two typical contour plots generated from the optical patternation data. The dark blue areas shown in Figure 4.24 are the areas of no fuel. The red areas indicate areas of high fuel concentration. The curve line thru the contour plots is the radial distribution of the fuel. The curve is an average concentration of the fuel around the nozzle centerline. It is interesting to note the contrast between the two contours. The only difference between the two atomizer tests shown in Figure 4.24 is the Outer Air Swirler. As predicted from the SDE the -5 Outer Swirler should improve Radial Uniformity and 12 Sector Uniformity. This is readily apparent in these contours.

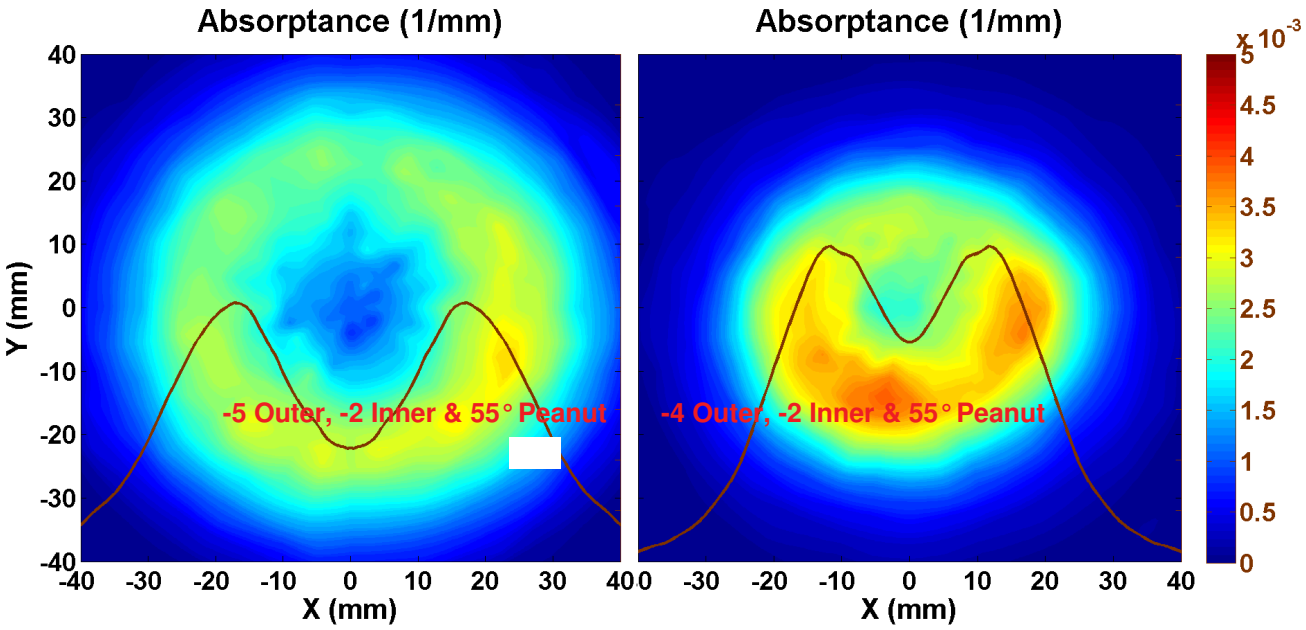

Figure 4.24: Contour Plots from Optical Patternation Testing

Phase Doppler Particle Analysis (PDPA) testing was next test completed on the preheating "Venturi" injector (Build II). Figure 4.25 shows the SMD results of this testing. The primary fuel for this test point was MIL-PRF-7024 Type 2 test liquid flowing 5pph at 22psig. The air flow was 25pph at 0.7inches of H_2O. This corresponds to a 5 kilowatt fuel cell operation point. The measurement was taken at an axial distance of 3 inches away from the injector face. The average SMD for this test was 72.9µm. This may appear high at first glance. However, this measurement is taken without the mixing chamber and at ambient temperature conditions with extremely low fuel and air pressures. It is expected that the SMD will only improve as the temperature is raised and the mixing chamber is added and optimized. The results are very promising when one accounts for the extremely low fuel and air pressure.

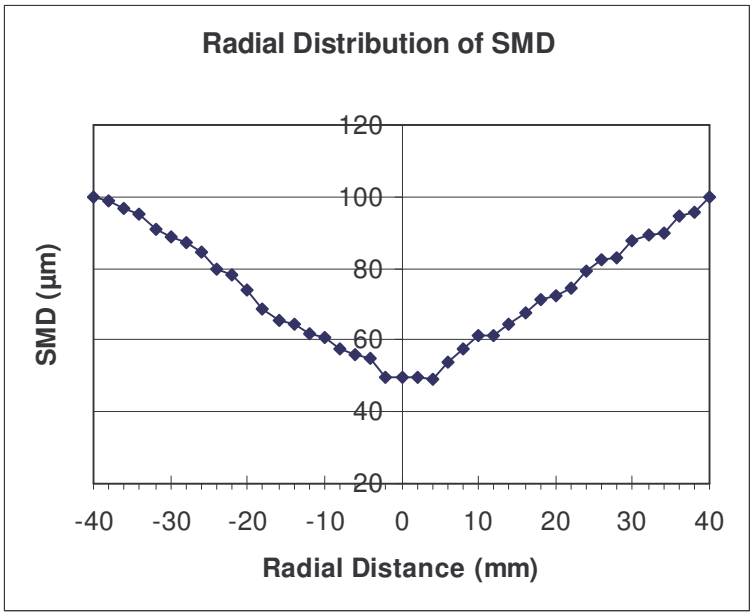

Figure 4.25: PDPA Results for the Build II Preheating Injector

Heated air uniformity TC testing was the next completed test on the preheating "Venturi" injector (Build II). There was some uncertainty upon previous results which required a retest of the injector. The atomizer was tested at eight different points. Test 6 results are shown in Figure 4.28. Test 6 had a 5 pph fuel/water flow rate (H_2O was utilized instead of diesel fuel for safety reasons) and a 25 pph air flow rate. The fuel/water was heated to 200° F at the injector exit. The air was heated to 460° F at the entrance of the injector. The injector and other components were insulated to minimize heat loss.

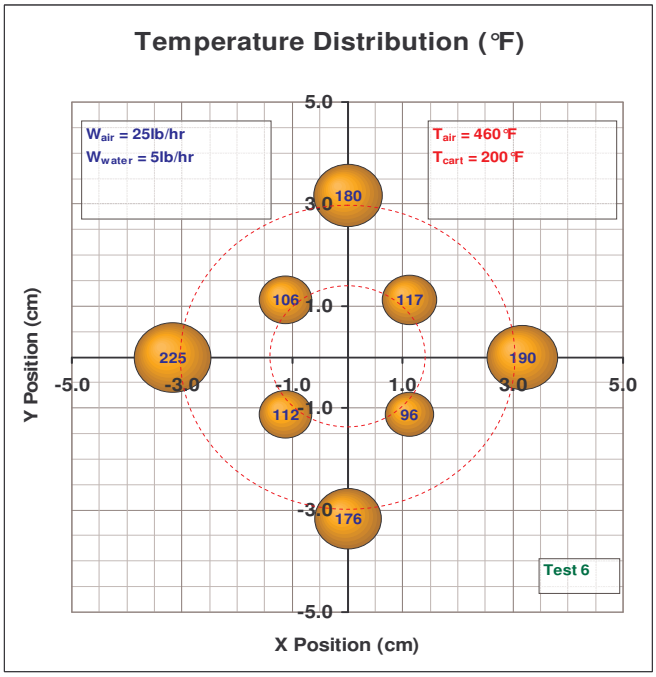

Figure 4.28: Build II Preheating Injector TC Uniformity Testing.

As seen from Figure 4.28 the average temperature of the inner ring of TC's is 108° F with the outer ring being 193° F. There are several theories that may explain this behavior. One of them is that a large recirculation zone is occurring down the nozzle center line. This recirculation zone could possibly pull cooler air from outside the injector. CFD supports this theory (see Section 6.0). Another theory suggests the center is cooler owing to more fuel/water vapor present in the center. The injector was designed to minimize recirculation zones. Because of this the outer air may not be mixing well with the inner column of fuel/water. This could allow for the temperature to decrease due to evaporative cooling. Either way, at this point the Build II injector does not show ideal temperature uniformity.

The next subtask completed of Milestone 3.0 was:

Task 3.11 Optimize feedback sensor location

The preheating injector utilizes a 500 watt electric cartridge heater to preheat the fuel for improved vaporization. The TC used in the temperature controller feedback in Phase I work was located within the fuel passage, near the injection point. Testing indicated that regulating the heater with fuel temperature feedback tended to cause instability, especially when transitioning flowrates or in the event that the fuel boils within the passage. It was apparent that using the base metal temperature near the exit of the atomizer would provide a more stable solution. This location was optimized for best performance. Shown in Figure 4.26 is the isometric view of the test specimen used in Task 2.0 ("back-to-back" coking rig test). The TC was relocated during this test to allow for temperature feedback measurements. Figure 4.27 is a cross-section of this same test specimen. As shown the TC is located near the fuel exit of fuel heating passage. The test specimen has the TC entering from the tip of the nozzle. In actual production the thermocouple will enter through the side of the fuel cartridge. The TC is positioned in such a way as to measure metal temperature near the heated fuel exit. In order to achieve this TC position for the current tests and to allow the inner passage to be removed for study, the TC must enter through the fuel outlet passage (this would not be the case in a production part). This allows for the wall temperature of the fuel passage to be controlled, preventing the heating element from overdriving the system and damaging any components. In this way the fuel temperature is indirectly controlled, and will prevent the heater from undergoing large fluctuations.

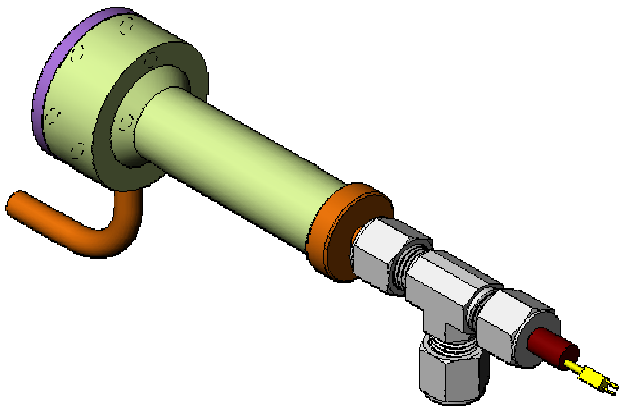

Figure 4.26: Model of Final Assembly with Thermocouple

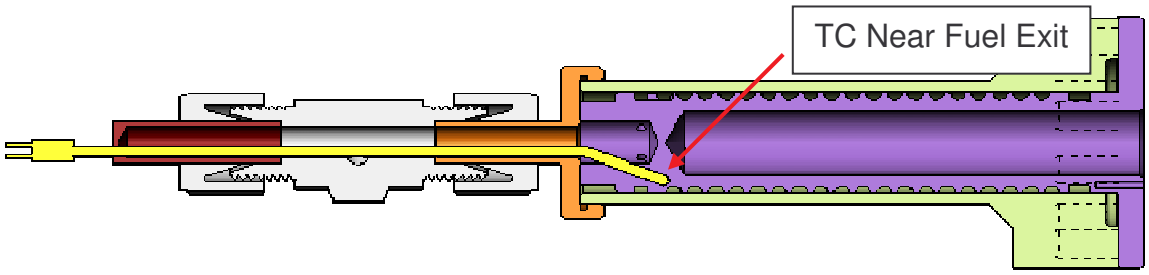

Figure 4.27: Optimized Thermocouple Feed Back Location.

The next subtask completed of Milestone 3.0 was:

Task 3.12 Improve Injector Response Time and Stability During Flow Transition

The injector response time and stability during flow transition was reviewed and completed. Originally there was a possibility of the preheating injector operating diesel fuel in the two phase regime. The idea was to bring the diesel fuel well into its boiling point range (>400°F) and allow fuel to begin to boil before exiting the injector. This type of operation often caused pressure surging and vapor locking within the nozzle. With the redesign of the preheating injector this two phase flow transition was no longer necessary. The current preheating injector preheats the diesel fuel to a temperature just below the minimum boiling point of diesel (~350°F) and then injects this fuel into the mixing chamber. This temperature is more in range of the anti-carbon coatings performance ability. The swirling heated air in the mixing chamber will quickly convert the 350°F diesel droplets into the 800°F diesel vapor. At this point the injector response time in bringing the fuel to 350°F is under 5 minutes which is adequate for fuel cell startup requirements. Since the nozzle is no longer designed for two-phase flow there is no need to optimize the nozzle for fuel phase transition thru the nozzle.

The only subtasks required of Milestone 3.0 that were not completed were:

Task 3.10 Optimize the Heating Efficiency and Miniaturize the Temperature Controller
Task 3.13 Perform Final Injector Tests With Improved Electronic Control

These tasks were reviewed and a miniaturized design was worked out on paper. However, this work was first placed on hold owing to personnel availability. The July - September quarterly financial report showed that very little money remained to complete the project. Milestone 6.0 was originally planned as the optional task in case funds ran short. Per NETL's request, Task 6.0 was brought up to run in parallel with Milestone 3.0 since it was deemed of high importance to the Department of Energy. Engine Components complied with this request. Because of this, funds ran short. Once personnel were available to complete the work of Task 3.10 and 3.13 there were no funds left. Thus, Task 3.10 and 3.13 of Milestone 3.0. were made optional and Milestone 3.0 was closed.

5.0 Milestone 4.0: Construct Integrated Preheating Injector/Mixer System

Milestone 4.0 builds upon Milestone 3.0 by adding a mixing chamber preheating injector developed in Milestone 3.0. Again, Engine Components feels that fuel/air stream preparation prior to the reform or fuel cell is critical to increase fuel cell and reformer life and performance. Because of this, Engine Components proposed a preheating simplex injector mixing system that could prepare the fuel and air prior to reformer injection that could accomplish these goals. The goals of this mixing chamber were to evenly mix the fuel and air throughout the mixing chamber exit and decrease the fuel and air pressures to as low as possible so that low cost solutions could be utilized to supply the fuel and air. This section summarizes the work and testing that was accomplished in developing a Preheating Simplex Injector Mixer.

Milestone 4.0 work began during the third quarter of this six quarter project and was not fully completed until the fifth quarter of the project. It was worked in parallel to Milestone 3.0. The first sub task that was completed was:

Task 4.1 Evaluate New Mixing Chamber Configurations for the Preheating Simplex Injector

This task is simply an evaluation of previous configurations and work completed on projects similar on nature to this project. One of the first initial concepts reviewed which became the starting point for this milestone can be seen in Figure 5.1 and Figure 5.2. Figure 5.1 shows the isometric view and Figure 5.2 shows the cross section of the atomizer and top portion of the mixing chamber. As shown, this mixing chamber top utilizes an extra drilled air swirler to encourage air and fuel mixing and discourage fuel from collecting on the mixing chamber's walls. The drilled hole air swirler could possibly have various air hole angles to accomplish the mixing. Again this concept was chosen as the platform for the mixing chamber build.

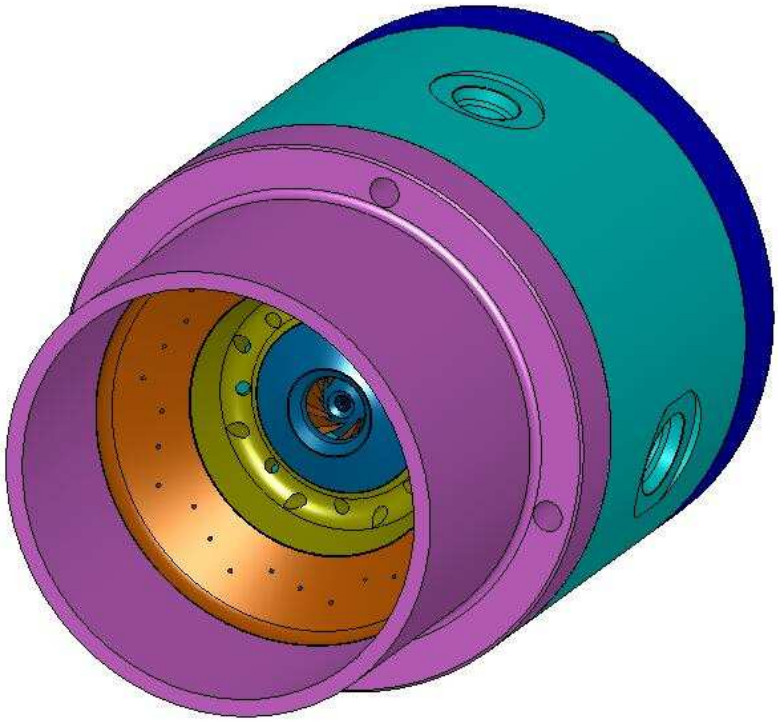

Figure 5.1: Isometric View of the First Mixing Chamber Option

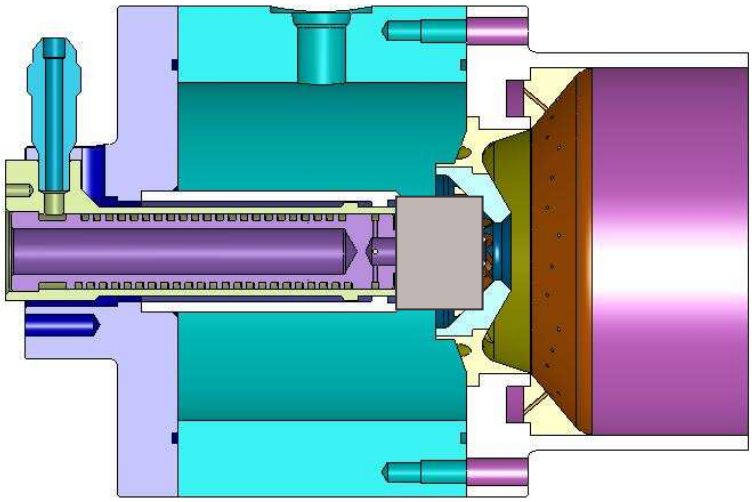

Figure 5.2: Cross Section of the First Mixing Chamber Option

With this platform selected the following task was then completed:

Task 4.2 Prepare Solid Model and Drawings For the Improved Mixing Chamber

The models and drawings were completed for this mixing chamber. This mixing chamber was customized to work seamlessly with the Build II ("Venturi") injector discussed in Section 4.0. Figure 5.3 shows the cross section of the "Venturi" atomizer and a completed mixing chamber. As shown, this mixing chamber utilizes a drilled-hole air swirler/diffuser to encourage air and fuel mixing near the mixing chamber swirler. These discrete air jets would also discourage fuel from collecting on the mixing chamber's walls. The drilled-hole diffuser has various air hole configurations to accomplish different amounts of mixing. These various diffuser configurations can be seen in Figures 5.4 and 5.5. These four configurations were tested to determine the optimum configuration (results discussed later in this section). In addition, the assembly has been designed to allow the center mixing chamber swirler to be located in several positions. This will allow for optimization of the swirler position.

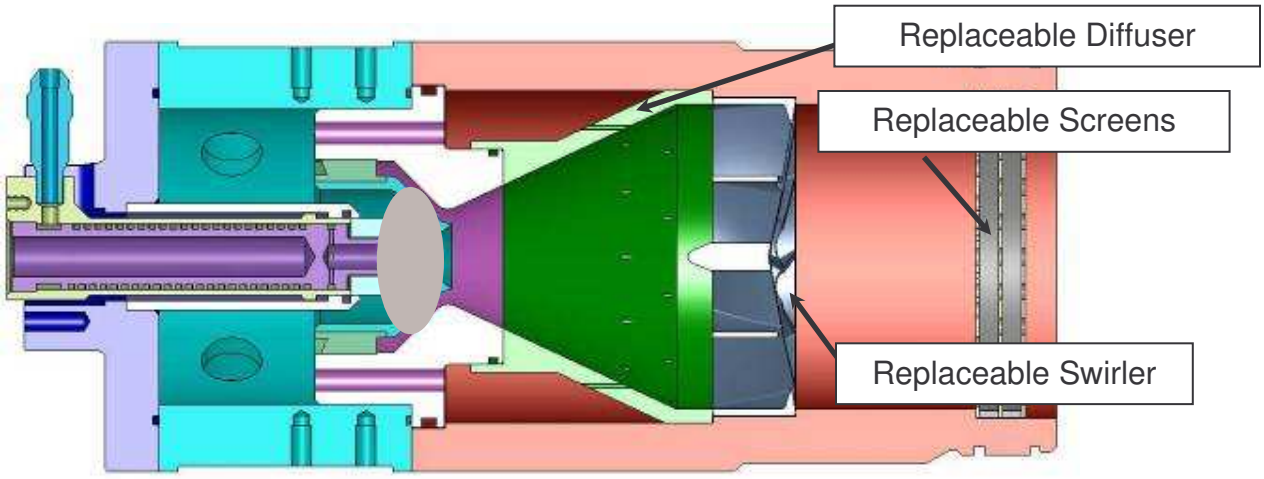

Figure 5.3: “Venturi” Atomizer and Mixing Chamber Cross Section

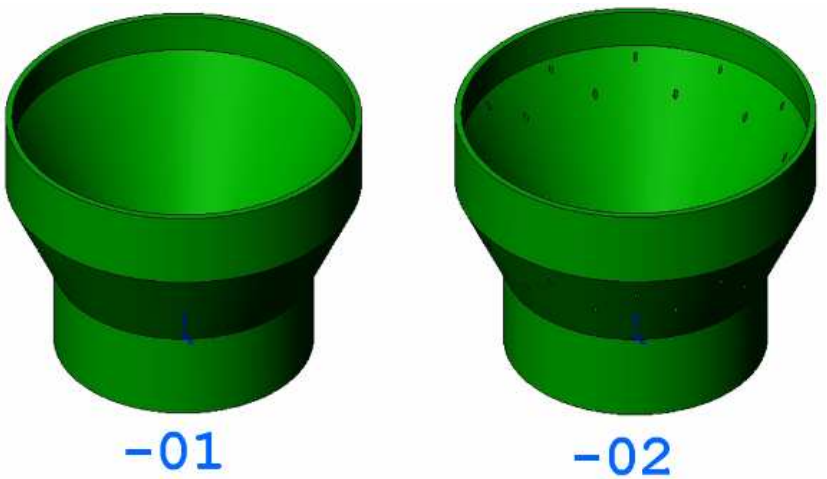

Figure 5.4: Dash 1 & 2 Mixing Chamber Diffuser Insert Options

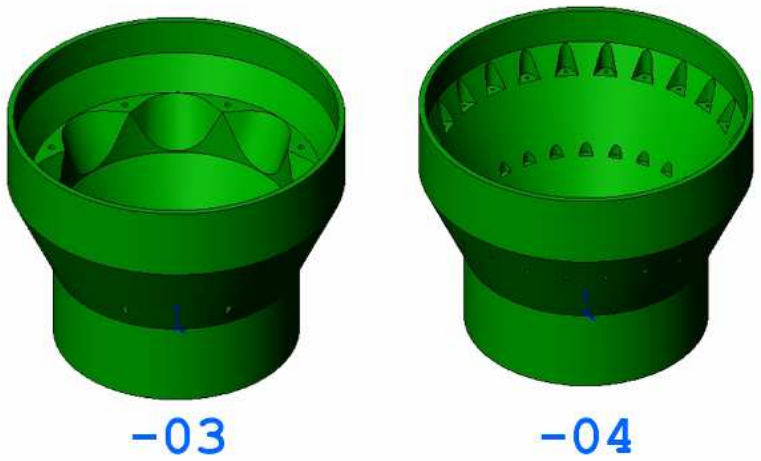

Figure 5.5: Dash 3 & 4 Mixing Chamber Diffuser Insert Options

After the drawings were completed the next task was:

Task 4.3 Fabricate and Assemble Mixing Chamber

The mixing chamber parts were manufactured and assembled in about two months time. The completed assembly and component pieces can be seen in Figures 5.6 through 5.10. As mentioned multiple configurations were tested to determine the optimum configuration. The testing will be discussed later in this section.

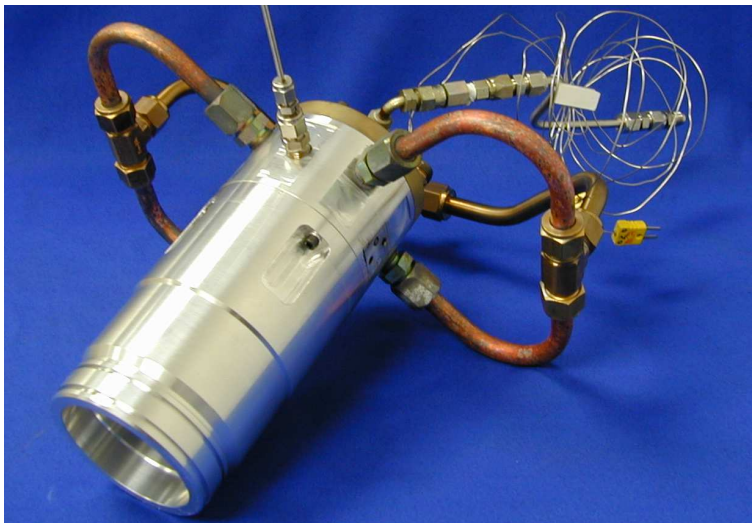

Figure 5.6: Completed Build II Injector and Mixing Chamber

Figure 5.7: View of Swirler Inside the Mixing Chamber

Figure 5.8: View of Removable Screens Inserted Into Mixer

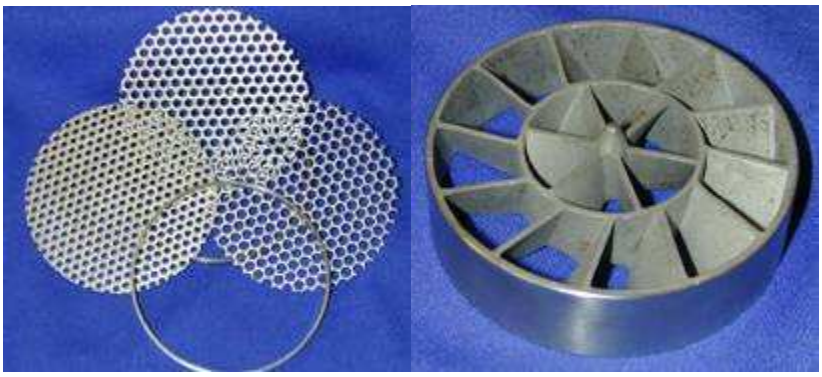

Figure 5.9: Screens and Swirler Used in the Mixer

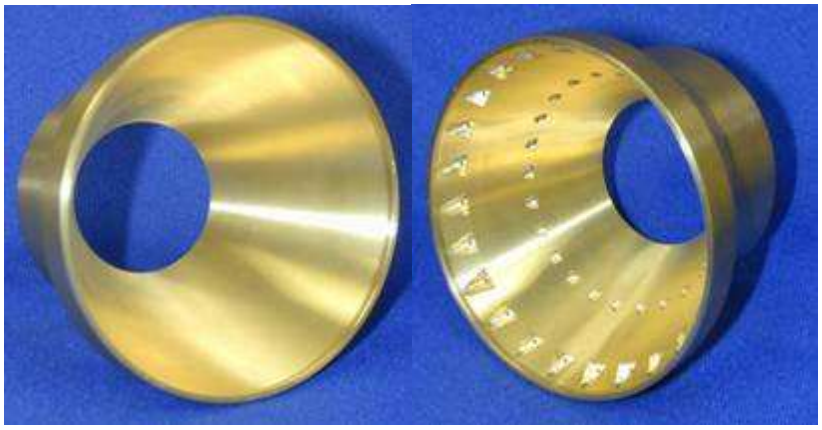

Figure 5.10: Alternate Diffuser Configurations Used in the Mixer

With all the components created the assembly was finalized and readied for testing. The following is a list of the sub tasks that were completed on the mixing chamber:

Task 4.4 Investigate Effect of Fuel Injection Location
Task 4.5 Optimize Injector Housing
Task 4.6 Optimize Swirl Mixer location, Configuration and Fabrication method
Task 4.7 Investigate Effect of Swirl mixer and Perforated Screens on fuel Mixture Characteristics
Task 4.8 Conduct Hot Flow Tests for the Optimized Injector/Mixer System

The mixing chamber assembly and its multiple diffuser configurations were first tested on the optical patternator. As mentioned in previously in this section, this mixing chamber has been customized for the Build 2 injector; the cross section is shown in Figure 5.3. As seen, this mixing chamber utilizes an exchangeable drilled-hole diffuser section to encourage air and fuel mixing near the mixing chamber swirler. These discrete air jets should also discourage fuel from collecting on the mixing chamber's walls. The drilled-hole diffuser has various air hole designs to test different methods of mixing. The resultant testing on the optical patternator can be seen in Figures 5.11 through 5.14. This testing did not include the replaceable swirler or screens shown in Figure 5.3. The swirler and screen caused large fuel droplets that confounded the optical patternator. It is theorized that the large drops would not be present if

the test was performed at operating conditions, as the fuel would be vapor before it came in contact with these components. As it is, we are not able perform these test at operating conditions because of test stand limitations, therefore the fuel is at ambient temperature and the droplets coalesce on any mixing components in the flow path. The data shown in this section was performed at ambient conditions with MIL-PRF-7024 Type II test fluid.

The following test data shown in Figures 5.11 thru 5.14 were with a fuel flow rate of 5pph and the air flow rate of 25pph. Figure 5.11 shows the patternation results with the -01 diffuser. Figure 5.12 shows the -02 results. Figure 5.13 shows the -03 results. Figure 5.14 shows the -04 results. These figures show the spray contour results of the heaviest fuel locations as it leaves the mixing chamber. The ideal flow would be evenly distributed fuel across the mixing chamber exit. The most even distribution can be seen in Figure 5.11 (-01 diffuser). An equation was developed that converted the spray contour into a single Radial Coefficient value. The lower the value, the more uniform the spray distribution. Figure 5.15 shows the results of all the testing and gives the Radial Coefficient. Figure 5.15 also includes the 9 pph fuel and 45 pph air test point. As seen, Diffuser -01 had the most uniform spray and thus the lowest Radial Coefficient.

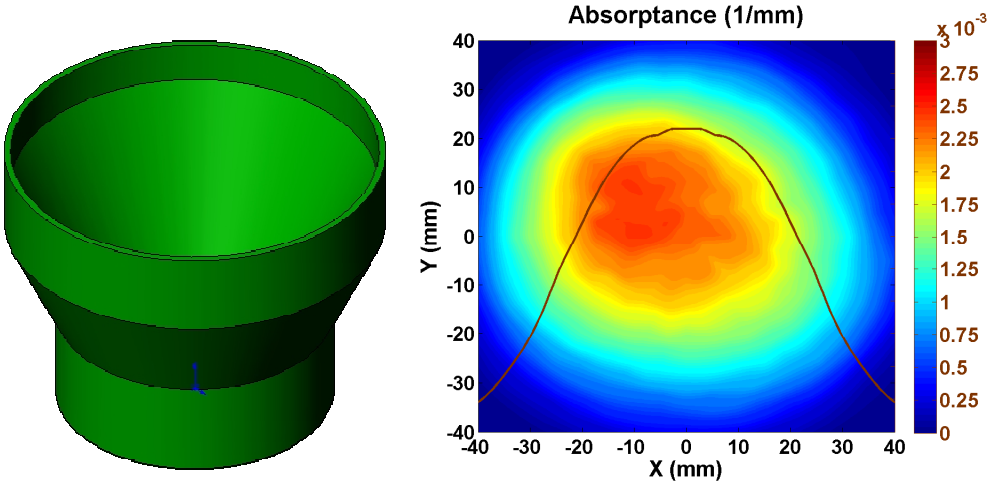

Figure 5.11: Diffuser -01 and Patternation Results

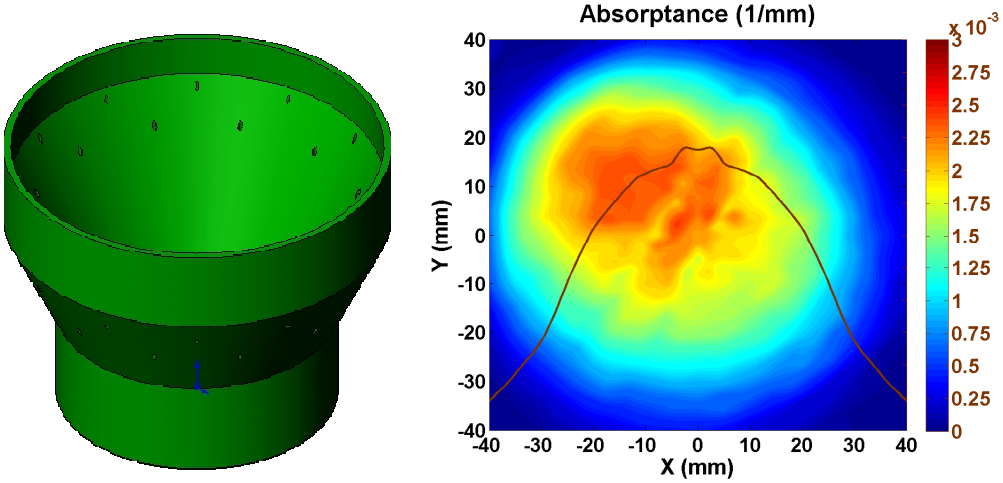

Figure 5.12: Diffuser -02 and Patternation Results

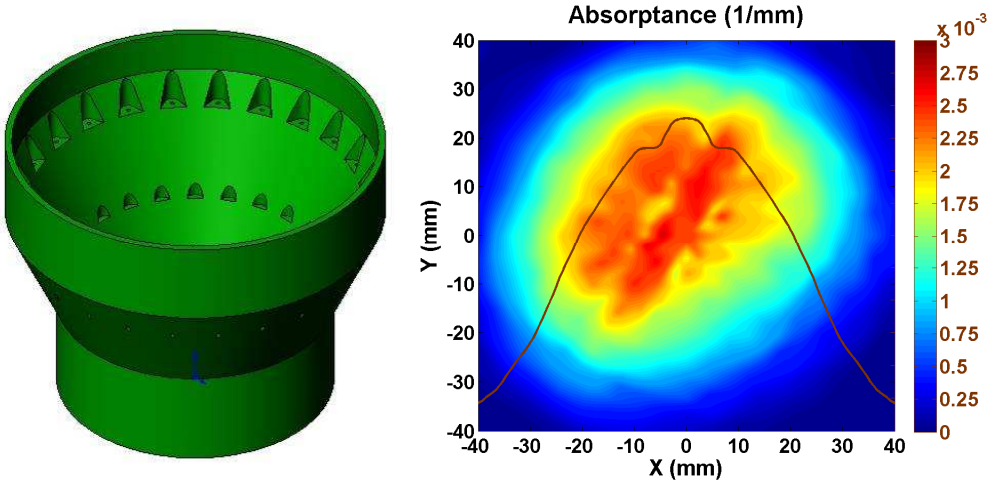

Figure 5.13: Diffuser -03 and Patternation Results

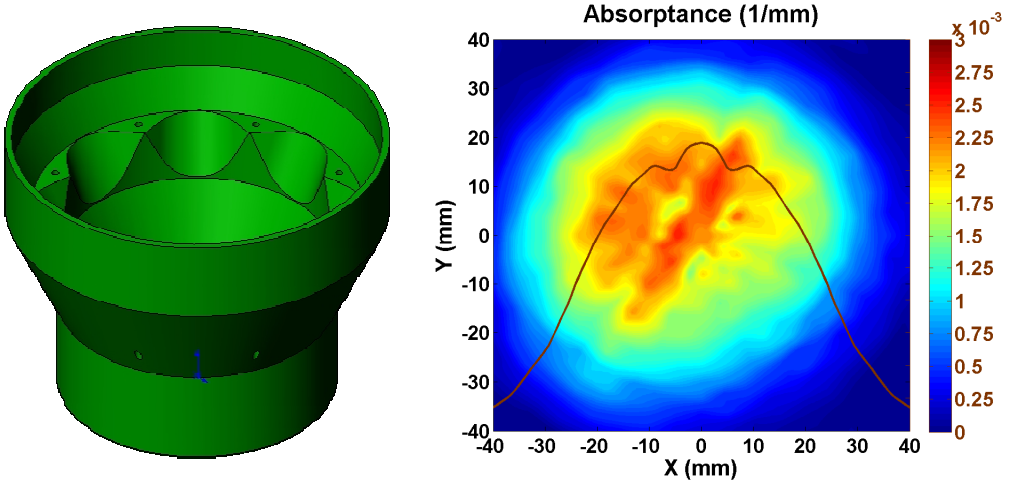

Figure 5.14: Diffuser -04 and Patternation Results

Effect of Diffuser on Fuel Distribution						
Test	Diffuser	Avg. Rad. Absorp.	Absorp. STD	Radial Dist.Coeff.	Avg. Radial Dist. Coeff.	Overall Radial Dist. Coeff.
-001	-01	0.00114	0.00010	0.085	0.083	0.077
-002	-01	0.00108	0.00009	0.081		
-003	-01	0.00115	0.00009	0.074	0.072	
-004	-01	0.00117	0.00008	0.069		
-005	-02	0.00098	0.00009	0.088	0.088	0.083
-006	-02	0.00097	0.00009	0.088		
-007	-02	0.00114	0.00009	0.082	0.079	
-008	-02	0.00126	0.00009	0.075		
-009	-03	0.00101	0.00009	0.091	0.091	0.087
-010	-03	0.00103	0.00009	0.091		
-011	-03	0.00111	0.00009	0.082	0.083	
-012	-03	0.00117	0.00010	0.083		
-013	-04	0.0009	0.00009	0.094	0.094	0.090
-014	-04	0.0009	0.00008	0.093		
-015	-04	0.00126	0.00011	0.086	0.086	
-016	-04	0.00122	0.00010	0.085		

Figure 5.15: Table of Overall Diffuser Performance

After both Computational Fluid Dynamic and experimental testing was performed, a mixing chamber and sub-components were selected based on fuel concentration and velocity uniformities. Figure 5.16 shows the fuel distribution measured one inch from the exit of the mixing chamber for the diffuser configuration which produced the most uniform distribution. Figure 5.17 illustrates the velocity magnitude distribution throughout the entire mixing chamber. The simplest diffuser was selected since it produced the most even fuel distribution at the chamber exit (with no swirler or screens). More complicated geometries were tested that added additional air at various locations. These other diffuser configurations were intended to promote mixing and to break up the swirl produced at the injector while reducing re-circulation. Such configurations added to the already high axial velocity near the outer wall, and would have therefore caused more fluid to pass through the outer section of the large mixing swirler downstream of the diffuser, reducing its effectiveness.

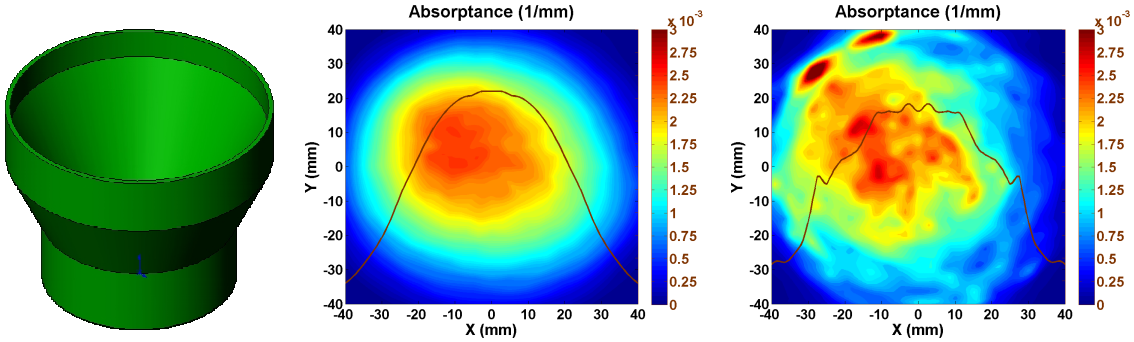

(a) (b) (c)

Figure 5.16: Results from Laser Extinction Topography Testing
(a) Optimum Diffuser (b) $\dot{m}_{air} = 25lb/hr$, $\dot{m}_{fuel} = 5lb/hr$ (c) $\dot{m}_{air} = 45lb/hr$, $\dot{m}_{fuel} = 9lb/hr$

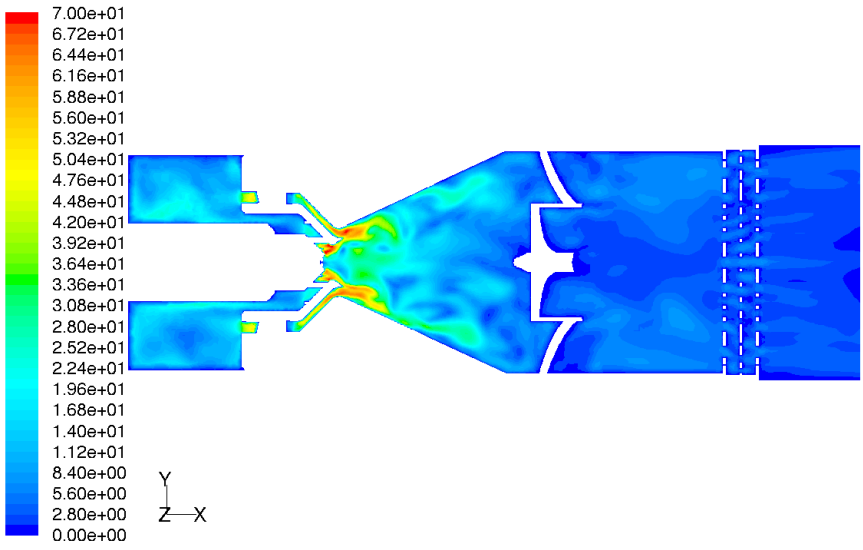

Figure 5.17: Snap-Shot from Time Accurate Computational Fluid Dynamic Animation of Complete Mixing System.

The downstream swirler has inner and outer sections that are respectively counter and co-swirling with respect to upstream swirler at the injection point. The swirler is intended to establish a shear layer generating a more turbulent region in which swirl strength is reduced and more rapid mixing can occur. However, the chamber length is not sufficient for the swirl to be completely eliminated before exiting. Three perforated metal plates with staggered hole-patterns were added near the exit of the mixing chamber to even out the velocity distribution and to eliminate any swirl from the exit flow. These plates also have the added bonus of aiding fuel and air homogeneity. The mixing swirler was positioned such that it is not too close to the fuel injection point in order for the fuel to have adequate distance to vaporize. This reduces the risk of liquid droplets collecting on the swirler surface and producing carbon deposits. Sufficient distance between the swirler and screens was provided to ensure that the more turbulent region downstream of the swirler has enough distance to enhance species concentration uniformity before entering the screens. Though the screens aid in mixing, they are not sufficient on their own, and their main purpose is to even out the velocity profile. The final mixing chamber configuration can be seen in Figure 5.18.

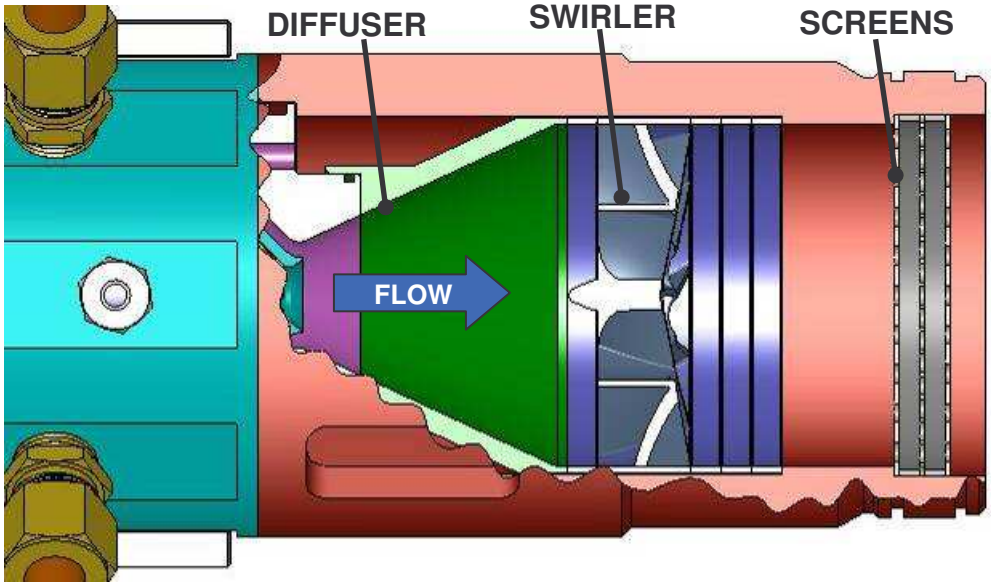

Figure 5.18: Cut-Away Section View of Mixing Chamber for Preheat Injector.

This completes the work performed on the mixing chamber development (Milestone 4.0). Much insight has been gained by the work in this section. This injector/mixing chamber has performed as desired. As always, there is room for improvement. However, the assembly is ready to be moved from the research phase to a production application if the right application can be found.

6.0 Milestone 5.0: Complete CFD analysis and Design of Experiment Study

Milestone 5.0 was created and accomplished to help confirm the results determined in Milestone 3.0 and 4.0 and to help developed improvements to the injector/mixer system.

Again, Engine Components feels that fuel/air stream preparation prior to the reformer or fuel cell is critical to increase fuel cell and reformer life and performance. Because of this, Engine Components developed a preheating simplex injector mixing system (see Sections 4 & 5) that could prepare the fuel and air prior to reformer injection. The goals of this injector and mixing chamber were to evenly mix the fuel and air throughout the mixing chamber exit and decrease the fuel and air pressures as low as possible so that low cost solutions could be utilized to supply the fuel and air. This section summarizes the CFD work that was accomplished to develop the Preheating Simplex Injector Mixer and verify the actual measurement results.

Milestone 5 began very early in the program but was not fully completed until the sixth quarter of the project. The first sub task that was completed was:

Task 5.1 Perform CFD Analysis for the Preheating Simplex Injector/Mixer Having a Large Plenum as the Outlet Boundary

The goal of the analysis was to determine an Inner and Outer Air Swirler combination that would lead to better mixing. These results are shown in Figure 6.1. The scale has been removed from the CFD results but the flow field trends can still be seen.

CFD Design Point Conditions For Figure 6.1 are:

Fuel Flow:	9.3 pph	Air Flow:	46.7 pph
Air Pressure:	3” H2O	Air Temperature:	375° F
Air Effective Area:	0.271 sq.in.		

One of the ideas pursued using CFD was to create a recirculation zone between the Outer Air Swirler and the Inner Air Swirler. The idea was to generate an area of mixing between the two flow fields that would allow the fuel to be evenly disbursed. However, as seen in Figure 6.1, this recirculation zone did not develop in the two modifications (MODs) analyzed. MOD 1 and MOD 2 utilized a different air swirler than that of the wax prototype testing. One positive that CFD was able to show is that this swirler concept allows the air to constantly wipe the outer walls. This may help remove any fuel from depositing on the outer wall and keep it free from carbon formation. Build 1 of the preheating injector did not utilize any of the swirler configurations shown in Figure 6.1. However, build 2 did.

Figure 6.2 shows the velocity contours of the Venturi Build configuration. One of the goals of this configuration was to avoid flow field separation on the diffuser wall. The idea is to reduce fuel build up on the diffuser wall and reduce recirculation zones which could lead to spontaneous ignition points. This atomizer successfully avoids flow separations near the diffuser wall. Testing was conducted on this atomizer to determine how well the fuel and air are mixed (see previous section).

One of the items noticed from this CFD result is the strong air jets found in the air box. As seen from Figures 6.2 & 6.3 the air box has two strong air jets just upstream of entrance of the air swirlers. These air jets are caused by the two inlet air ports on the air box. The air ports on the air box were not optimized for this injector. These air jets could have an effect on air flow thru

the swirlers. To reduce this affect, a new air box was created with four air ports instead of only two. This air box improvement reduced any possible effects caused by these strong air jets.

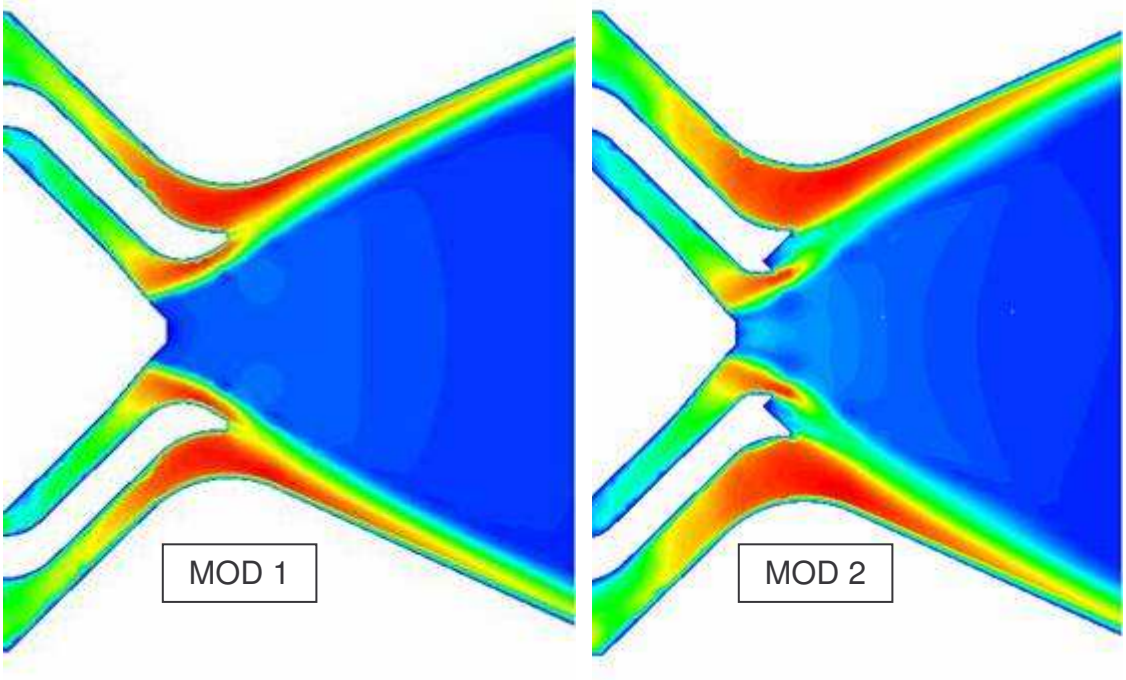

Figure 6.1: CFD Modeling Of Preliminary Concept MOD 1 and MOD2

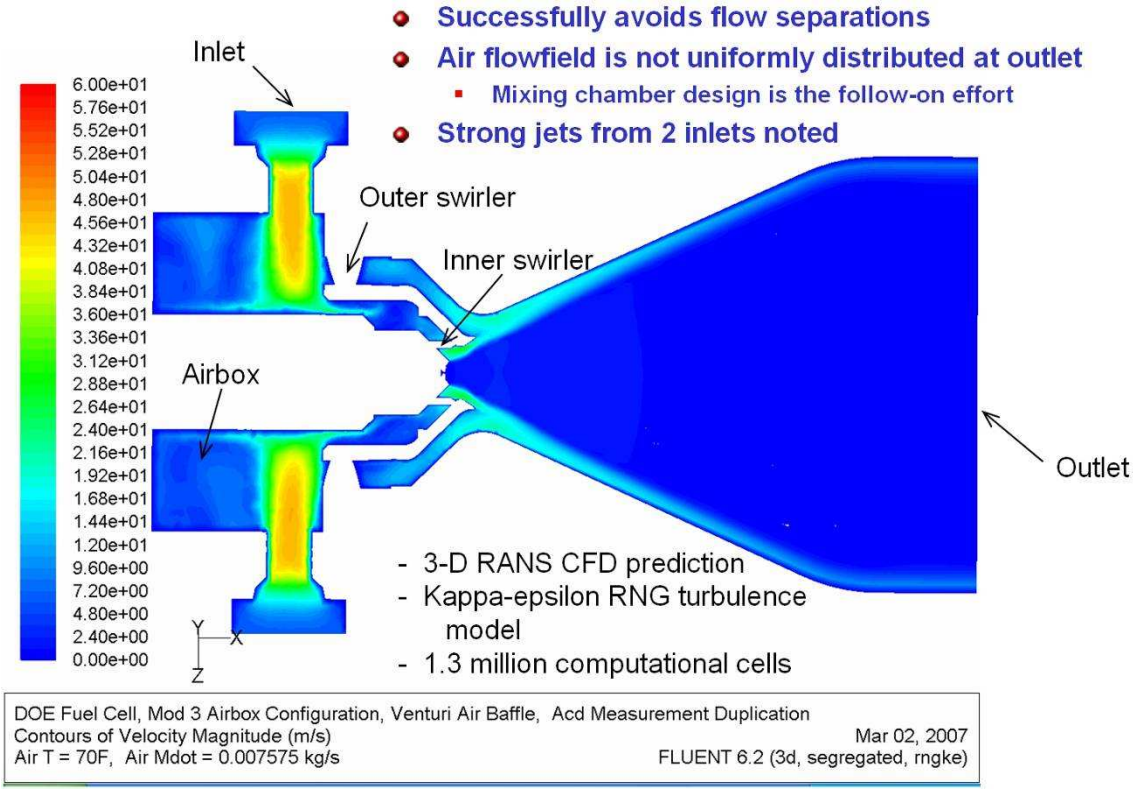

Figure 6.2: Velocity Contours of the Venturi Atomizer Configuration

Figure 6.3 shows the air flow velocity vectors on the surface of the outer air swirler as well as velocity vectors down the atomizer center plane. These velocity vectors are used to determine recirculation zones in the flow field. As shown the velocity vectors are as desired and there are no recirculation zones near the diffuser walls.

Figure 6.4 shows the tangential velocity contours at a plane just down stream of the atomizer exit. This figure clearly shows the counter rotating flow field generated by the outer air swirler. The counter rotation caused by the outer swirler is designed to cause a shear layer between the inner and outer air flows. It is hoped that this shear layer will promote fuel mixing between the inner and outer air flows. Tests with the optical patternator were used to determine if the fuel flow is more uniformly distributed with this configuration.

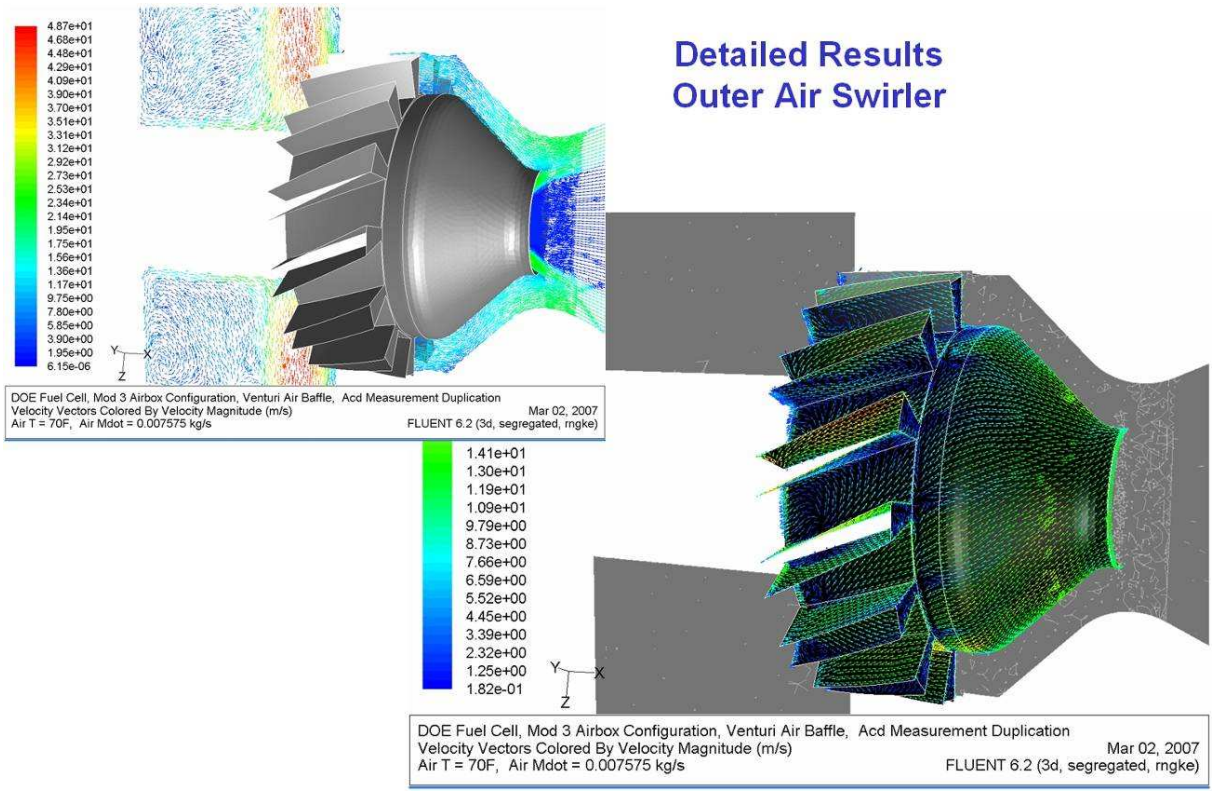

Figure 6.3: Velocity Vectors of the Venturi Atomizer Configuration

The final CFD required for Task 5.1 is shown in Figure 6.5. Figure 6.5 shows axial (X-axis) velocity contour predictions of this assembly. This is a steady state prediction of the baseline assembly. It utilizes the no-hole diffuser, mixing swirler, and three flow straitening screens. Figure 6.5 is at a 10 kilowatt test point with 400°C inlet air. The CFD results shown in Figure 6.5 show a very large recirculation zone down the atomizer center line. This recirculation zone helps explain the large temperature variations seen during the heated air testing. See the Milestone 3.0 section for more information regarding the heated air testing. This CFD model was also run in a “time accurate” solution. This “time accurate” solution was used to determine the unsteadiness of the flow field and possibly resolve the recirculation zones.

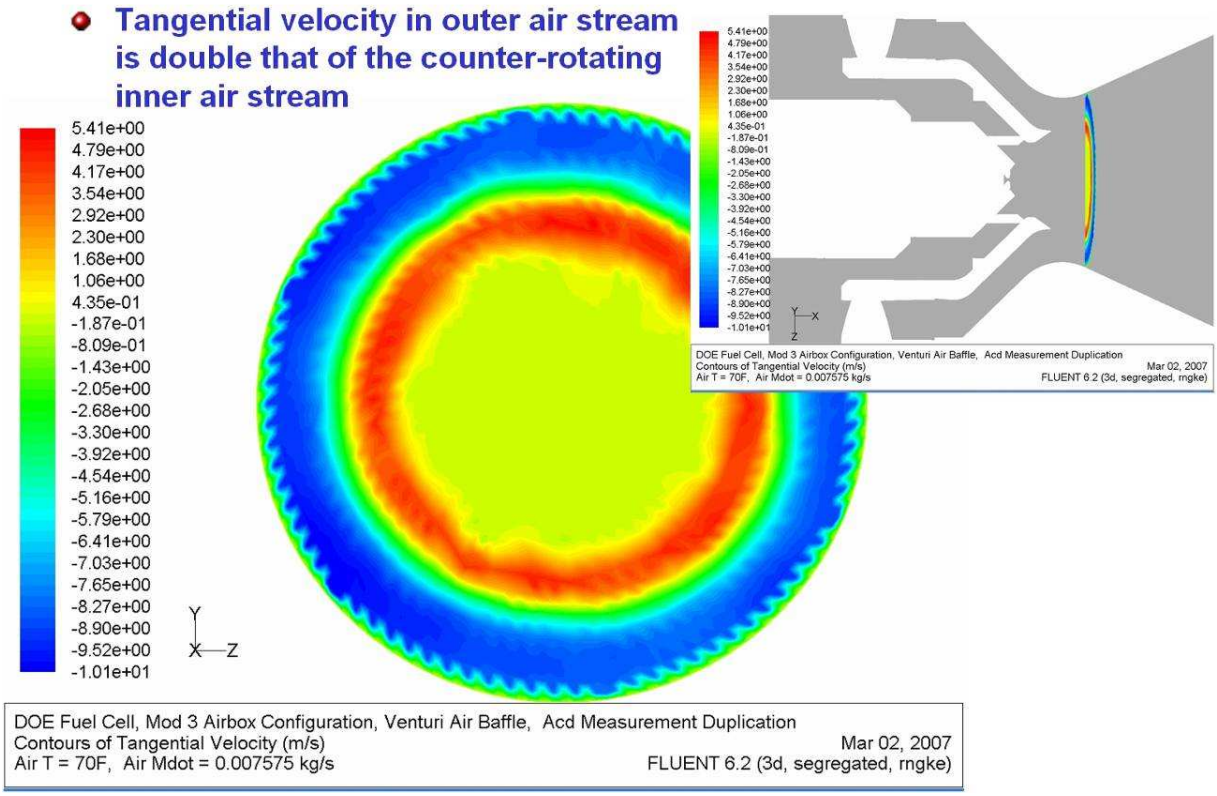

Figure 6.4: Tangential Velocity Contour of the Venturi Atomizer

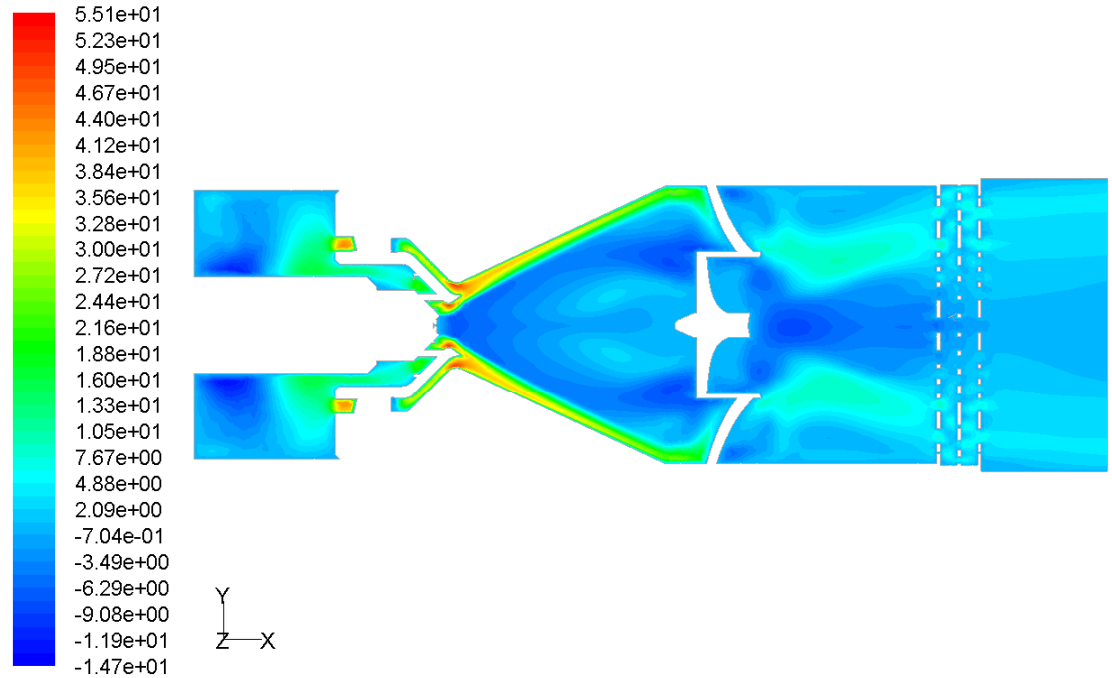

Figure 6.5: X Axis Velocity Contour Predictions

Task 5.2 Conduct Flow Field Measurements to Validate CFD Predictions

The original intent of Task 5.2 was to measure the fluid mixture velocity exiting the mixing chamber (air and fuel mixture). This was to be accomplished by use of a pitot tube. This did not work as originally planned. The CFD predictions suggested that the fluid velocities would be extremely low exiting the mixing chamber (very low inlet pressures). It was determined that the accuracy of the Engine Components pitot tube was not enough to resolve the fluid flow rates. The velocities are low enough to be near the noise floor of the test device. CFD does confirm a low fluid velocity near the mixing chamber exit. Engine Components was unable to determine exactly how they compare to each other but did confirm that the velocities were indeed very low.

Task 5.3 Perform CFD Analysis for the Preheating Simplex Injector/Mixer Having a Simulated Reactor as the Outlet Boundary

CFD was further developed on the build 2 preheating injector and mixing chamber by completing CFD with a simulated reformer reactor as the outlet boundary. Figure 6.6 shows axial velocity contour predictions of this assembly first without the reformer boundary. This figure is a snap shot of a time-accurate CFD solution. This time accurate solution shows the unsteadiness of the air flow field. It also shows the large recirculation zone down the center of the mixing chamber. This time-accurate solution utilizes the no-hole diffuser (Diffuser -01 shown previously), mixing swirler, and three flow straightening screens (not shown).

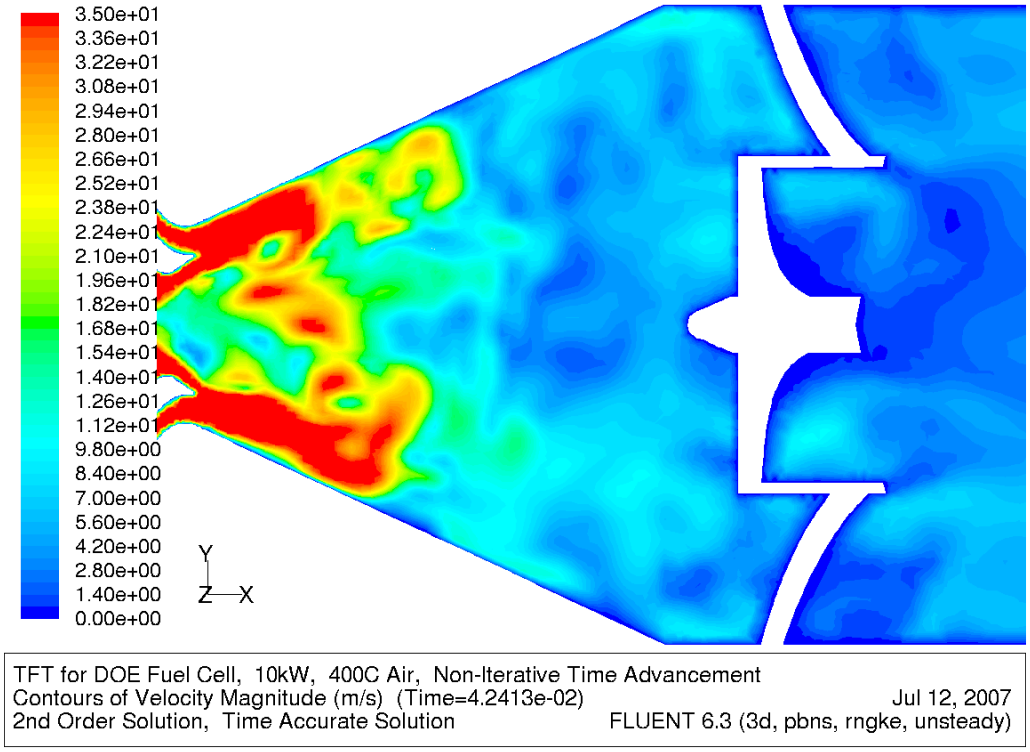

Figure 6.6: Preliminary X Velocity Contours Predictions

Figure 6.6 is at a 10 kilowatt test point with 400℃ inlet air. The CFD results shown in Figure 6.6 show a very large recirculation zone down the atomizer center line. The goal was to minimize this recirculation zone. It appears that this was not accomplished in this build. This recirculation zone helps explain the large temperature variations seen during the heated air testing discussed previously.

Figures 6.7 thru 6.13 are the results of this CFD analysis with a simulated reformer down stream of the injector. Figure 6.7 is a snap shot of the time-accurate animation solution. The simulated porous medium reformer is just down stream of the screen baffle plates and is modeled as 0.04% pressure drop. Figures 6.7, 6.8, and 6.9 show that the simulated porous medium does not affect the large recirculation zone down the injector center line near the fuel injection point. This large recirculation zone was shown previously in this section.

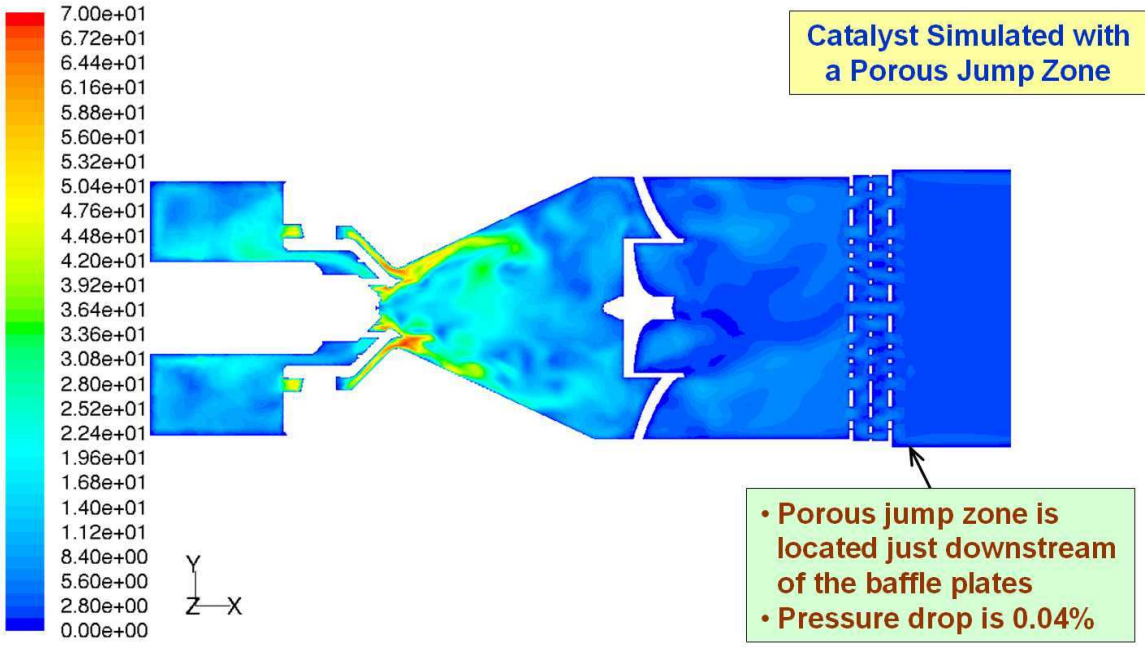

Figure 6.7: Velocity Contours of Entire Mixing Chamber

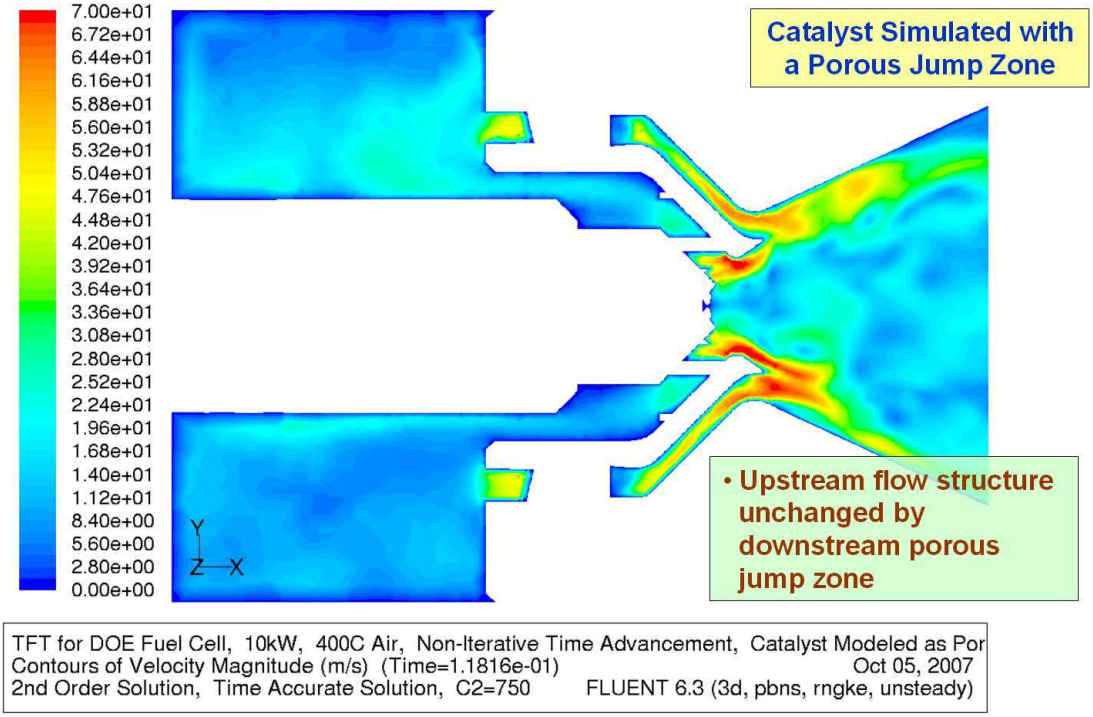

Figure 6.8: Velocity Contours Showing the Exit of the Injector

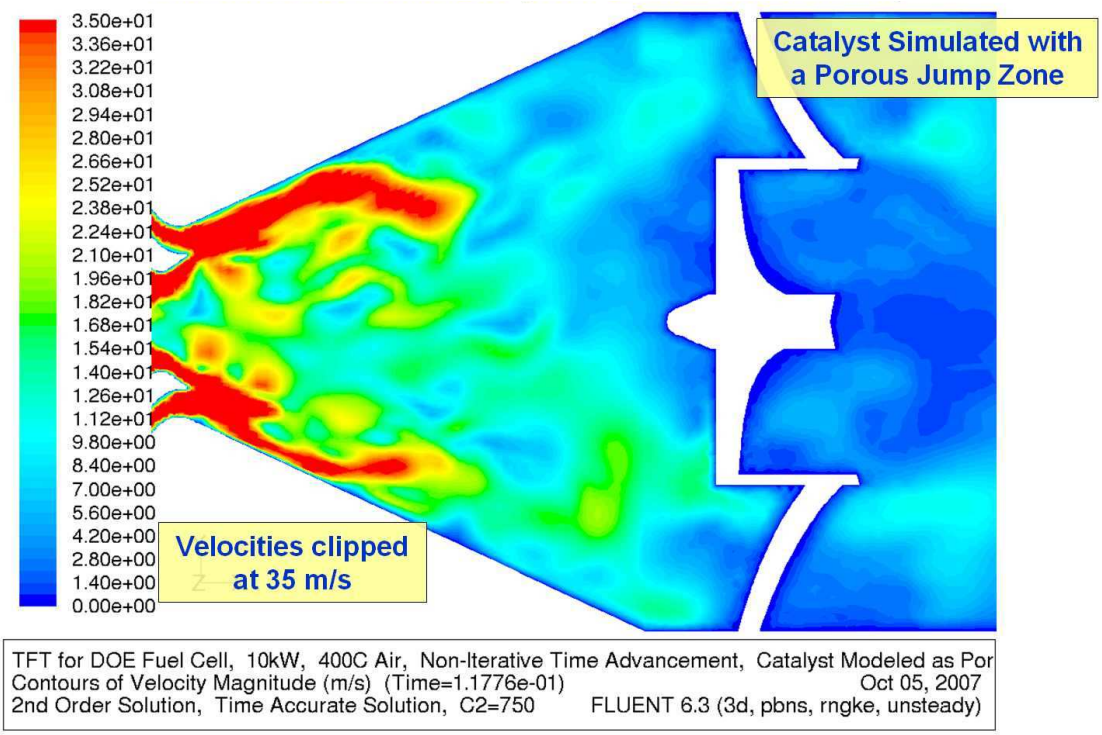

Figure 6.9: Velocity Contours of Injector Exit and Large Mixing Chamber Swirler.

Figure 6.10 shows the pressure contours near the flow distribution screens and the simulated porous medium. As seen the pressure contours even out as the flow passes through the screens. The pressure drop near the simulated porous medium can be clearly seen near the

flow distribution screens. Figure 6.11 shows the Time Accurate velocity contours of this same area. Some of the unsteadiness down the chamber center line is dampened out because of the porous medium. This can be better seen in Figure 6.12 and Figure 6.13.

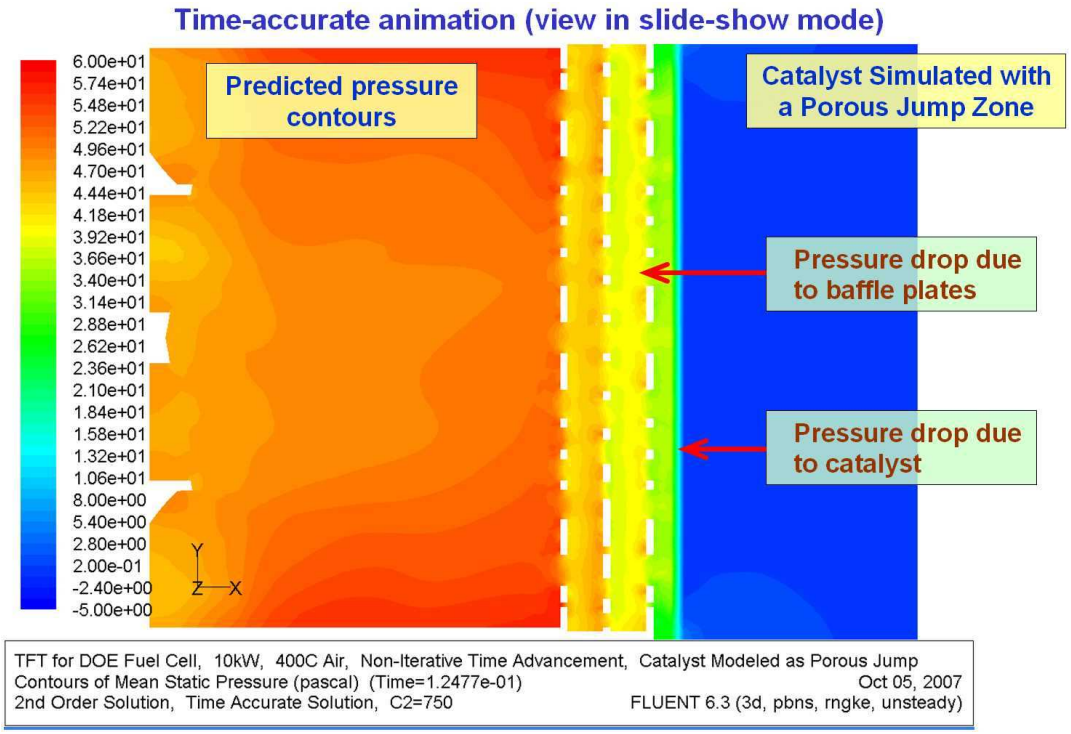

Figure 6.10: Pressure Contours near the Screens and Simulated Porous Medium

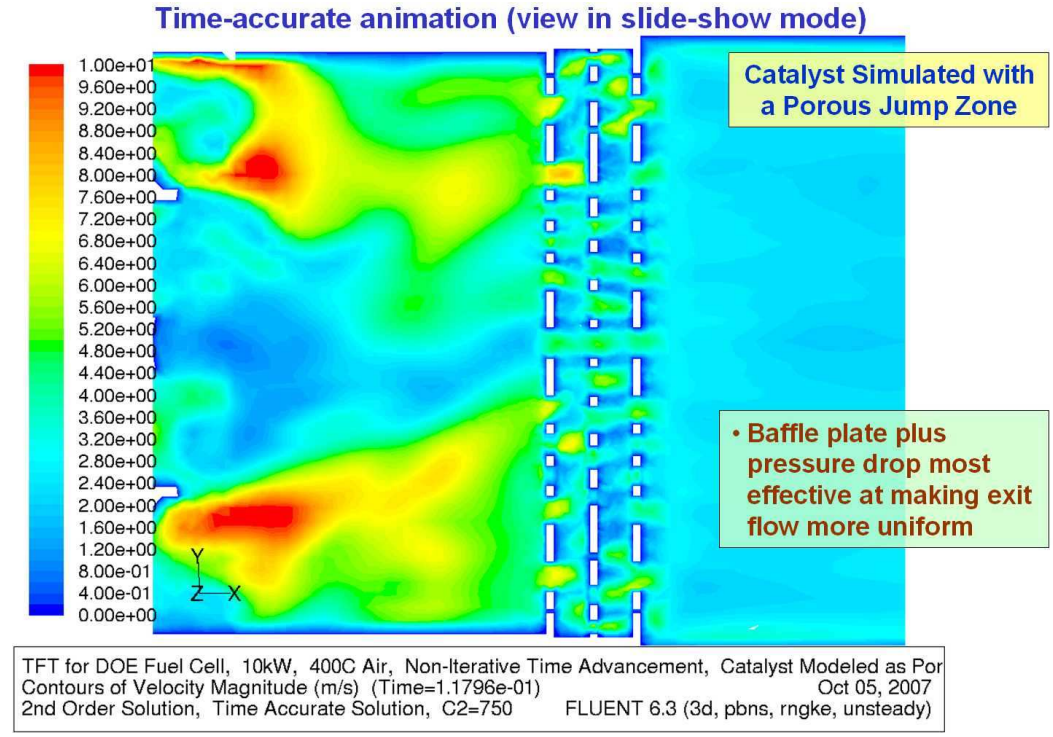

Figure 6.11: Velocity Profiles near the Screens and Simulated Porous Medium

Figure 6.12 shows the CFD results of the baseline atomizer/mixer (no porous medium near the mixing screens). It is important to note that Figure 6.12 and 6.13 are Time-Averaged solutions (not time accurate). This means that Figure 6.12 and 6.13 are average velocity contours. They do not vary with time and do not show the fluctuations in the flow field. Figure 6.13 shows the CFD results of the atomizer/mixer with a porous medium in place. As shown in Figure 6.5 there is a low velocity zone on the centerline (possible recirculation zone) near the mixing screens. This low velocity zone is not present when the porous medium is added to the model.

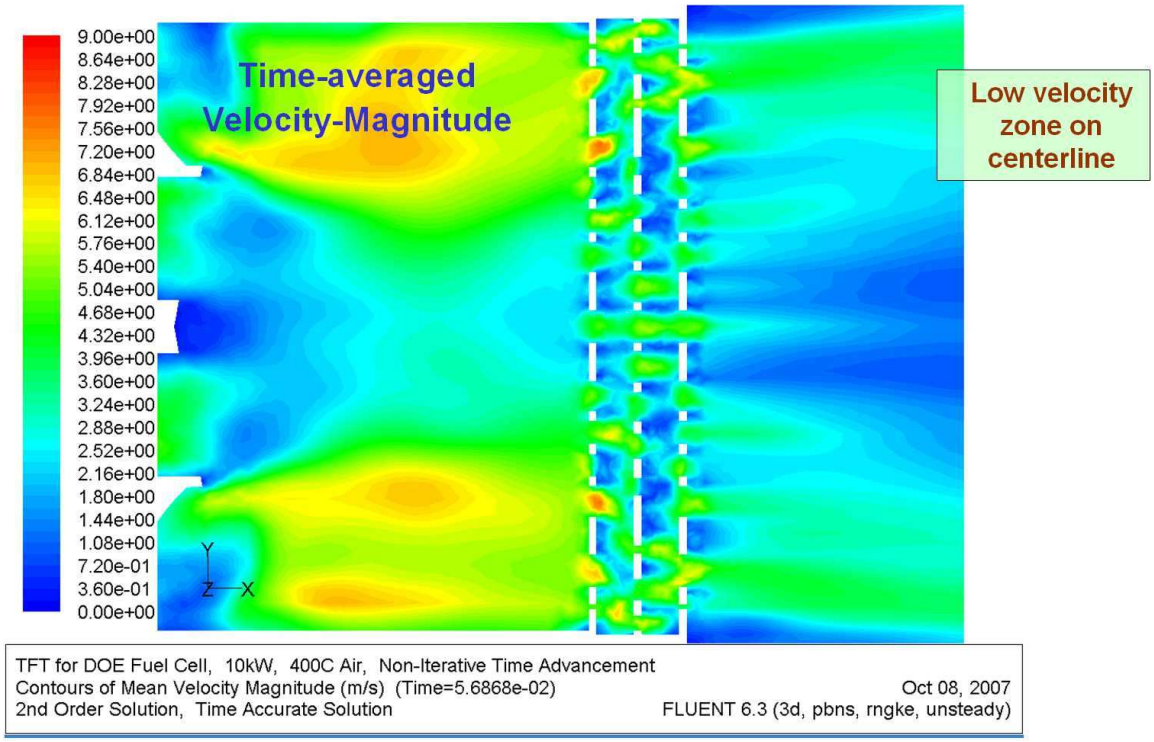

Figure 6.12: Baseline Time Averaged Velocity Contours (No Simulated Porous Medium)

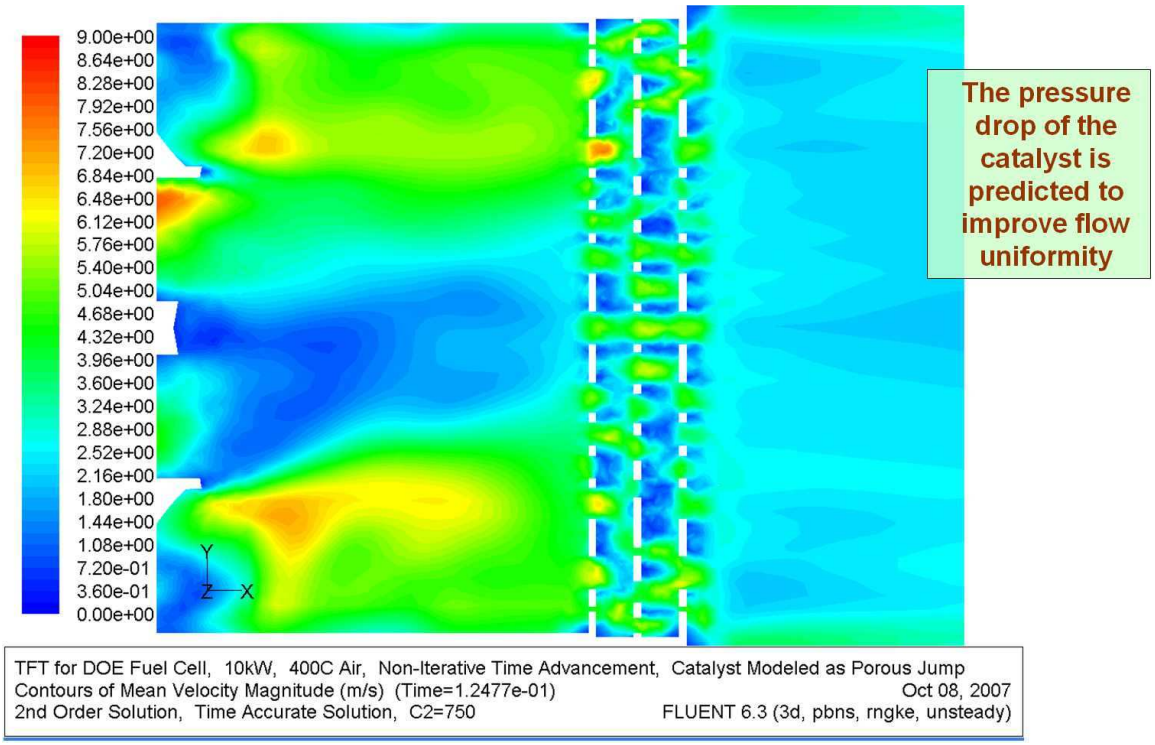

Figure 6.13: Time Averaged Velocity Contour with Simulated Porous Medium

Task 5.4 Conduct FE Analysis For the Injector Thermal and Material Stress Improvement

One of the goals of the Finite Element Analysis (FEA) was to design a nozzle that will keep the fuel wetted wall temperatures below 450°F while heating the fuel to 350°F at the injector exit. The two sources of heat for the fuel are the heater cartridge and the air entering the swirler passages. Another goal of this FEA is to minimize the amount of heating required by the electric cartridge heater. The less electricity required by the nozzle the more efficient the injector system could be.

Figure 6.14 shows some of the first preliminary FEA results obtained. As seen the max wetted wall for this 5 kilowatt test case was 420°F which is below the 450°F max target. This condition is with an 800°C air inlet into the injector and a 5 pph fuel flow rate. The heat shield (not shown) was optimized for this test case. The idea is to control the gap between the fuel cartridge and the heat shield to bring the fuel temperature up to 350°F without bringing the fuel wetted wall above 450°F. As a side note, the 450°F max wetted wall is based upon current work with anti-carbon coatings. It was anticipated that one (if not more) of the current anti-carbon coatings will resist carbon formation up to this 450°F temperature. This carbon testing is discussed in more detail in the Milestone 2 section.

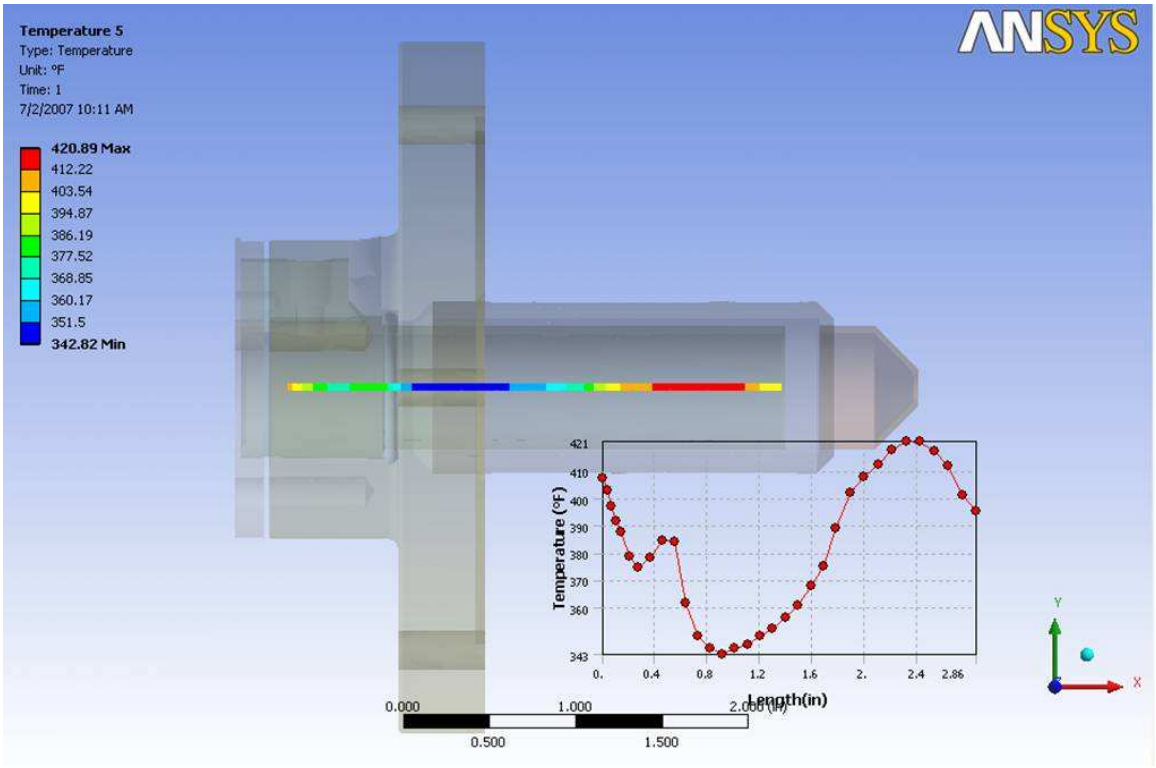

Figure 6.14: Wetted Wall Temperature of Fuel Passage

The next analysis completed was Case One and it was used to evaluate the wetted wall temperatures of the fuel passage using the current design with the existing heat shield removed. This was to establish a baseline for wall temperatures before beginning a re-design. Figure 6.15 thru 6.16 shows some of the FEA results for this case one.

As indicated in Figures 6.15-6.16, wetted wall temperatures were calculated to rise to over 800°F at the fuel passage outlet near the tip. While this particular analysis did yield bulk temperature fuel rise above 350°F, the design was not feasible since the anti-coking coatings are projected to only defeat carbon growth at temperatures much lower than the predicted 800°F wall temperatures.

One of the main problems with the current injector design is the lack of a thermal barrier between the outer heat shield components and the fuel cartridge. A braze joint currently exists between the outer sleeve and the heat shield cap, creating a thermal bridge. Heat can also transfer to the barber pole due to the existence of another braze joint between the outer sleeve and the barber pole.

In addition to the braze joints, the current design did not indicate any type of seal on the inside surface between the flange/heat shield and the outside surface of the outer sleeve. Without a proper seal present hot air can leak out of the system through the heat shield cavity, subsequently leading to a higher heat transfer coefficient.

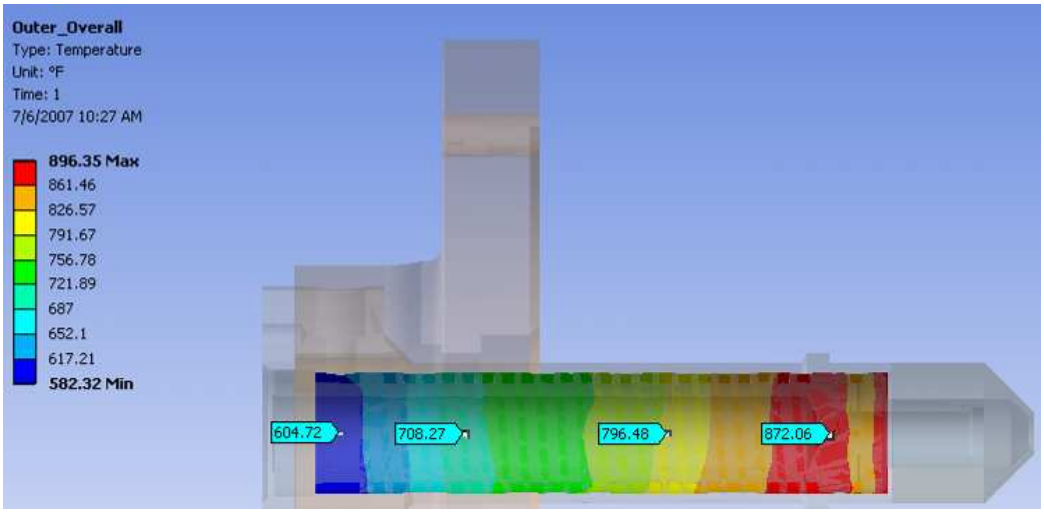

Figure 6.15: Case One (No Heat Shield) Outer Wetted Wall Temperatures

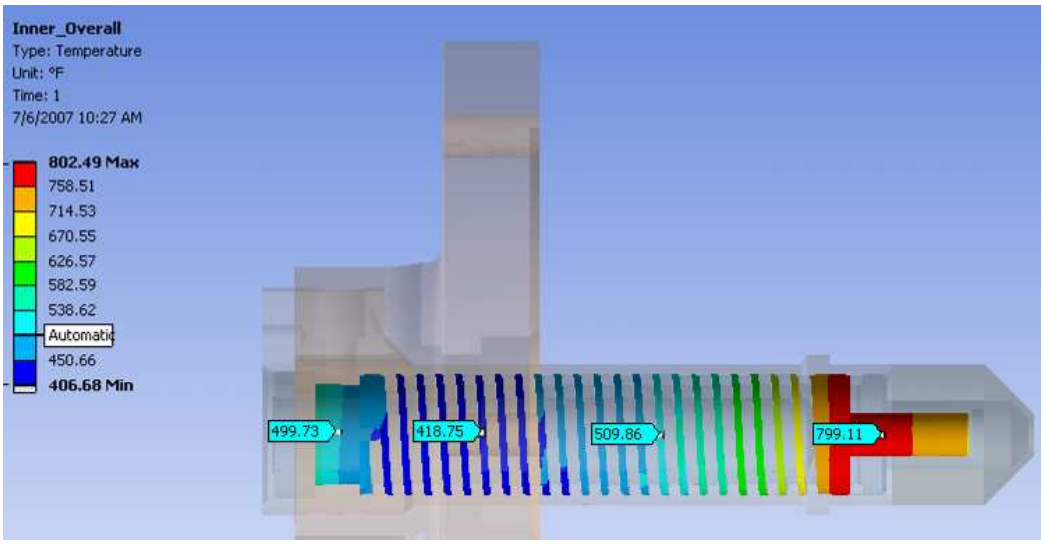

Figure 6.16: Case One (No Heat Shield) Inner Wetted Wall Temperatures

Case Two was the next FEA case study. Case Two uses a recommended heat shield design that completely isolates the fuel passage from the outer heat shield. The design also includes a metallic C-Seal where the outer shield bottoms out with the flange. This seal eliminates air flow through the injector air gaps, making the air a better insulator. The results of this design change can be seen in Figures 6.17 and 6.18.

The results from these analyses shows that the heat-flux into the fuel passage can be controlled using the air gap between the outer sleeve and the heat shield. For this particular iteration, wetted wall temperatures were kept well under 450F. It was further predicted that the bulk temperature fuel rise would be around 247°F given the ANSYS defined wall temperatures based on the constant heat flux analysis method.

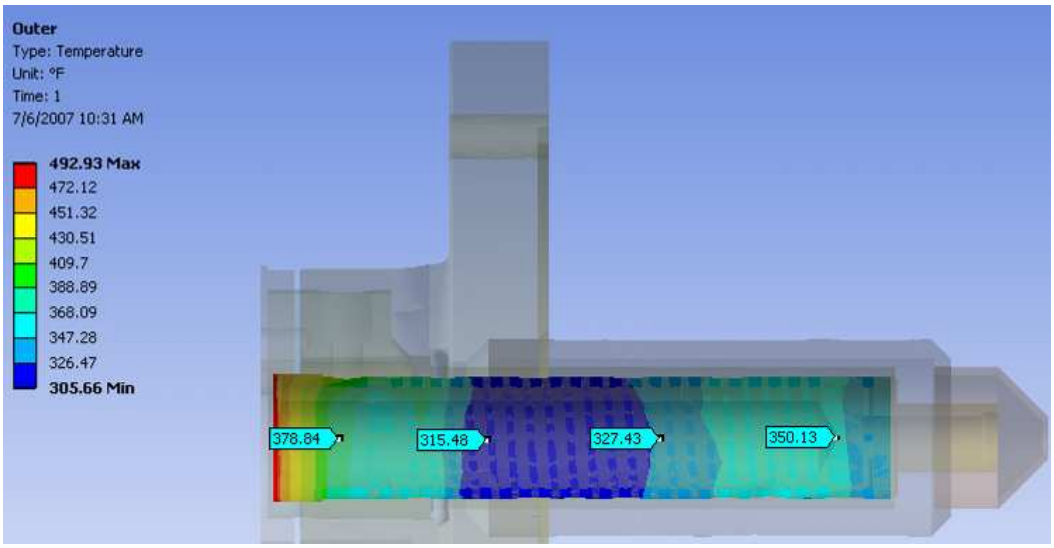

Figure 6.17: Case Two (Heat Shielded) Outer Wetted Wall Temperatures

Based on the analyses, heating the fuel over 300°F is not a difficult challenge given the heat of the air supplied to the injector. However, maintaining wetted wall temperatures below 450°F has proven to be of concern. The two analyses conducted with a modified heat shield prove that maintaining a wetted wall temperature below the coking limit of the metal coatings is possible. However, by doing so, the ability to heat the fuel above 300°F is compromised.

Cases 2 and 3 indicate that the wetted wall temperatures in the fuel passage can be readily controlled by use of a sealed air gap between the heat shield and the fuel passage. Furthermore, thermal bridging via metal-on-metal contact and braze joints should be not used when attempting to minimize wetted wall temperatures.

Since the fuel is only in the injector for approximately 1.5 seconds, it is inherently difficult to impart enough energy into the fuel before it leaves the injector without having much higher wall temperatures. As such, it is a recommendation that future design work research the possibility of preheating the fuel to a higher temperature before it enters the fuel injector. By doing so, it may be possible to heat the fuel to the desired temperature of over 300°F before it exits, while still keeping wetted wall temperatures in the functional limits of the coatings.

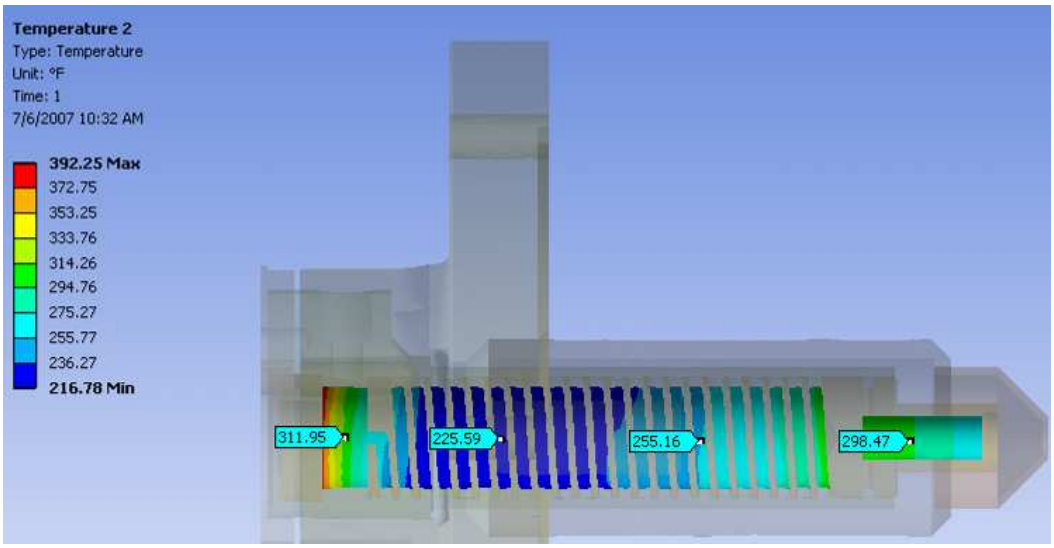

Figure 6.18: Case Two (Heat Shielded) Inner Wetted Wall Temperatures

Task 5.5 Conduct SDE Study Using the Optimized Preheating Simplex Injector for Performance Prediction and Correlation

Task 5.5 is a repeat or a restatement of sub tasks 4.6 through 4.8. Sub task 5.5 just reiterates the work to ensure that CFD was consulted during the injector optimization processes. The optimized preheating simplex injector and mixing chamber can be seen in Section 5 in this report.

In summary, CFD shows that there are recirculation zones present near the atomizer/mixer centerline. These results can be confirmed by the testing performed on the injector/mixer. Recirculation can be useful for mixing the fuel and air. The FEA results suggest that it would be possible to increase the fuel preheat by allowing more interaction time with the fuel and the hot inlet air. Something that could be readily added during a follow on phase to this work.

7.0 Milestone 6.0: Optimize Piezoelectric Injector and Mixer (Optional)

Milestone 6.0 is a competing approach to the preheating injector work completed in Milestones 3 & 4. Instead of using heat to increase atomizer efficiency the piezoelectric injector uses small piezoelectric vibrations to induce atomization of the fuel. In this way, very low fuel and air pressures could also be utilized. This section focuses on the work that was done on the piezoelectric injector.

Originally Milestone 6.0 was an option task to be completed if funds were available towards the end of the project. However, NETL expressed interest that this milestone be brought up in priority and worked in parallel with the other milestones. This allowed this milestone to be fully completed with only Task 3.10 & 3.13 of Milestone 3 made optional because of funding.

The first subtasks completed of Milestone 6.0 were:

Task 6.1 Evaluate Improvement Ideas for the Piezoelectric Injector
Task 6.2 Prepare Solid Model and Drawings
Task 6.3 Fabricate and Assemble Test Hardware

Figure 7.1 shows an isometric view of the piezoelectric injector assembly. The components for this assembly were completed and assembled per this model. Figure 7.2 and 7.3 show two flow points that were tested on the piezoelectric injector fuel horn (two horns with different horn angles) without the air swirlers and air box. A significant change was made to the vibrating injector tip from the Phase 1 work. Instead of producing a narrow spray angle, the tip has been modified to create an extremely wide spray angle (>180°). With this wide angle the fuel will be better mixed with the low pressure, low velocity air. This wide spray angle can be clearly seen in Figures 7.2 and 7.3. This portion of the injector testing showed very favorable results. As seen, the fuel demonstrates very small droplets and appeared to be uniform, even with a single fuel injection point. The fuel pressures at this test condition were lower than 1.0 psi which demonstrates the advantage of the piezoelectric injector (the preheating injector operated near 20 psi fuel pressure). A single point injection point was used in the testing shown. The final build assembly utilized a multi-point fuel injection system which improved fuel distribution on the injector tip.

This preliminary injector demonstrated a natural frequency near 70 kHz. This is below the 80 kHz predicted natural frequency but within expected ranges. Also, the atomizer demonstrated effective atomization up to 8 pph. Flow rates above 8 pph caused the tip to flood with fuel which resulted in no atomization. This fuel flow range was within the desired targets.

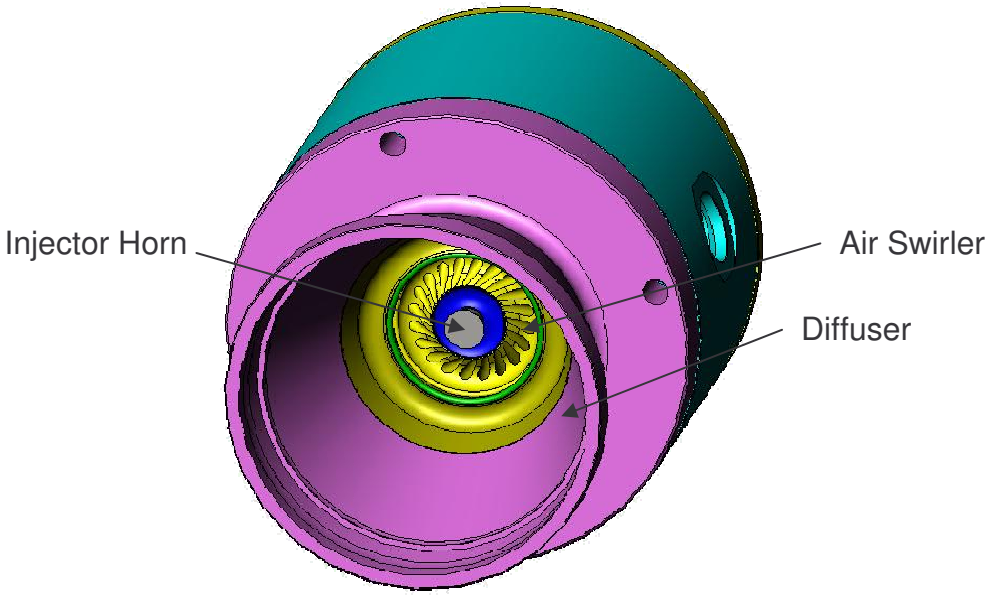

Figure 7.1: Isometric View of Piezo-Electric Nozzle Assembly

Figure 7.2: 3 PPH Fuel with 70° Tip Cone

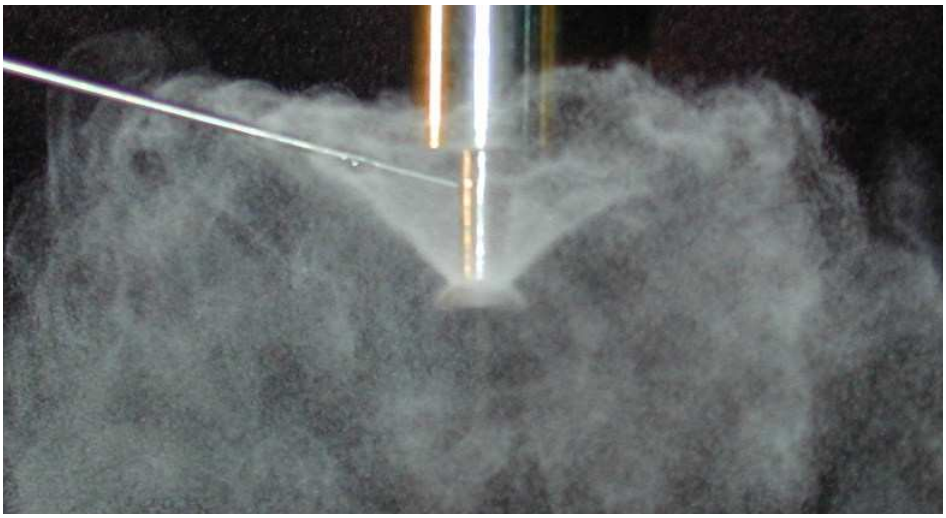

Figure 7.3: 1 PPH Fuel with 90° Tip Cone

After this testing the complete atomizer assembly was tested with and without heated air (with out the diffuser shown in Figure 7.1). Figure 7.4 and 7.5 show the 5 pph fuel flow test point utilizing 70°F PS133 test fluid and 25 pph of 70°F air. Figure 7.4 shows this test point utilizing the flash to capture the individual droplets. As seen the droplets are extremely small and evenly distributed. Figure 7.5 does not use the flash to show the fuel flow path and the resulting fuel spray angle.

Figure 7.6 & 7.7 show the 3 pph fuel flow test point utilizing 70°F water and 15 pph of 560°F air. At this temperature the droplets are smaller and difficult to detect with the same camera setup. These results were excellent first pass results. As a side note, the injector demonstrated a natural frequency near 63 kHz. Again, this is below the 80 kHz predicted natural frequency but within expected ranges since the natural frequency is a factor of fuel flow rate and temperature of the injector. The atomizer demonstrated effective atomization up to 5 pph. Flow rates above 5 pph caused the tip to flood with fuel which resulted in very little atomization. This

fuel flow range is within the desired target but is expected to improve with performance development.

Figure 7.4: 5 PPH 70°F PS133 Test Fluid, 25 PPH 70°F Air

Figure 7.5: 5 PPH 70°F PS133 Test Fluid, 25 PPH 70°F Air

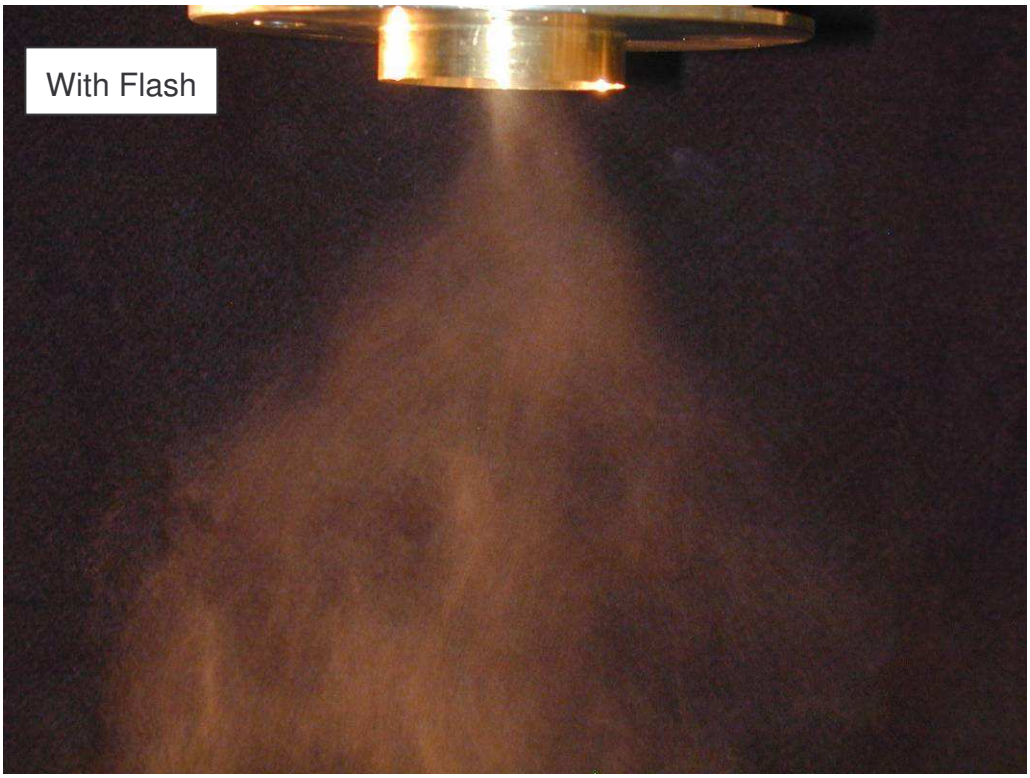

Figure 7.6: 3 PPH 70°F Water, 15 PPH 560°F Air

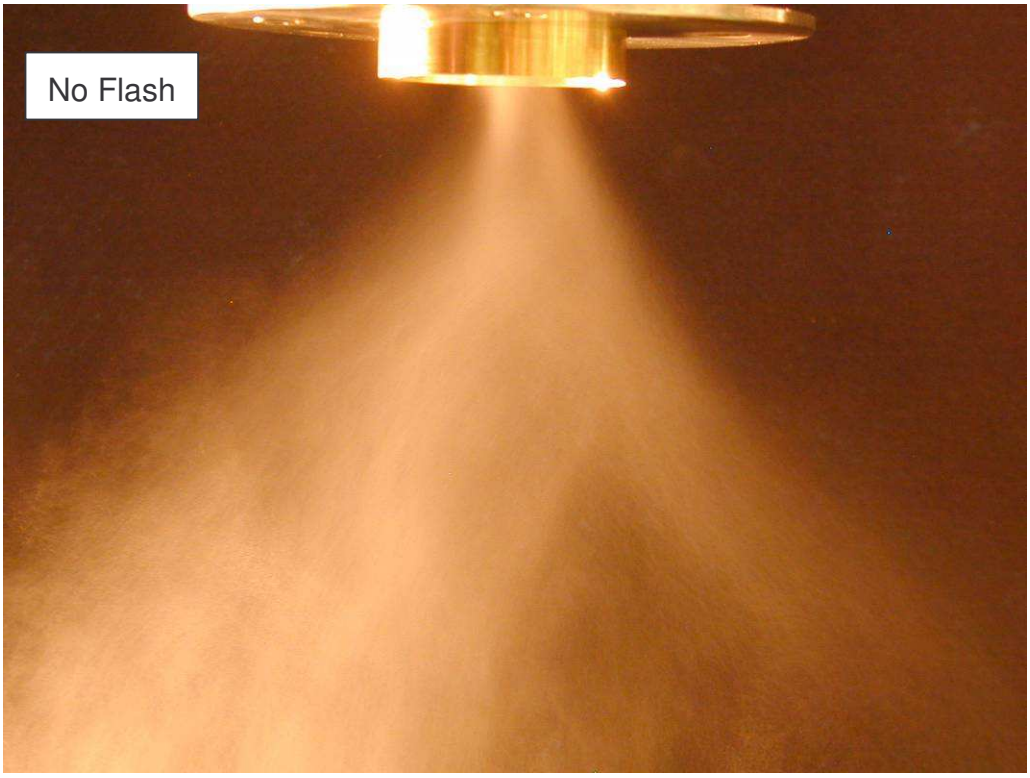

Figure 7.7: 3 PPH 70°F Water, 15 PPH 560°F Air

These piezoelectric assembly test results are very encouraging. The atomizer spray angle is much wider than the phase 1 work. It was anticipated that this injector would have better mixing capabilities than the phase 1 piezoelectric injector. The next sub-task of Milestone 6.0 that was completed was:

Task 6.4 Conduct Experimental Tests

PDPA testing was next performed on the piezoelectric injector. Figure 7.8 shows the SMD results of this testing. The primary fuel for this test point was MIL-PRF-7024 Type 2 test liquid flowing 5pph at less than 1 psig. The air flow was 25 pph at 0.6 inH_2O. This corresponds to a 5kW fuel cell operation point. The measurement was taken at an axial distance of 3 in. away from the injector face. The average SMD for this test was 109.9µm. This SMD is higher than anticipated but still within acceptable limits and comparable to the preheating injector. In review, this measurement was taken after heated air testing was attempted on the injector. This heated testing damaged the o-rings used in the injector. The o-rings became hardened due to the high temperature allowing the piezoelectric vibration to be dampened by the air-box reducing the energy transferred to injector tip. The testing shown in Figure 7.8 was completed with this dampening effect. Design changes were made to improve performance, and testing was repeated once the injector was rebuilt with these new changes. Again, PDPA testing shown in Figure 7.8 was performed without the mixing chamber and at ambient temperature conditions with extremely low fuel and air pressures. It is expected that the SMD will only improve as the temperature is raised and the mixing chamber is added and optimized. These preliminary results were very promising. The PDPA retest results can be found in the task 6.5 and 6.7 discussed next.

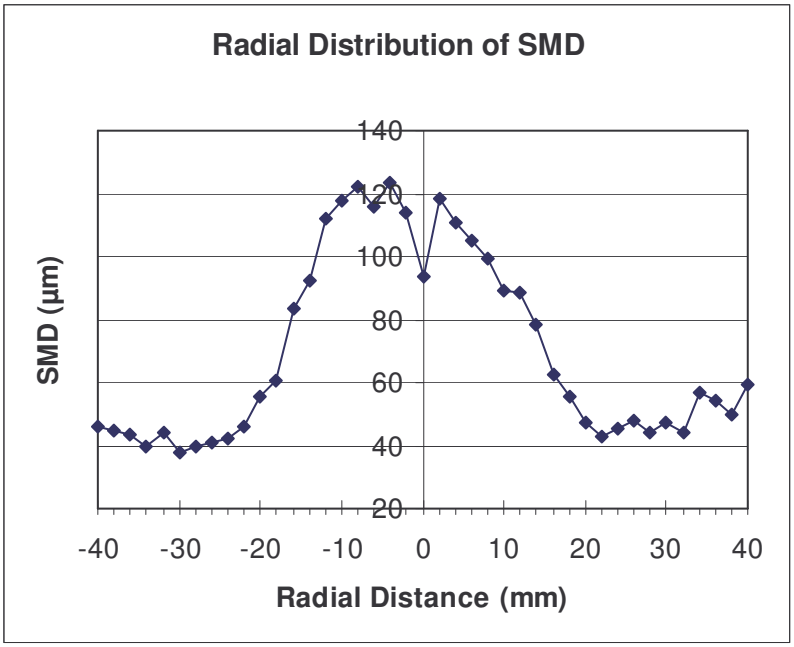

Figure 7.8: PDPA Results for the Piezoelectric Injector

The next subtasks completed were:

Task 6.5 Investigate Effect of Flow Rate, Temperature, and Fluid properties
Task 6.7 Conduct SDE Study to Fully Characterize the Injector performance

Because of the problems that occurred during high temperature air testing previously discussed, five new components were manufactured for the piezoelectric injector. The first piezoelectric injector required super glue for assembly. The super glue was used to isolate fuel passages and air passages. This super glue showed favorable results at room temperature testing. It was quickly learned during heated air testing that the super glue was not temperature resilient. Five new parts were created that were brazed together in the final assembly. These braze joints will be able to stand the higher air temperature testing. This new assembly was created and was tested. Figure 7.9 and 7.10 are pictures of the completed piezoelectric injector.

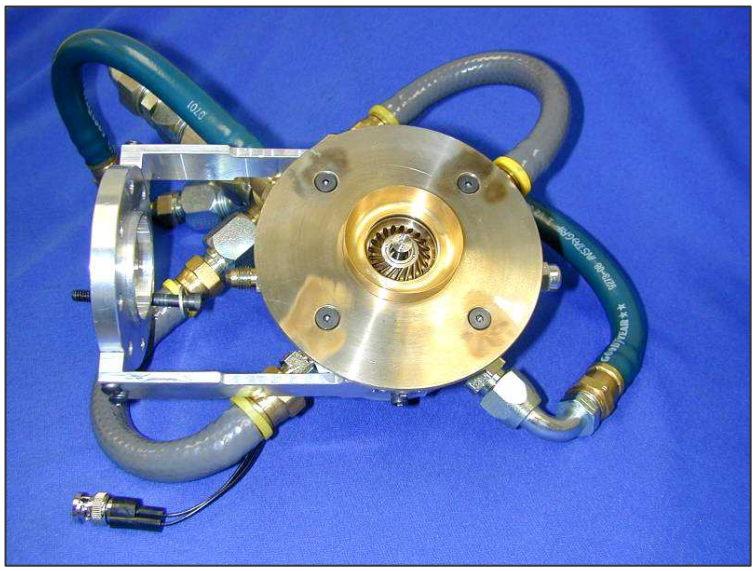

Figure 7.9: Piezoelectric Injector Face

Figure 7.10: Piezoelectric Injector Back View

The piezoelectric injector shown was retested on the Phase Doppler Particle Analyzer (PDPA). As mentioned previous testing results were found to be somewhat unreliable. As a reminder, the piezoelectric injector had been subjected to high air temperatures which caused the o-rings to solidify. This allowed the vibration to be transferred into the air box which caused significant dampening in the injector. Previous PDPA work was completed with this dampening effect. Due to the need to eliminate this effect and to create a more robust prototype, the piezoelectric injector was redesigned and several improvements were incorporated. O-rings were eliminated from the hot section, the fuel delivery was simplified, and an improved controller was fabricated. Retesting was delayed because the PDPA test instrument was sent to the vendor for refurbishment, cleaning, and calibration. The PDPA rig returned from the vendor and was reassembled. Figure 7.11 thru 7.13 shows the results of the PDPA tests with the redesigned injector (Config 3) and controller. Measurements were taken at two locations downstream, 1 inch and 3 inches.

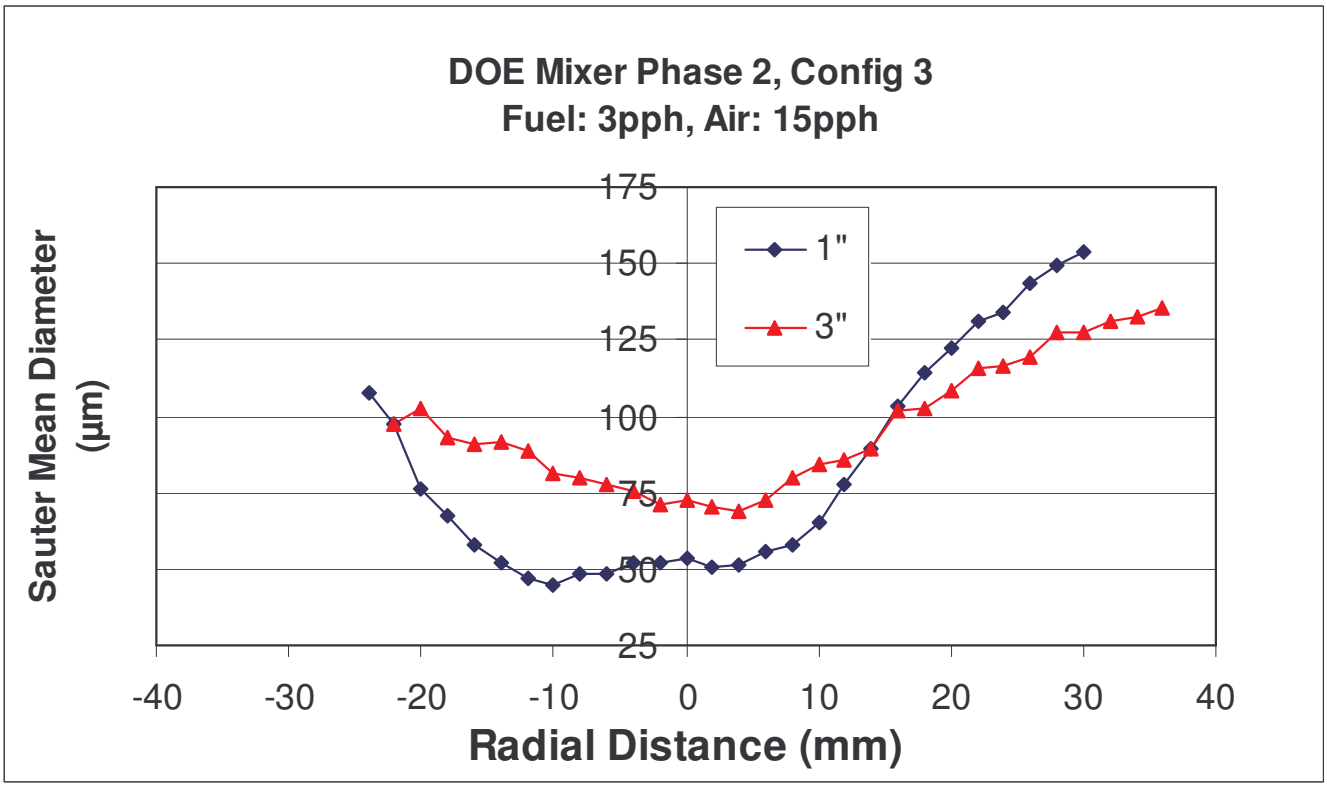

Figure 7.11: Radial SMD <1 psi Fuel, 0.25 inches H_2O of Air

Figure 7.14 shows the PDPA results of the latest test and Figure 7.15 shows the o-ring dampened test results (previous PDPA test). At the 5 pph test point there is a 50 µm SMD improvement with the new injector. However, at the lower flow rates (2 and 3 pph) the previous PDPA shows superiority over the new injector. This is likely due to the new components for fuel delivery. The new components deliver fuel slightly differently and were targeted for the 5 pph flow rate. In summary, the results are extremely pleasing since the air pressure is 2.0 in of H_2O or less, the fuel pressure is less than .5 psi and the global SMD is less than 100 µm. This is extremely good news for the piezoelectric injector.

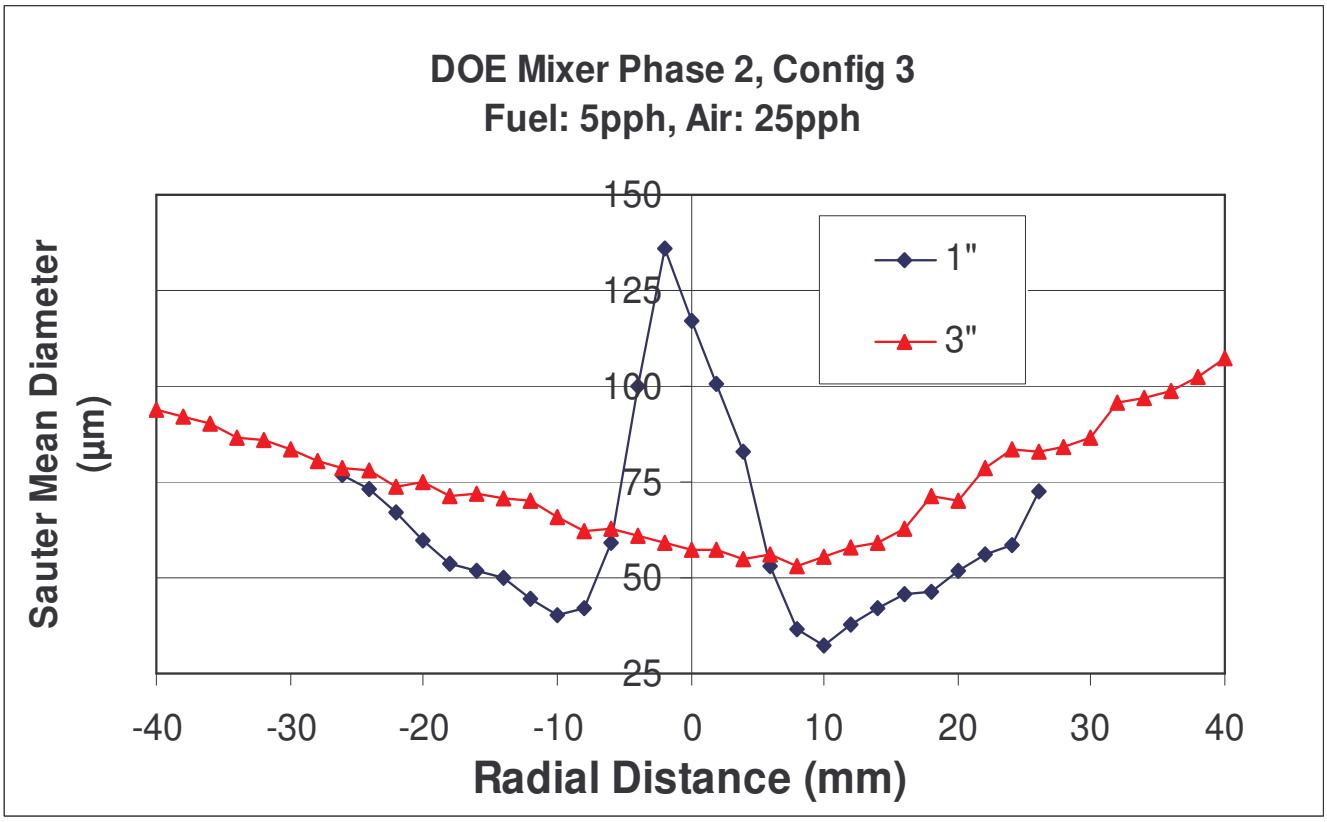

Figure 7.12: Radial SMD <1 psi Fuel, 0.5 inches H_2O of Air

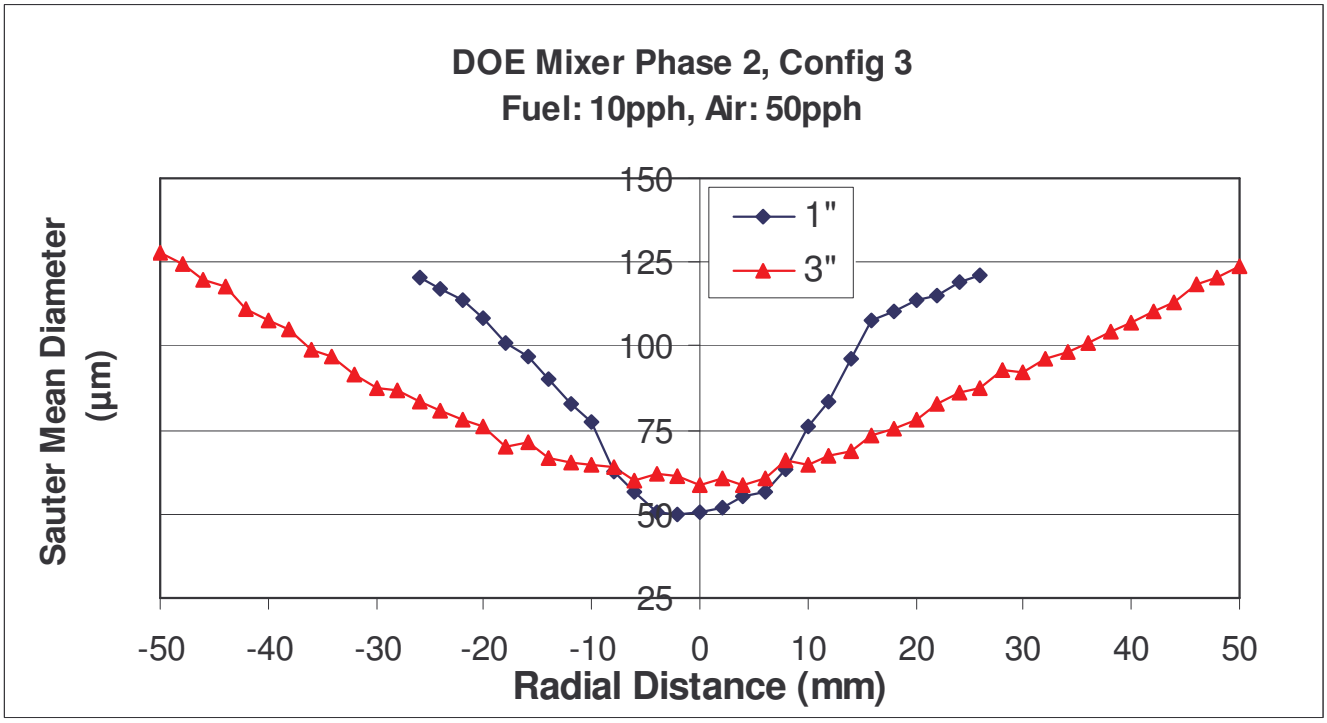

Figure 7.13: Radial SMD <1 psi Fuel 2.0 inches H_2O of Air

Phase 2 Data (Brazed Fuel/Air Assembly, Optimized Lower Voltage Driver)

PN: Phase 2 Config 3 (-3, -5) **Axial Dist.:** 3 inches

			Rosin-Rammler				
	Test Fluid	**SMD (µm)**	**Xbar**	**N**	**Hertz**	**Amps**	**Volts**
Fuel: 3 pph, Air: 15 pph	PS133	103.1	138.4	3.05	62,400	1.52	17.0
Fuel: 5 pph, Air: 25 pph	PS133	73.4	95.6	2.84	62,500	1.25	16.3
Fuel: 10 pph, Air: 50 pph	PS133	82.9	110.5	2.73	62,400	0.70	17.0

PN: Phase 2 Config 3 (-3, -5) **Axial Dist.:** 1 inch

			Rosin-Rammler				
	Test Fluid	**SMD (µm)**	**Xbar**	**N**	**Hertz**	**Amps**	**Volts**
Fuel: 3 pph, Air: 15 pph	PS133	84.1	131.2	2.06	62,300	1.51	17.0
Fuel: 5 pph, Air: 25 pph	PS133	59.4	84.0	2.11	62,300	0.58	17.0
Fuel: 10 pph, Air: 50 pph	PS133	74.4	114.8	1.95	62,600	1.38	17.0

Figure 7.14: PDPA Data Summary (Config 3)

Another important item to note is the operational flow rate range of this injector. The new controller, completed during the month of August, was able to increase the operation range of the piezoelectric injector (2 pph to 11 pph). Previously the max fuel flow rate for the injector was ~6 pph. As seen in Figure 7.14 and 7.15, the injector operated consistently at 3 and 10 pph. This injector demonstrated a turn down ratio of 6:1. This turn down ratio is an improvement over the phase one work as well as first nozzle developed in this section. Also the new controller operates much more efficiently: 17 volts rather than 32 volts.

Phase 2 Legacy Data

PN: Phase 2 Config 2 (-3, -4, -1, -2) **Axial Dist.:** 3 inches

			Rosin-Rammler				
	Test Fluid	**SMD (µm)**	**Xbar**	**N**	**Hertz**	**Amps**	**Volts**
Fuel: 2 pph, Air: 10 pph	PS133	66.2	92.7	2.36	62,800	0.600	31.6
Fuel: 5 pph, Air: 25 pph	PS133	127.6	187.6	2.59	64,440	0.570	31.6
PN: Phase 2 Config 1 (-3, -5, -1, -5)							
Fuel: 2 pph, Air: 10 pph	PS133	50.2	69.7	2.14	62,750	0.550	31.6
Fuel: 5 pph, Air: 25 pph	PS133	117.4	175.4	2.39	62,440	0.580	31.6
Fuel: 5 pph, Air: 25 pph (Sweep)	PS133	109.9	184	2.01	62.43-62.47	.69-.70	31.6

Figure 7.15: PDPA Data Summary (O-Ring Dampened)

The last sub-task completed of Milestone 6.0 was:

Task 6.6 Incorporate Pulse Modulation Device and Controller

The only item remaining in the piezoelectric injector work was to add phase tracking to the piezoelectric injector controller. With all the testing shown in this section, the frequency of the controller was adjusted manually. Phase tracking allows the controller to vary the driving frequency. The driving frequency is phase matched to the natural frequency of the injector. It was found that the natural frequency in the injector changed during operation. This was due to temperature change (heat up and cool down) and fuel flow rate changes. As the nozzle heats up to operating condition, the temperature rise causes the metal components to increase in length. This increase in length causes the natural frequency to change. Similarly, the more fuel

that is placed on to the vibrating injector tip, the more the natural frequency of the atomizer would shift. The phase tracking controller changes the driving frequency automatically. This eliminates the need for an operator to continually tweak the injector during operation. The phase tracking was bench tested and shown to track the natural frequency exceptionally well.

Another item added to the frequency controller was a burst mode option. During testing it was found that the injector would stop atomizing fuel when near the upper flow rate limit. If the fuel flow rate became too large, the injector tip would saturate and the vibration would not induce enough energy into the fuel to atomize it. This event was termed flooding. Flooding was used to determine the top end of the injector operating range (~10 pph). To recover from flooding, the fuel flow rate was decreased and high pressure air was used to blow the fuel off the end of the vibrating cone. The burst mode was developed to eliminate the need for the high pressure air to clean the tip. When the tip floods with fuel, the fuel flow rate is slightly decreased and the burst mode is activated. The controller causes a high amplitude spike to be delivered. This allows the injector to shake off any extra fuel and then continue to operate normally. The burst mode was bench tested and worked well. Burst mode was not able to take the injector to a higher operating point (>10 pph) but it did show that it could shake off extra fuel during the normal operating range.

This work closes Milestone 6.0. No more actions are required for Milestone 6.0. The piezoelectric injector showed great promise for flow rates between 2.0 and 10.0 pph. There are still some thermal management issues to work out (keep piezoelectric crystals cool) but this injector could be and is ready to be used in fuel cell applications.

8.0 Summary

There are many data related conclusions from each section of this report. This section will summarize some of the main conclusions from each section. First, three anti-carbon coatings have shown improvement over a non coated baseline (347 stainless steel). SEM analysis has shown that no carbon was generated on the test specimens after 70 hours of continuous back to back testing. Without the formation of carbon it was impossible to draw conclusions of which anti-carbon coating showed the best performance. It was theorized that the fuel obtained for this test did not produce the carbon growth rates seen in the previous tests. This was one of the many unplanned variations that occurred during testing. Because of the lack of carbon growth that occurred on the final back to back test, a single best anti-carbon coating could not be selected. The three coatings that showed improvement over the baseline uncoated specimen were:

Dash #	Coating Vendor	Coating Type	Application Technique
-1A	AMCX	Inertium	Diffusion Bonded
-1B	AMCX	AMC26	Diffusion Bonded
-2	Restek	Silcosteel AC	Chemical Vapor Deposition

These results would not have been possible without the construction of the coking formation test rig which was built during Milestone 1. Engine Components highly recommends that future

tests be completed on this rig to obtain more reliable test results. As a side note, the final back-to-back testing was able to show that AMCX AMC26 demonstrated the lowest discoloration of the metal out of the three down selected anti-carbon coatings. This discoloration did not relate to carbon but could be a useful result when carbon growth rate is not the only concern. Also, unplanned variations in the series of tests must be considered and may have altered the results. Reliable conclusions could only be drawn from consistent, repeatable testing beyond the allotted time and funding for this project.

Next, a single configuration from the SDE of the preheating injector Build 1 has shown a very uniform fuel spray flow field. This injector was improved upon by the creation of Build 2 which attempting to reduce recirculation zones by diffusing the air through a venturi region prior to the mixing chamber swirler. Build 2 of the preheating injector demonstrated promising SMD results with only 22psi fuel pressure and 0.7in H_2O of Air. However, it is apparent from testing and CFD that this Build 2 still had flow field recirculation zones. These recirculation zones may indicate that this Build 2 atomizer and mixer may require steam injection to reduce the auto ignition possibilities. It is also important to note that to achieve uniform mixing within a short distance, some amount of recirculation is necessary. Although the mixing chamber could be improved to reduce recirculation, this would likely have a negative impact on mixture uniformity which may be a bigger factor in reformer life.

CFD results confirmed the recirculation zones seen in test data and confirmed that the flow field would not change when attached to the reformer. The FEA predicted fuel wetted wall temperatures which led to several suggested improvements that could possibly improve nozzle efficiency. CFD was a valuable tool in evaluating injector performance at operating conditions that were not possible in lab testing.

The piezoelectric atomizer showed acceptable SMD results with fuel pressure less than 1.0 psig and air pressure less than 1.0 inH_2O. These SMD values were improved once a few components were changed, and it is expected would reduce further still at elevated air temperatures. The real conclusion of this project is that the piezoelectric injector has shown great promise. The addition of phase tracking and a burst mode to the frequency controller increased the usability of the piezoelectric injector. This injector is ready to move onto the next phase of development and be added to a working fuel cell application.

Engine Components has met the required program milestones of this project. Again, these Milestones were adjusted to allow Milestone 6 to be completed in parallel with the other Milestones. Because of this, Task 3.10 and 3.13 were made optional instead of Milestone 6. Engine Components was extremely grateful for the support that was provided by NETL in support of this work.